A Role for Focal Adhesions and Extracellular Matrix in Traumatic Axonal Injury

Citation

Permanent link

Terms of Use

Share Your Story

A Role for Focal Adhesions and Extracellular Matrix in Traumatic Axonal Injury

A dissertation presented

by

Matthew Allen Hemphill

to

The School of Engineering and Applied Sciences

in partial fulfillment of the requirements

for the degree of

Doctor of Philosophy

in the subject of

Engineering Sciences

Harvard University

Cambridge, Massachusetts

July, 2014

Dissertation Advisor: Professor Kevin Kit Parker   Author: Matthew Allen Hemphill

A Role for Focal Adhesions and Extracellular Matrix in Traumatic Axonal Injury

Abstract

Traumatic Brain Injury (TBI) is linked to a diverse range of diffuse pathological damage for which there is a severe lack of therapeutic options. A major limitation to drug development is the inability to identify causal mechanisms that link head trauma to the multitude of secondary injury cascades that underlie neuropathology. To elucidate these relationships, it is important to consider how physical forces are transmitted through the brain across multiple spatial scales ranging from the whole head to the sub-cellular level. In doing so, the mechanical behavior of the brain is typically characterized solely by its material properties and biological structure. Alternatively, forces transmitted through distinct cellular and extracellular structures have been shown to influence physiological processes in multiple cell types through the transduction of mechanical forces into cellular chemical responses. As an essential component of various biological processes, these mechanotransduction events are regulated by mechanical cues directed through extracellular matrix (ECM) and cell adhesion molecules (CAM) to mechanosensitive intra-cellular structures such as focal adhesions (FAs). Using a series of *in vitro* models, we have implicated FAs in the cellular mechanism of traumatic axonal injury by showing that forces directed through these structures potentiate injury levels and, moreover, that inhibition of FA-mediated signaling pathways may be neuroprotective. In addition, we show that localizing trauma forces through specific brain ECM results in differential injury rates, further implicating mechanosensitive cell-ECM linkages in the mechanism of TBI. Therefore, we show that FAs play a major role in axonal injury at low strain magnitudes indicating that cellular mechanotransduction may be an important mechanism underlying the initiation of cell and sub-cellular injuries ultimately responsible for the diffuse pathological damage and clinical symptoms observed in diffuse axonal injury. Furthermore, since these mechanisms may present the earliest events in the complex sequelae associated with TBI, they also represent potential therapeutic opportunities.

Contents

List of Figures

List of Tables

Acknowledgements

1 Mechanisms of Diffuse Damage Caused by Traumatic Brain Injury

1.1 Introduction

Traumatic Brain Injury (TBI) is caused by a mechanical insult to the head and is estimated to affect 1.7 million people annually in the United States [92] and 235 per 100,000 people annually in Europe [274]. TBI is categorized as mild, moderate, or severe based on clinical symptoms often in combination with imaging and post mortem histology. Pathological lesions consisting of contusion, hemorrhage, and edema are clinical indicators of head injuries. As such, traumatic cell death in regions directly adjacent to sites of trauma is often viewed as the primary neurological damage [3,105,116,238,308]. However, it is now understood that additional forms of neuropathology contribute significantly to the ensuing morbidity associated with TBI.

Broadly described as diffuse TBI, a complex array of microscale pathologies including diffuse axonal injury (DAI), microvascular damage, and diffuse neuronal injury can develop throughout the brain parenchyma following trauma. Even though clinical symptoms may improve, the microscale damage can persist and potentially contributes to an increased likelihood of future neurodegenerative disease [102,189,114]. Although the risk associated with diffuse damage has clearly emerged, a comprehensive understanding of the mechanical and biological processes that initiate this damage remains elusive.

Difficulties in identifying the events that initiate diffuse pathologies are likely due in part to the complexity of characterizing forces distributed through structures ranging in size from the whole brain down to subcellular levels [60]. Understanding the biomechanical events that initiate brain injuries has typically relied on determining how neural tissue responds to rapidly applied loads through both mathematical modeling and experimental techniques [164,60,52]. In order to understand disease pathogenesis, there has been a tendency to focus on forces that

disrupt the integrity of the networked architecture of the brain [275,152]. However, establishing a causal link between a mechanical insult and the ensuing diffuse pathology observed in TBI has been met with limited success.

In this dissertation, we begin by introducing the known diffuse neuropathological damage associated with TBI and the multi-scale biomechanics that may explain patterns of cell-level injury in the brain. We propose that to improve the mechanistic understanding of diffuse brain damage, it may be necessary to consider how mechanical forces below the threshold for mechanical failure influence cellular physiological processes. Specifically, we hypothesize that injury forces directed through extracellular matrix molecules activate cellular mechanotransduction mechanisms that cause axonal injury. The importance of cellular mechanotransduction, or the ability of cells to convert mechanical forces into biological signals, has been widely established in many organs, tissues, and cells across multiple species [292,289,291]. Cell-cell and cell-matrix interactions have been shown to influence both physiological and pathophysiological processes [131,139], suggesting that they play an important role in brain injury and remodeling after TBI. Herein, we focus on understanding whether the brain ECM serves as a conduit to direct forces associated with mechanical trauma through mechanosensitive cellular structures that affect axonal injury.

1.2 Biomechanics and Neuropathology of Traumatic Brain Injury

1.2.1 Trauma Induced Local and Distributed Loading Within the Brain

Many studies have explored the role of sudden impact, acceleration, and blast force in brain injury [221,220,17] (Fig. 1-1). Localized forces are typically associated with impact injuries where the brain deforms against the skull, while distributed loading is typically attributed to both inertial forces due to rapid head acceleration [220] as well as pressure transients due to

Figure 1-1: Mechanical Loading of the Brain Due to Trauma.
A mechanical insult to the head resulting from impact, acceleration, or blast forces can generate both localized and distributed forces throughout the brain. Localized forces typically occur due to impact of the brain against the skull. Distributed forces can be caused by inertial effects during rapid acceleration or by increased pressure transients caused by explosive blast.

explosive blast waves [17]. Although these loading patterns are not mutually exclusive, we will focus on the current limitations in understanding the effects of diffuse loading patterns and the complexity of understanding the cellular damage and injury mechanisms associated with them.

1.2.2 Assessing and Diagnosing Anatomical Brain Injury

Diagnosis of TBI typically relies on a neurological assessment followed by imaging to detect pathology. Classes of TBI pathology, termed focal and diffuse, have been attributed to local and distributed loading in the brain. Povlishock and Katz suggested a distinct classification between focal and diffuse injuries predicated upon both clinical and basic science perspectives, with the acknowledgement of some overlap in pathobiology and clinical outcome [235]. They classified a typical focal injury as consisting of contusion and hemorrhage located near the site of impact and a diffuse injury as consisting of diffuse axonal injury (DAI) and petechial white matter hemorrhage located at multiple sites throughout the brain.

While pathological lesions consisting of contusion and hematoma formation associated with focal injures are readily distinguishable by CT and traditional MRI scans, DAI and other

3

subtle hemorrhages are not. For example, abnormalities were detected by CT scan in only 5-30% of patients exhibiting clinical symptoms consistent with mild TBI (mTBI) [35], and the extent of pathology detected by CT scan and MRI did not correlate with the clinical outcomes [167]. Therefore, identifying diffuse pathology following head injury has historically relied on postmortem histological analysis in which DAI is detected by the presence of punctate, swollen axons [269]. The inability to measure the extent of diffuse pathology demonstrates a deficiency in diagnostic methods that may contribute to the debate about the etiology of TBI.

A major breakthrough occurred in 2002 when Arfanakis et al. showed that Diffusion Tensor Imaging (DTI), a form of MRI, could detect abnormalities not found on CT scans in patients diagnosed with TBI within 24 hours of trauma [11]. DTI abnormalities were measured as regional reductions in diffusion anisotropy, which were later shown to correlate with regions of axonal damage from histological analysis [180]. Subsequent studies further correlated reductions in diffusion anisotropy with neuropsychological dysfunction in longitudinal studies [20] while also showing that DTI abnormalities can be used to predict cognitive outcome [117]. The incorporation of DTI as a diagnostic technique has improved the ability to identify diffuse brain damage and may contribute to an understanding of how diffuse pathology may contribute to TBI related morbidity.

Recent reports have shown that diffuse damage can occur even after mild insults with no previously identifiable neuropathology [190,265,218], supporting the notion that diffuse damage may contribute more greatly to morbidity than previously understood. Concussion and repetitive sub-concussive impacts are now linked to progressive neurodegeneration classified as Chronic Traumatic Encephalopathy (CTE) [190]. This disease was first reported in boxing as dementia pugilistica where it was characterized clinically by declining mental capacity, lack of

coordination, and behavioral problems [63]. McKee et al. showed that professional athletes who suffered repetitive mTBI developed diffuse, microscale injury patterns characterized by post-mortem identification of neurofibrillary and glial tangles, hyperphosphorylated tau, axonal degeneration, and immunoreactive microglia [189]. Moreover, blast combat casualties from the wars in Afghanistan and Iraq exhibited similar tissue damage [114] as well as additional pathology such as cerebral vasospasm [12] and traumatic axonal injury [181]. The diffuse neuropathological changes associated with CTE and explosive blast, some of which are distinct from those previously attributed to TBI, suggest that the extent of diffuse brain damage, especially following mTBI, may be greater than previously understood.

While traumatic cell death attributed to focal injuries was for many years viewed as the primary contributor to morbidity following TBI, it is now understood that pathophysiological conditions may ensue even without widespread cell death [91]. For example, an acute phase of neuroexcitation was shown to occur in the brain immediately following impact. This event has been linked to the indiscriminant release of neurotransmitters, such as glutamate, that activate excitatory neurons [314,6]. Diffuse patterns of metabolic change throughout the brain of live human patients have been detected following trauma using Positron Emission Tomography (PET) [22]. These abnormal activity patterns have been shown to initiate immediately and persist up to weeks following the initial insult. Furthermore, these changes were identified in patients diagnosed with mTBI based upon neurological assessment, in which neither focal pathology nor, in some cases, diffuse pathology was detected. Glutamate release combined with a loss of ionic homeostasis may manifest in mitochondrial dysfunction [112] and lead to general cellular dysfunction. A combination of acute neuroexcitation and potential vascular damage is believed to lead to a cellular energy crisis. Furthermore, progressive degeneration linked to this

energy crisis may lead to deafferentiation, or a loss of synaptic terminals [86], affecting regulation of neuronal activity patterns that are crucial to brain function. Recently, patients with mTBI were shown to exhibit decreased connectivity between brain regions, as measured by magnetoencephalography [322]. Therefore, a diverse range of pathophysiological events may occur following TBI. The diffuse patterns of pathology and functional impairment in patients lacking focal injuries supports the notion that diffuse damage may contribute significantly to the morbidity associated with TBI.

While multiple forms of diffuse pathology have been identified and the extent of associated pathophysiological change is still emerging, many questions remain regarding the development of diffuse tissue damage. In addition to questions surrounding the initiating events, a difficult problem remains in understanding the spatiotemporal distribution of diffuse pathology.

1.2.3   Regional Susceptibility to Diffuse Pathology

Identification of diffuse damage throughout the brain has revealed non-uniform distributions of injury suggesting that certain tissue and cellular structures may be more vulnerable than others. Blumbergs et al. compared the extent of DAI occurring in multiple brain regions by analyzing histological slices from patients diagnosed with either mild or severe TBI [34]. Following mTBI, no evidence of DAI was detected in the cerebellum, one half of the patients exhibited injury in the brainstem, and all patients exhibited injury in the cerebral hemispheres. Following severe TBI, patients exhibited evidence of DAI in all examined regions. White matter within the cerebral cortex and large axonal tracts within the cerebral hemispheres, such as the corpus callosum and fornices, were especially susceptible to injury. These vulnerabilities were supported by findings in patients in which MRI was used to detect a greater number of lesions located in the cerebral hemispheres compared to the brainstem, which also

correlated with injury severity [146]. A preferential decrease in diffusion anisotropy has been measured in structures such as the corpus callosum, internal capsule, and the centrum semiovale [137], confirming the susceptibility of large axonal bundles to damage. DAI lesions have also been shown to localize to the interface of cerebral white and gray matter [258]. Therefore, diffuse damage appears to differentially affect tissue regions and structures within the brain.

Although diffuse pathology appears primarily in certain brain regions and tissue structures, heterogeneity at the cellular level also exists within these damaged regions. For example, injured regions are typically distributed in a multi-focal pattern [259]. Furthermore, injured axons are typically dispersed amongst neighboring uninjured axons within these focal regions [34]. Heterogeneity in axonal vulnerability is also suggested by reports indicating differential injury responses in myelinated versus small caliber, non-myelinated axons [241]. Within myelinated axons, DAI has been shown to occur preferentially at the Nodes of Ranvier [240], which are the periodic regions of exposed axon between regions of myelination.

Additional heterogeneity in injury distribution is observed in relation to the microvasculature. Evidence of diffuse damage in the vasculature has been suggested by micro-hemorrhage of small vessels, which often occurs diffusely within the white matter similar to that of DAI [34]. Furthermore, tau-immunoreactive neurofibrillary and astrocytic tangles associated with CTE have been shown to exhibit perivascular localization [189] suggesting a role for the vasculature in the injury process.

Biomechanical studies provide some explanation for diffuse injury distributions [220,130], however, the growing diversity of diffuse pathology combined with the inability to explain cellular and sub-cellular injury patterns highlights the difficulties in understanding how this damage occurs. Purely mechanical explanations provide some insight into injury initiating

mechanisms. For example, Ommaya and Gennerelli posited that head rotation results in an injury distribution consistent with the degree of inertial forces generated by centripetal acceleration [219]. However, explaining the subsequent distribution of diffuse tissue, cellular, and sub-cellular damage due to head trauma is complicated by several orders of spatial magnitude that separate these anatomies. Therefore, to understand the diversity of injury that comprises diffuse damage, it may be necessary to consider the multi-scale mechanics that characterizes brain trauma.

1.3 Multiscale Biomechanics and Mechanisms of Diffuse Traumatic Brain Injury

1.3.1 Multiscale Structural Organization and Mechanical Properties of the Brain

Biomechanics of TBI are complicated by the brain's diversity in structure and range of material properties. Although the brain is a relatively soft tissue, it is encased by multiple layers of tissue and fluid that provide protection from mechanical forces. These protective layers include the skin (~1.0 MPa), the skull (~8.0 GPa), the dura matter (31.5 MPa), the pia matter (11.5 MPa), and the cerebral spinal fluid [318]. Together, these multiple layers provide a relatively rigid structure that protects the much softer underlying brain tissue from normal environmental factors, such as mechanical trauma. The underlying brain tissue is characterized by large brain regions such as the cerebral hemispheres, the cerebellum, and the brain stem (Fig. 1-2A), which are defined by anatomical features and functional properties [39,150]. Early studies on human brain tissue reported shear stiffness between 0.6 and 1.1 kPa [89], indicating that the brain is relatively soft and susceptible to deformation compared to other biological tissues. Subsequent studies highlighted the variation in mechanical properties due to age, region, and sample preparation [236], reporting values between 0.7-33 kPa [276]. Brain tissue also exhibits viscoelastic behavior, with loss modulus ranging between 2.8-81.4 kPa [256], indicating

the greater the rate of an applied load the greater the apparent stiffness. The variation in material properties of brain tissue is clearly indicated by elasticity maps of rodent brains showing regional variations in shear stiffness ranging between 2-25 kPa [182,286]. Therefore, the brain is considered a heterogeneous material.

Differences in material properties between brain regions are attributed to differences in cell population demographics, network architectures, and other micro-architectural attributes that facilitate functional uniqueness. The adult human brain consists of a diverse cellular population of approximately 100 billion neurons and at least as many non-neuronal cells [14]. Neuronal, glial, and vascular cells are the primary constituents of the brain parenchyma and together form intricate cellular and multicellular structures (Fig. 1-2B). Neurons are polarized cells that transmit electrical signals through small diameter processes (axons and dendrites) that extend away from their cell body (soma) to neighboring cells [39,150]. While the typical neuronal cell body is 10 - 50 μm in diameter, neuronal processes extend up to 500 μm (dendrites) or several centimeters to a meter (axons) away while remaining only 0.2-20 μm in diameter [150,4,239].

In addition to neuronal processes, other cellular constituents also exhibit polarized morphologies that form complex multi-cellular structures. For example, oligodendrocytes wrap multiple layers of cellular processes around axons at consistently spaced intervals to form myelination. It is this precise wrapping that forms periodic regions of exposed axon called Nodes of Ranvier that are important for electrical conduction. Astrocyte processes interact with axons and dendrites to form synapses that are critical for transmitting signals between neurons. The cerebral vasculature forms prominent structures within the brain with vessels existing in a large range of diameters:1-3 mm for large arteries and veins [88], 10-60 μm for small arterioles and venules, and 4-8 μm for capillaries [321]. While larger vessels near the surface of the brain
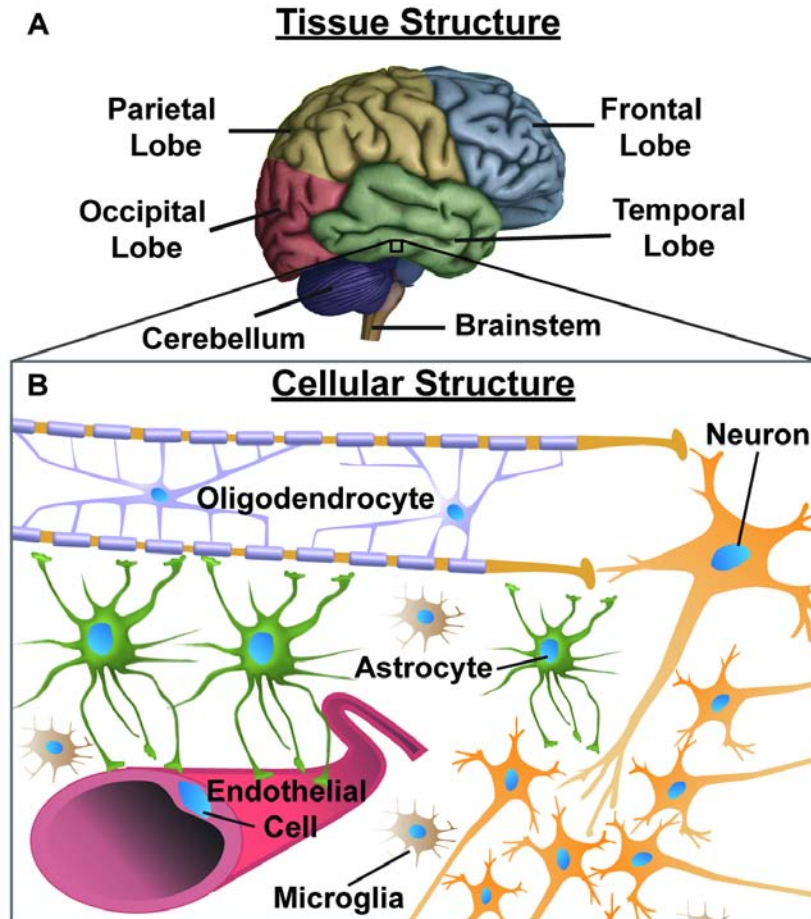
Figure 1-2: Structural Organization of the Brain.
Understanding the occurrence of diffuse pathology at the cellular level is complicated by the intricate cell and tissue structures that span ~4 orders of magnitude in spatial scale to form the human brain. (A) Large brain regions such as the cerebral hemispheres (comprised of four lobes), the cerebellum, and the brain stem are well defined by anatomical features and functional properties. (B) Within each tissue structure, there is an underlying multicellular composition comprised of neurons, neuroglia, and vascular cells. Many of these cells are highly polarized and together form intricate multi-cellular structures. Differences in material properties between brain regions are attributed to differences in cell population demographics, network architectures, and other micro-architectural attributes that facilitate functional uniqueness.

are sparse, smaller vessels within the parenchyma have been reported at high densities ranging from 25 per mm^2 in the corpus callosum to 150 per mm^2 in the hippocampus [51]. Together, these multicellular constituents form complex micro-structures throughout the brain.

In addition to structural complexity, neural cells exhibit differences in mechanical properties. Heterogeneity in mechanical properties is important because it indicates that

different regions or cell types may deform differently when experiencing the same load. For example, astrocytes may deform to a greater extent than neurons since elasticity measurements have shown neuronal somas to vary between 480 Pa and 970 Pa [23,74] and astrocyte somas to vary between 300 Pa and 520 Pa [177]. A difference may also exist between sub-cellular regions, as neuronal soma stiffness was reported to be ~ 500 Pa [25,177] while axons were reported to be ~12 kPa [23,74]. Evidence of delayed elasticity has been observed in some axons following rapid stretch, in which a return to their initial length occurs over timescales much larger than the initial stretch [275,260]. Therefore, traditional mechanical metrics such as elasticity may not fully capture the behavior of these biological structures.

Heterogeneity in mechanical properties is also important because of the potential for shear forces to occur at the interface between regions with different shear stiffness. These interfaces exist between prominent structures such as cerebral white and gray matter [258], which were measured in humans to have shear stiffnesses of 13.6 kPa and 5.22 kPa, respectively [160]. Additionally, the stiffness of human arteries was reported to be ~20 MPa and veins to be ~3MPa [200], 2-4 orders of magnitude larger than bulk brain tissue. Although the largest arteries and veins course superficially in the brain, smaller arterioles, venules, and capillaries permeate the brain parenchyma and account for ~2.5% of the total volume [214], providing for regional material heterogeneity.

The complexity of the cellular and multi-cellular structures within the brain can likely explain the heterogeneous mechanical properties observed within the tissue. The structural and mechanical properties at the cellular and sub-cellular level must therefore be considered in mechanical analyses to properly understand the brain's vulnerability to trauma.

1.3.2   Linking Biomechanics to Mechanisms of Diffuse Traumatic Brain Injury

Mathematical modeling and experimental techniques are providing insight as to how forces applied to the brain are transmitted to the cellular level. By including cellular anisotropy, multi-scale models have recapitulated the effect of cellular structures, such as the microvasculature and axonal bundle orientation, on localized cellular strain and have begun to incorporate these effects over the spatial scales of TBI [55,306,60].   These models have suggested that vessels can create microscale heterogeneities that increase localized stress or strain generation near the vessel, potentially explaining the susceptibility of these structures to injury [61]. For example, microscale inclusions were predicted to increase localized cellular strain levels by 60% compared to the gross tissue level. Furthermore, the same modeling effort suggested that vessels may force abrupt changes in axonal orientation that can affect localized strain distribution along the axon. Mathematical predictions of microscale variations in strain have been verified by high-speed optical measurements of tissue deformation that indicate inhomogeneity in strain fields in local regions containing both white and grey matter [166]. Therefore, gross tissue deformation may not completely describe the distribution of forces exerted on the underlying cellular structures or the variability in cellular injury within a region of the brain.

Although forces exerted on the brain initiate biological processes associated with diffuse pathology, the sequence of events between initial injury and subsequent pathology is poorly understood. Transient membrane tearing, termed mechanoporation has been suggested as a possible mechanism in axonal injury [152,106].   Mechanoporation is believed to occur in response to a rapid increase in axonal strain, which has been shown using *in vitro* stretch models of axonal injury. In these experiments, 30% uni-axial strain applied at a rate of $10s^{-1}$ resulted in brief tearing of the membrane that is observed through the cellular uptake of a membrane

impermeable marker [104]. It is proposed that transient membrane tearing causes a loss in cellular homeostasis that initiates a cascade of secondary events that ultimately result in DAI.

The presence of punctate swollen axons, the hallmark morphology associated with DAI, has been linked to a progressive series of cellular pathologies believed to result from mechanoporation. Previous studies have suggested that cytoskeletal abnormalities occur due to impaired axonal transport, causing an accumulation of vesicles and organelles leading to axonal swelling [2,59,108,233,234]. This disruption is thought to result from the action of cysteine proteases, such as calpains and caspases that degrade the cytoskeleton [47]. The involvement of protease activation in cytoskeleton disruption is supported by improved injury outcomes in rats that were administered protease inhibitors prior to or following experimental brain injury [45,245,231,246,161]. Pathological activation of proteases has been linked to an influx of ions, such as Ca^{2+} and Na^{+}, that occurs due to mechanoporation [152,103,153]. As such, one therapeutic candidate, Poloxamer 188, has shown the potential to treat DAI by promoting membrane resealing. Although Poloxamer 188 has exhibited neuroprotective effects following TBI in animal models, it has yet to be tested in humans [15,254]. Therefore, no therapeutic treatment options currently exist that effectively target a specific injury mechanism of DAI.

1.3.3 Current Limitations in the Understanding of Diffuse Traumatic Brain Injury Mechanisms

While membrane poration has been linked to much of the secondary injury cascade associated with DAI using experimental models, its role as the sole injury mechanism is not without controversy. Evidence of cytoskeleton breakdown, as indicated by calpain-mediated proteolysis [90,305], as well as impaired axonal transport [267], have been reported to occur without evidence of membrane poration, challenging the membrane poration hypothesis. Additional injury markers such as neurofilament compaction have also been shown to occur in

different cell populations than impaired axonal transport implicating the existence of multiple injury mechanisms [76]. Although not investigated as extensively as mechanoporation, additional injury mechanisms, including traumatic mechanical failure of microtubules [275] and impaired sodium channel function [138] can be linked to the secondary injury cascades associated with DAI.

Therefore, additional mechanisms likely exist by which neural cells respond to mechanical forces associated with TBI resulting in subsequent injury. While mechanical failure of biological structures such as the cell membrane or cytoskeleton is likely to occur when sufficient forces are applied, the potential for physical forces below mechanical failure thresholds to influence physiological processes provides additional mechanisms to explore.

1.4   Mechanobiology and the Cellular Microenvironment of the Brain

1.4.1   Mechanisms of Conversion of Mechanical Signals to Biochemical Signals

Cellular mechanotransduction, or the ability of cells to convert physical forces into biological signals, is a widely established phenomenon that has been linked to the regulation of diverse cellular physiological processes [131] including morphogenesis, growth, and survival [110,123]. Mechanotransduction pathways are influenced by interactions between intracellular structures, such as the cytoskeleton, and extracellular structures, such as the ECM or neighboring cells, through CAMs in the cell membrane. Mechanical coupling of the intracellular and extracellular space allows cells to 'sense' their local mechanical environment through physical interactions directed through these structures [144], and their mechanosensitive properties have been demonstrated in many cell types [122].

Several mechanisms exist by which exogenous forces are converted by sub-cellular mechanosensitive components into biochemical signals that influence cellular processes. Both

properties of the cellular microenvironment, such as ECM stiffness [176,313,77], and dynamic conditions, such as a change in cellular force distribution [185,187,316], can affect development, differentiation, disease, and regeneration by influencing gene expression and biochemical signaling pathways [165,132,298]. Redistribution of forces within a cell can be initiated by intracellular events, such as alterations in the cytoskeleton due to remodeling of microtubules [18], and also by extracellular events, such as an exogenous force directed through CAMs [292]. The conversion of force to biological signals is accomplished by changes in interactions and properties of proteins, often localized to intracellular structures such as the integrin associated focal adhesion complex, that regulate the activation of biochemical signaling pathways [168,185]. For example, changes in the relative force balance between the intracellular and extracellular space have been linked to acute cytoskeleton remodeling [282] through the activation of Rho signaling pathways [319]. The mechanochemical control mechanism is believed to occur through force induced enzymatic activation of protein kinases. Interestingly, a single mechanical perturbation has been shown to activate Src kinase in both endothelial and smooth muscle cells [209,253], suggesting that an acute insult may be sufficient to influence biological signaling pathways. Moreover, this activation can occur at locations distant to the stimulus site and over time scales that cannot be accomplished by diffusion or active transport, suggesting mechanical propagation through the cytoskeleton. Force transmission through the cytoskeleton has been previously postulated to explain how mechanotransduction may alter signaling pathways in the nucleus that affect gene expression [298]. While extensive literature has focused on mechanotransduction in multiple cell types, relatively few have focused on it within the developed brain. Nonetheless, the ubiquitous nature of these sub-cellular components

and signaling pathways suggest a potential for similar phenomena to occur within the developed brain.

1.4.2   Mechanobiology of the Developed Brain

Although the brain is typically viewed as a mechanically isolated organ, mechanical interactions at the cellular and sub-cellular level are critical components of normal biological function. Both the existence of endogenous forces as well as their influence on cellular function within the developed brain have been reported [281]. Specifically, mechanical interactions between sub-cellular structures such as the cell membrane, CSK, ECM, CAMs, and ion channels have been shown to influence diverse neural functions including ion channel activity [13], synaptic vesicle clustering [257], neurotransmitter release [57], and axonal growth cone dynamics [261]. Signaling pathways associated with mechanotransduction have also been linked to important neuronal functions. For example, integrin binding forms a mechanical linkage at the synapse, but subsequent activation of integrin mediated signaling pathways is a critical step in the formation and regulation of synapse morphology and maturation [24]. Moreover, RhoA activation has been shown to influence synaptic plasticity [311] potentially by affecting the structural stability of dendritic spines through cytoskeleton remodeling. Integrin mediated RhoA-Rho Associated Kinase (ROCK) signaling also affects the potential for remyelination in damaged white matter [215], indicating the broad influence of these pathways in neural function. Although a comprehensive understanding is far from complete, the potential for physical forces to influence cellular function in the developed brain via cellular mechanotransduction is clearly evident.

The cytoskeleton, CAMs, and ECM are important sub-cellular structures that contribute to the mechanical integrity of the cell. The cytoskeleton consists of multiple filamentous

polymers including actin, microtubules, and neurofilaments that form an interconnected network with extracellular structures, such as the ECM (cell-ECM) or neighboring cells (cell-cell), through CAMs located in the cell membrane (Fig. 1-3) [144]. Actin filaments are 5-9 nm in diameter and, with cross-linking proteins, form load bearing structures within the cell [94,163,48]. Microtubules are ~25 nm in diameter and form rigid structures with stiffness measurements of ~100 MPa that can bear compressive loads [94,36,156]. Intermediate filaments are ~10 nm in diameter and have shown the ability to resist tensile forces by stretching up to 3.5 fold [158,127]. Therefore, the cytoskeleton consists of biologically active filamentous structures that can provide mechanical integrity to the cell.

Cell adhesion molecules, consisting of members of the integrin, cadherin, immunoglobulin, selectin, and proteoglycan superfamilies, are integral membrane proteins that provide mechanical continuity across the cell [120,198,290]. CAMs exhibit binding specificity to both intracellular and extracellular components, some of which are indicated in Table 1. For example, tenascin binds integrins but not L1 IgCAMs [198,172], and CSPGs bind L1 IgCAMs but not integrins [183,290]. Furthermore, intracellular components, such as the focal adhesion complex, bind to integrins but not to cadherins [73,121]. This selective binding provides the ability to regulate mechanical coupling between the cell and its local microenvironment by influencing the organization of structural elements within the cell in response to both intracellular and extracellular cues.
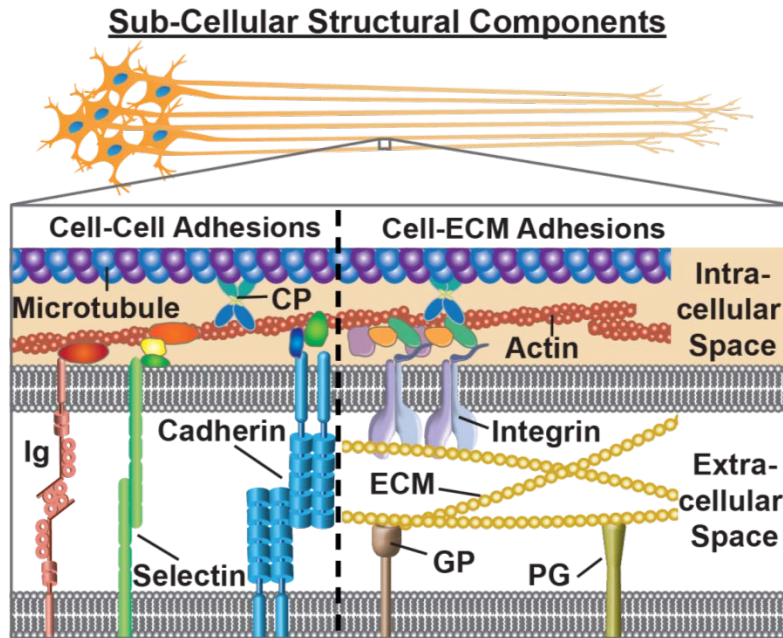
Figure 1-3: Protein networks maintain connectivity and structural integrity of neural networks.
Within all cell types, there are sub-cellular components that dictate cellular architecture by providing mechanical structure. Such structure is formed by interconnected networks of proteins in both the intracellular and extracellular space. Intracellular structures include cytoskeleton components such as actin, microtubules, neurofilaments, and crosslinking proteins (CP). Extracellular structures include extracellular matrix proteins as well as neighboring cells. These structures are connected through transmembrane receptors called cell adhesion molecules that include IgCAM (Ig), Selectin, Cadherin, Integrin, and other glycoproteins (GP) and proteoglycans (PG). The resulting networks bear loads and distribute forces throughout the cell and across the cell membrane to the extracellular space and neighboring cells.

Table 1: Cell Adhesion Molecules and Binding Partners Expressed in the CNS

Receptor Family	Sub-Types Expressed in the CNS	Intracellular Cytoskeleton Binding	Extracellular Binding	Associated Signaling Pathways	References
Integrin	α(1,5,6,v) β(1,3)	FAC → Actin α –actinin → Actin	ECM proteins (Laminin, Tenascin Reelin) CAM (Ig, Cadherin	Rho-family GTPases PTK, PTP	[73,175,133,148, 134]
Cadherin	N-Cadherin E-Cadherin	Catenin → Actin Desmoplakin → IF	Cadherin Integrin ECM (Reelin)	Rho-family GTPases PTK Wnt signaling Src-family kinase	[121{Nelson, 2004 #385,303,10,148, 212,155,21] [212,303,10,148, 155,21,118,119]
IgCAM	L1, NCAM	Ankyrin→spectrin → Actin Ezrin → Actin	IgCAM, Integrin, HSPG, CSPG	PTK, PTP, MAPK Src-family kinase	[119,68{Juliano, 2002 #84,148,223,155, 21]
Selectin		α –actinin → Actin	Selectin PSGL-1	MAPK, c-Src	[148]
Additional Glycoproteins and Proteoglycans	CD44 Neurexin Neuroligin	ERM → Actin Ankyrin → Actin	HA, laminin, Neuroligin, Neurexin	PTK (p195HER2, c-src) Rho-family GTPases	[285{Goodison, 1999 #456,280,115,21]

HA: Hyaluronan, CSPG: Chondroitin Sulfate Proteoglycan, HSPG: Heparin Sulfate Proteoglycan, FAC: Focal Adhesion Complex, IF: Intermediate Filament, PTK: Protein Tyrosine Kinase, PTP: Protein Tyrosine Phosphatase, MAPK: Mitogen Activated Protein Kinase

1.5 Conclusion

Given the critical importance of sub-cellular structures such as ECM and cell adhesion molecules in cell mechanics, we sought to determine their potential involvement in TBI. Specifically, we sought to determine if pathological cellular mechanotransduction may provide a mechanism by which axons are injured during diffuse TBI. To do so, we utilized multiple *in vitro* models of DAI allowing the greatest level of control over the cellular structures necessary to address the following specific aims:

1. Determine if focal adhesions transmit forces in such a way as to potentiate axonal injury as observed in Traumatic Brain Injury

2. Determine if localizing injury forces through different ECM affects axonal injury levels

2 Focal Adhesion Density Affects Levels of Strain Induced Axonal Injury

2.1 Introduction

Over the past decade, investigators have attempted to establish the pathophysiological mechanisms by which non-penetrating injuries induce diffuse damage in the brain. A primary motivator for the increased attention to non-penetrating injuries arose from the increased incidence of Blast-induced mild Traumatic Brain Injury (mTBI). Blast mTBI is the most frequent wound of the conflicts in Afghanistan and Iraq [29], with approximately 60% of total combat casualties associated with blast events generated by improvised explosive devices. Furthermore, recent studies suggest that nearly 16% of US combatants have been diagnosed with mTBI [129]. Although how blast energy is transmitted to the brain is not well understood, *in vivo* studies and clinical reports have shown that exposure to blast can cause mTBI [84,129,53]. Interestingly, the neuronal injury observed in these studies resembles DAI, a common pathology observed following mTBI *in vivo* [107]. DTI studies have identified structural alteration in white matter tracts in military personnel who previously suffered Blast-induced mTBI [263], and experimental mouse models have linked these structural alterations to DAI [179]. However, the mechanisms that initiate this pathophysiological response are unclear.

In vitro models of TBI may not fully recapitulate the complexity of the brain structure or mechanical trauma, but they provide unique insight into its cellular pathology by allowing the manipulation of specific biological components. Previous models of mTBI have proposed that a strain magnitude and rate dependent disruption in ion homeostasis initiates a sequence of secondary events ultimately leading to neuronal death. However, evidence of membrane poration is not observed in all injured neurons [153,90], and excitotoxicity due to loss of ion channel homeostasis [262] cannot account for observations of axonal retraction.

We hypothesized that cellular mechanotransduction events at the focal adhesion initiate secondary injury cascades that cause axonal injury. Focal adhesions are clusters of proteins containing transmembrane integrin receptors that couple the cytoskeleton in the intracellular space to the ECM network in the extracellular space, providing mechanical continuity across the membrane [296]. Mechanical forces propagating through these coupled networks can activate signal transduction pathways, alter ion channel currents, and initiate pathological cascades [140,194]. In the brain, roles for integrin signaling have been studied extensively in development and memory potentiation [54,152,198,247,270,300], however, there are no reports on the role of integrin signaling in mTBI.

To test our hypothesis, we built a high velocity tissue stretcher to deliver an abrupt mechanical perturbation to cultured neonatal rat cortical neurons exhibiting varying amounts of ECM adhesion coupling. These experiments demonstrated that neuronal injury is a function of focal adhesion size and density, with greater FA presence corresponding to increased injury susceptibility. Membrane poration was only observed at extreme strains in a subset of experiments, whereas at lower strains, neurite focal swelling was observed without membrane poration. The injury was not mitigated with the use of a calpain inhibitor, suggesting a calpain-independent injury mechanism. Treatment with a Rho-kinase inhibiter decreased neuronal injury, suggesting a role for mechanochemical signaling events in neuronal injury.

2.2   Results

2.2.1   High Speed Stretchers Induced Strain-Dependent Injury

The spatio-temporal profile of the mechanical perturbation, such as a blast wave, in the brain during mTBI is likely variable and, given the timescale of blast wave propagation, quite rapid.

In order to mimic this sudden mechanical stimulus, we designed and built a high speed stretcher (HSS) system to deliver an abrupt strain to a population of neurons cultured on a flexible silicon elastomer substrate coated with PLL (Fig. 2-1A), similar to previous *in vitro* stretch models [85]. We seeded primary neonatal rat cortical neurons on stretchable membranes five days before experiments to allow dendritic and axonal extension. During experiments, the substrates underwent an abrupt, uniaxial stretch (at 1% per ms) to generate a strain field of defined magnitude (Fig. 2-2). Neuronal injury was defined as the appearance of focal swellings along neurites, neurite retraction, or abrupt mechanical failure of the neurite (Fig. 2-1B), similar to injury morphologies reported in previous *in vitro* fluid shear models of injury [153] and similar to swellings seen in DAI *in vivo* [232]. We found that neuronal response to stretch was heterogeneous and dependent upon strain magnitude (Fig. 2-1C), similar to what has been reported *in vivo* [90]. Few neurons were lost, defined as abrupt failure of all attachment to the substrate, due to the stretch at strain magnitudes less than 10% and a small increase in loss was observed at 25% strain. At 10 minutes following stretch, a significant increase in focal swelling was observed for strain magnitudes greater than 5%. For all subsequent studies, we focused on strain magnitudes of 0-10%, as this range captured the threshold of inducing neuronal injury. Also, in this strain range only a small percentage of neurons exhibited signs of mechanoporation, as indicated by the uptake of membrane impermeable dye from the extracellular solution (Fig. 2-1D), or apoptosis, as indicated by TUNEL staining (Fig. 2-3). Thus, we identified a strain dependent injury response in our neuronal populations that is not explained by membrane poration.

23
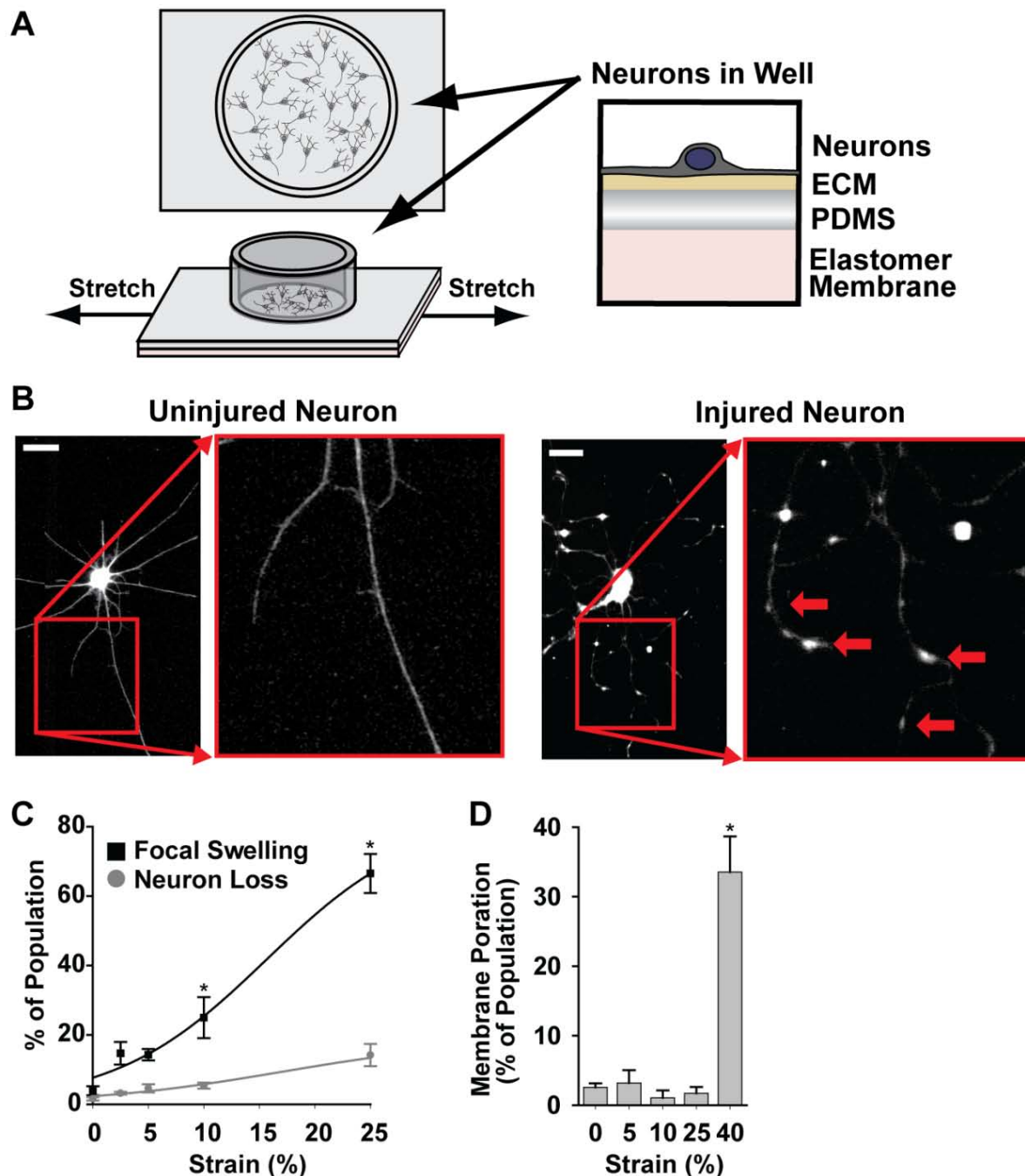
Figure 2-1: High speed stretch model of neuronal cultures indicates a strain dependent injury response identified by focal swelling of the neurites without porating the membrane.
(**A**) Neurons were cultured on elastomer membranes that were quickly stretched, transferring injurious forces to neurons. (**B**) Beta-3-Tubulin immunofluorescence imaging showed that prior to stretch, neurons exhibited highly branched, smooth neurite morphology. After stretch, many neurons developed widespread focal swellings along their neurites (red arrows) (Scale Bar = 20 µm). (**C**) Quantification of neuronal injury showed an initial significant response between 0% and 10% strains ($n \geq 4$). Neuron loss due to stretch also increased with strain magnitude. (**D**) Mechanoporation cannot account for the injury morphology as strain magnitudes less than or equal to 25% showed no significant uptake of a membrane impermeable dye following stretch ($n \geq 3$). All bars SEM for all panels, $* \, p < 0.05$.
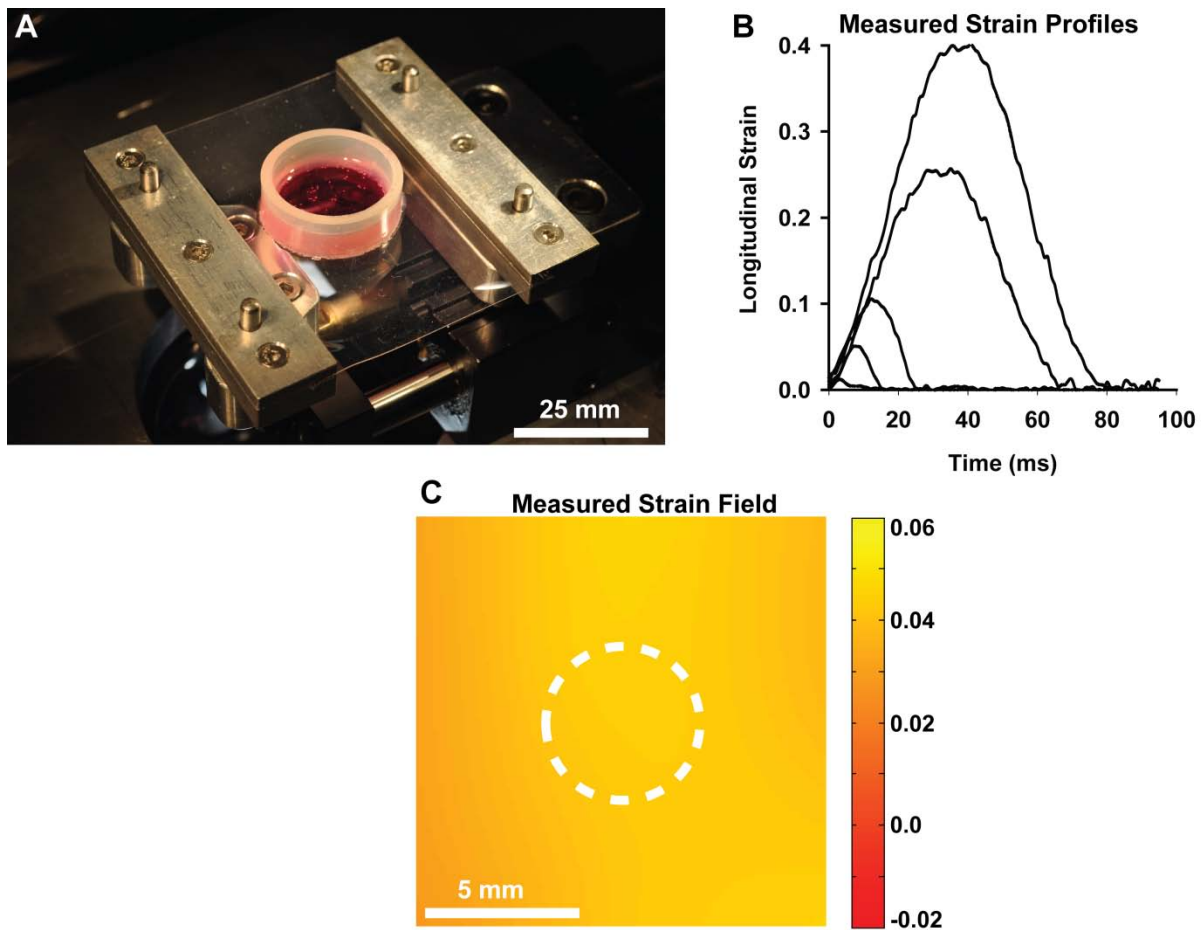
Figure 2-2: Characterizing Substrate Strain Levels.
(A) The high speed stretcher induces a rapid strain within the culture substrate. **(B)** Strain profiles indicating magnitude and rate are measured by **(C)** high speed imaging (80FPS) of the distortion of a grid printed onto the substrate surface and subsequently calculating 3-point strain values (max values indicated here for 40% strain field).
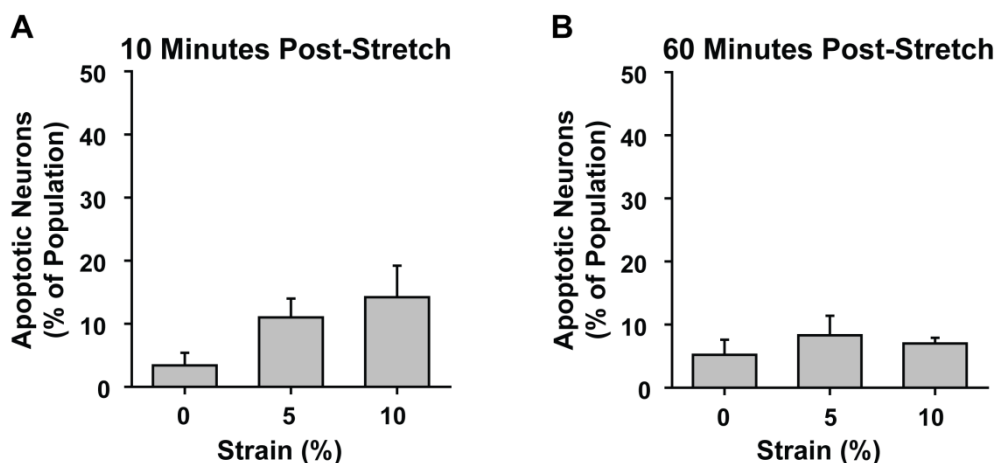
Figure 2-3: Stretch Induced Cell Death.
The extent of induced cell death following stretch was measured using TUNEL staining at both **(A)** 10 minutes and **(B)** 60 minutes post stretch. Significant increases in cell death were not observed at either time point. All bars SEM.

2.2.2   High Speed Stretcher Injury is Focal Adhesion Density-Dependent

The cytoskeleton of the neuron is anchored to the substrate through FAs [266] providing a link for force propagation in the cell (Fig. 2-4A). We reasoned that we could control FA density by culturing neurons on microcontact printed surfaces coated with PLL or saturated FN. On PLL surfaces, extracellular matrix (ECM) deposition from media serum provides specific attachment sites for neuronal FAs (Fig. 2-4B). We found that neurons cultured on FN-coated substrates formed FAs throughout ~25% more of their neurite area compared to PLL-coated substrates (Fig. 2-4C). FAs were also smaller and appeared less dense on PLL-coated substrates as compared to those in neurons on FN-coated substrates.

We asked how neuronal focal adhesion density affected the neuronal injury. We coated the culture wells of the stretchable substrates with either FN or PLL prior to seeding them with neurons to regulate the density and number of FAs. After five days in culture, we subjected the neuronal networks to an abrupt strain with the HSS system. We observed an increase in the

26
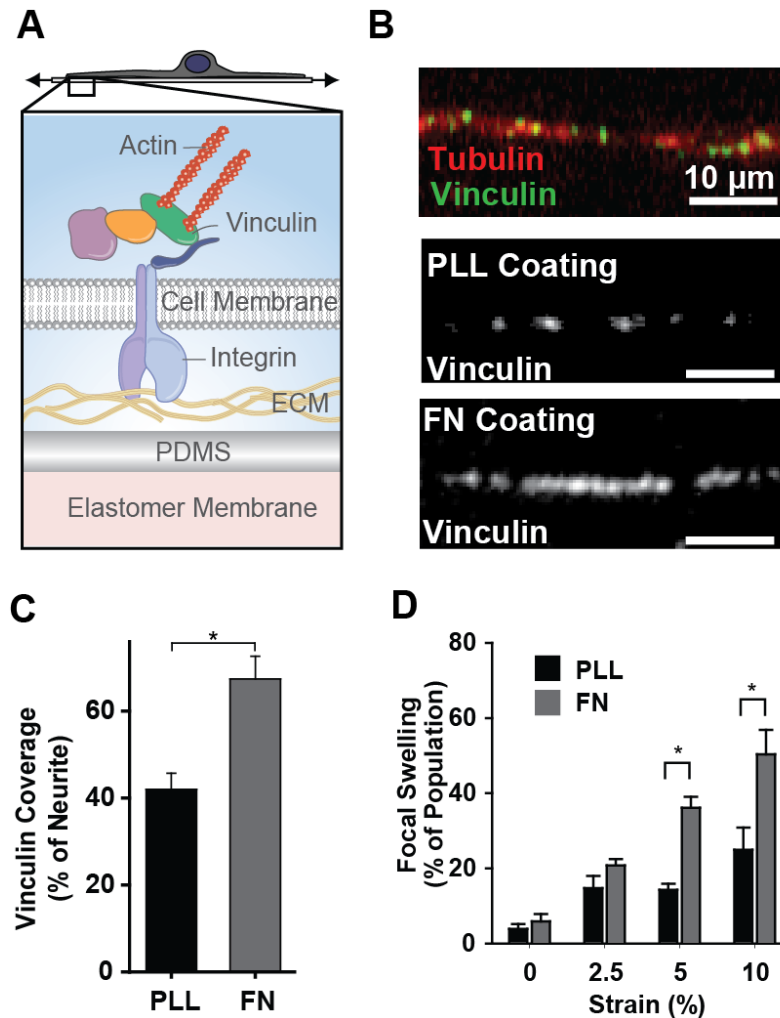
Figure 2-4: Substrate coating influences neuronal FA formation and injury progression.
(A) Neurons are mechanically coupled to the substrate via FAs that couple the intracellular cytoskeleton to the ECM. (B) Immunofluorescence imaging of vinculin puncta indicated the presence of FAs. Scale bars correspond to 8 and 10 µm, for PLL and FN respectively. Quantification of (C) total vinculin puncta area ($n = 8$) indicated that a fibronectin coated substrate induced FA formation over a larger area and with greater average cluster size compared to a PLL coated substrate ($n = 5$). (D) The percentage of neurons that exhibited widespread focal swelling following stretch injury was greater on a FN coated substrate compared to a PLL coated substrate at 10 minutes ($n \geq 4$ for PLL and $n \geq 8$ for FN). All bars SEM for all panels, * $p < 0.05$.

proportion of neurons exhibiting focal swellings on FN-coated substrates when compared to neurons cultured on PLL at both 5% and 10% strains (Fig. 2-4D). Since PLL-coated substrates induce the formation of smaller and less dense FAs when compared to neurons cultured on FN, the difference in injury rates as a function of FA size and density suggests a role for an integrin-mediated injury mechanism. In this case, abrupt stretch of the cell substrate uniformly injures the more robust focal adhesion architectures of the FN-seeded neurons because they are more rigidly adhered at networked points throughout the neuron's soma and neurites.

2.2.3 Injury is ROCK-Dependent

Mechanochemical coupling may activate secondary signaling cascades which cause neuronal injury. Previous reports suggest that cysteine proteases, such as calpains, actively degrade the cytoskeleton and that their inhibition can reduce neuronal injury [90,46]. Others, however, have suggested the involvement of additional or multiple pathways leading to different forms of neuronal injury [268,186]. We asked if a calpain inhibitor would reduce the instance of focal swelling in our model. Using the HSS system with neuronal cultures seeded on PLL substrates, we observed that the application of MDL-28170 to inhibit calpain activation either before (Fig. 2-5), or immediately following, abrupt stretch yielded no significant change in neurite focal swelling, suggesting that calpain activation cannot explain neuronal injury in our model (Fig. 2-6A). Previous work has shown that integrin mediated RhoA activation may cause cytoskeleton reorganization, stiffening, and contraction in other cell types [188,199]. Since increased RhoA activity has been noted in previous *in vivo* TBI models [82], and more recently inhibition of ROCK, a downstream effector of RhoA, has been shown to be an important therapeutic target in various neurodegenerative disease [206], we asked whether integrin-activated Rho-ROCK signaling may contribute to neuronal injury in our model. Immediate

28
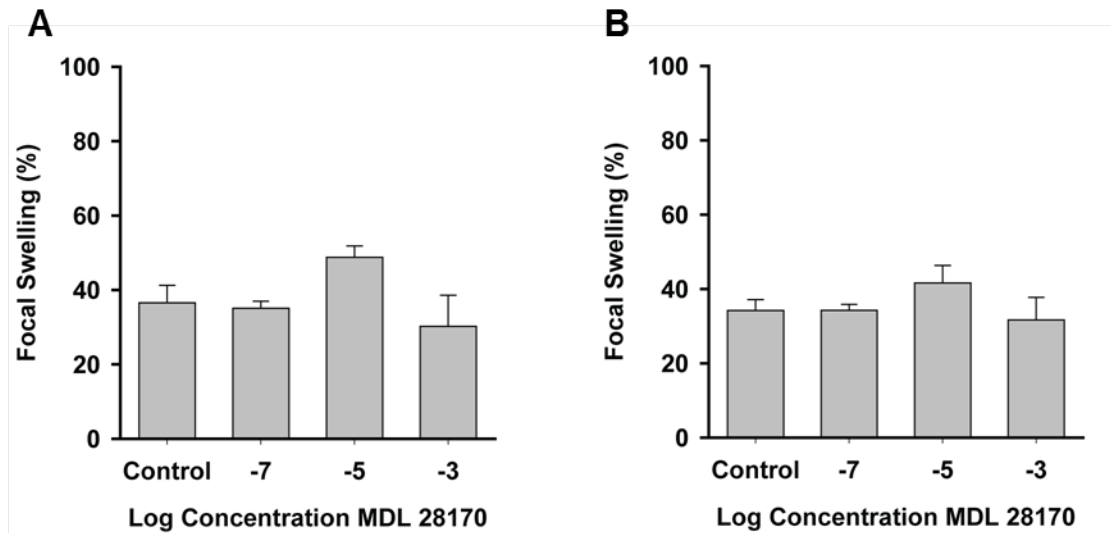
Figure 2-5: Effect of Calpain Inhibition on Injury Levels
Neither **(A)** pre-administration 30 minutes prior to nor **(B)** post-administration immediately following stretch of Calpain inhibitor elicited neuroprotective effects against stretch induced focal swelling. All bars SEM for all panels

application of HA-1077, a ROCK inhibitor, following stretch with the HSS system resulted in a dose-dependent decrease in the percentage of neurons exhibiting focal swellings (Fig 2-6B). This apparent neuroprotective effect of HA-1077 was observed at both 5% and 10% strain magnitudes (Fig 2-6C). These studies suggest that a FA mediated signaling cascade may be converging on a ROCK-mediated pathway, identifying a series of potential targets for future *in vivo* therapeutic intervention studies following TBI.
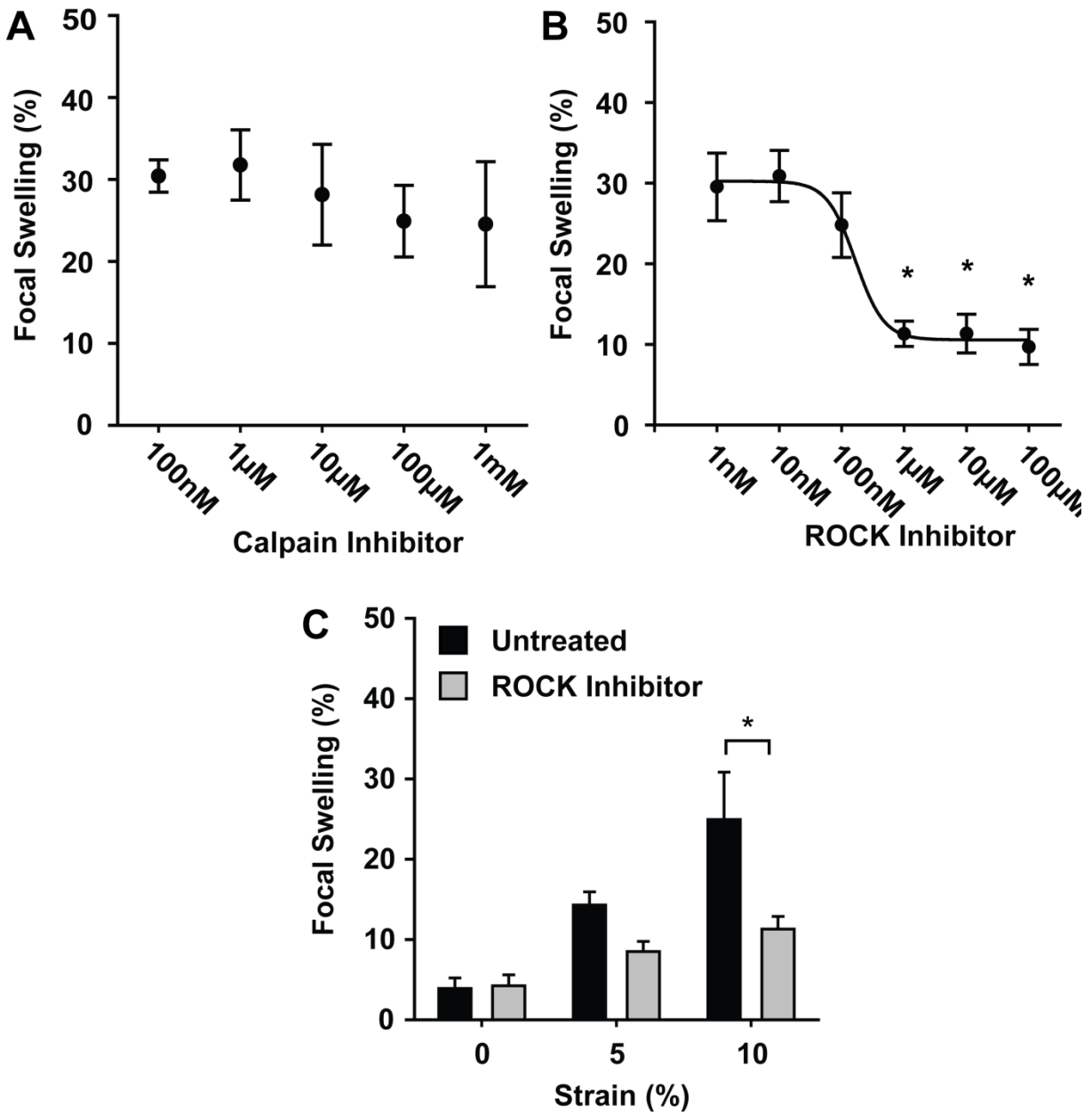
Figure 2-6:Pharmacological inhibition of secondary injury pathways may reduce neuronal injury.
(**A**) Immediate administration of a Calpain inhibitor MDL 28170 following 10% stretch of neurons seeded on PLL substrates was unable to reduce the percentage of injured neurons 10 minutes later ($n \geq$ 4). (**B**) However, immediate application of a ROCK inhibitor, HA-1077, was able to reduce neuronal injury in a dose dependent manner ($n \geq 5$). (**C**) Decreases in injury were observed at both 5% and 10% strain magnitude ($n \geq 5$). All bars SEM for all panels, * $p < 0.05$.

2.3 Discussion

Here we have shown that given the same mechanical stimulus, neurons exhibiting increased FA density are more likely to experience axonal injury. Previous studies have attributed this injury to a loss of ionic homeostasis caused by either a disruption of the cell membrane [104,153,90] or changes in ion channel function [262,305]. However, we have shown that injury can be induced by applying small strains, less than what can disrupt the cell membrane, at high rates directly through mechanically sensitive FAs. A recent *in vitro* study directly linked focal swelling to the pathological influx of calcium and activation of calpains which degrade the cytoskeleton [153]. Other studies have shown that not all neuronal injury is dependent on membrane disruption and calpain activity [90,268], but offer little evidence for an alternative mechanism to account for the calpain-independent injury. Our *in-vitro* study indicates that integrin mediated Rho-ROCK activation may account for calpain independent pathways of injury.

Concurrent with this study, our group showed that axons may be more vulnerable to injury than the soma because the failure strength of FAs in neurites is significantly lower than in the soma. Furthermore, force transmission via integrin binding ECM proteins always produced widespread focal swelling, whereas non-specific force transmission through the membrane produced only local injury [126]. A previous study has demonstrated a similar sensitivity of neuronal injury to ECM composition in the 3D cell microenvironment [43]. Neurons embedded in a 3-D gel composed of collagen conjugated to agarose exhibited increased cell death following an acute, high rate deformation when the collagen concentration was increased, indicating that the degree of cell-ECM contacts may influence neuronal injury [69]. Cell-matrix interactions have also been shown to be involved in pathological processes following acute mechanical stimulation in other cell types such as vascular smooth muscle cells [302] and epithelial cells

31

[283,32]. These reports, coupled with the data reported herein, suggest ECM-cell adhesions may be important conduits for mechanical cell trauma.

Previous reports suggest a role for calpains in neuronal injury [153,90,268]. In our low strain model, we were unable to mitigate neuronal injury with a calpain inhibitor. However, we were successful in reducing neurite injury with the use of a ROCK inhibitor. Integrin stimulation can activate many signaling cascades, but activation of the Rho-ROCK pathway is of particular interest because of its known effects on the cell cytoskeleton. ROCK activation can affect cytoskeleton remodeling by activating downstream targets that regulate cytoskeleton tension [154], actin polymerization [217], neurofilament depolymerization [125], and microtubule stability [9]. Interestingly, studies have shown that axon focal swelling may be a result of the breakdown of microtubules and impairment of the axonal transport system [151]. Furthermore, axon retraction following mTBI can be linked to active remodeling of the neuronal cytoskeleton [178]. The activation of RhoA in *in vitro* studies has demonstrated neurite retraction in neuroblastoma cell lines [143] and dendritic retraction in brain slices [33]. A genetic study in *Drosophila* indicates that in mature neurons, the RhoA-mediated axon retraction pathway is actively repressed by negative regulators [31]. The synaptic degeneration associated with DAI implies that the activation of RhoA is a maladaptive response. Blocking activation with a Rho antagonist can reduce injury related apoptosis in the CNS [83], suggesting that blocking Rho activation may be effective in treating TBI. Furthermore, recent studies on axon growth cone retraction have demonstrated a link between ECM protein type, integrin activation, cyclic AMP levels, and Rho activity [169]. With the growing concern about the lack of therapeutic options for treating mTBI [145], our results suggest that further exploration of cellular

32

mechanotransduction mechanisms associated with ECM-cell adhesions may identify novel therapeutic opportunities.

This chapter has focused on introducing the concept that axonal injury may be affected not only by the magnitude or rate of applied insult, but also by mechanochemical coupling at the focal adhesion. We utilized a standard *in vitro* TBI model with a subtle, but important modification to substrate surface chemistry to indicate that mechanosensitive properties of the neuron must also be considered in addition to the mechanics to fully understand the neurons response to trauma forces. This is equivalent to saying that the neuron is not a passive material, but has an active response to applied force. Future chapters of this dissertation will aim to elucidate additional factors that influence this active response.

2.4   Materials and Methods

2.4.1   Ethics Statement

All procedures were approved by the Harvard Animal Care and Use Committee under Animal Experimentation Protocol permit number 24-01. This protocol, entitled "Harvest and Culture of Neural and Cardiac Tissue from Neonatal Rats and Mice for In Vitro Disease Models," meets the guidelines for the use of vertebrate animals in research and teaching of the Faculty of Arts and Sciences of Harvard University. It also follows recommendations included in the NIH Guide for the care and use of laboratory animals and is in accordance with existing Federal (9 CFR Parts 1,2&3), state and city laws and regulations governing the use of animals in research and teaching.

2.4.2   Neuron Harvest and Culture

Cortical neurons were isolated from 2-day old neonatal Sprague-Dawley rats (Charles River Laboratories, Boston, MA). Reagents were obtained from Sigma-Aldrich (St. Louis, MO)

unless otherwise indicated. Cortices were surgically isolated and minced in Hanks' balanced salt solution (Invitrogen, Carlsbad, CA) followed by digestion with trypsin (USB, Santa Clara, CA) overnight at 4°C. The cell suspension was then filtered through a nylon filter of 40μm pore size (BD Bioscience) and finally separated using a Percoll gradient (GE Healthcare Life Sciences, Piscataway, NJ). Subsequently, cells were re-suspended in DMEM culture medium (Invitrogen) supplemented with 10% (v/v) heat-inactivated fetal bovine serum (Invitrogen), 30 mM Glucose, 2mM L-glutamine, 25 mM KCl, 50 mU Insulin, 7μM *p*-Aminobenzoic acid, 100 U/mL penicillin, and 100μg/mL streptomycin. Cells were seeded at a density of 30,000 cells per cm^2 and supplemented with 10 μM cytosine arabinoside for the first 48 hours of culture on substrates coated with either 100μg/ml PLL or 50 μg/ml FN. Samples were incubated under standard conditions at 37°C and 5% CO_2. After 48 hours cells were washed 3 times with PBS to remove non-adherent cells. Media was replaced every 48 hours until experiments were executed. All experiments were performed on either day 4 or 5 post seeding.

2.4.3   High Speed Stretcher *in vitro* TBI Model

Medical grade silicone elastomer membranes   (SMI .010" NRV) were spin-coated with Sylgard 527 (Dow Corning, Midland, MI) polydimethylsiloxane (PDMS) that was mixed at a 1:1 base to curing agent ratio and allowed to cure for at least 4 hours at 70°C. The elastomer membranes were then clamped into custom made brackets to maintain tension, and a reducing well to hold cell media was adhered using additional PDMS which was allowed to cure again for at least 4 hours at 70°C. Samples were then oxidized using UV ozone (Model No. 342, Jetlight, Irvine, CA) for 8 minutes to sterilize the surface and increase hydrophilicity for protein adsorption. Either isotropic Poly-l-Lysine (PLL) or Fibronectin (FN) (BD Biosciences, San Jose, CA) was then deposited on the PDMS at a concentration of 100 μg/ml or 50 μg/ml, respectively,

in sterile deionized water for at least 20 minutes. Excess PLL or FN was removed by washing with deionized water. Neurons were seeded and cultured inside the reducing well as indicated previously. Each sample was loaded into a custom made High Speed Stretching (HSS) device which used a high precision linear motor (LinMot Model P01-23x80F-HP, Elkhorn, WI) to displace the brackets and strain the elastomer sheet to a desired magnitude at a rate of 1% per ms (Movie S1). Membrane strain was verified by recording the deformation of a 1x1 cm grid using a high speed camera (FasTec Troubleshooter Model #: TS1000ME) and calculating the strain using a three-point strain algorithm [8].

2.4.4 Immunofluorescent Staining and Microscopy

Cells were washed 3 times in PBS at 37°C and fixed for 10 minutes in 4% paraformaldehyde and 2.5% TritonX-100 in PBS at 37°C. Cells were then washed 3 times in PBS and an initial blocking step using 5% Bovine Serum Albumin (Jackson ImmunoResearch, West Grove, PA) in PBS was performed for 1 hour at 37°C. The blocking solution was aspirated away and the primary antibody solution was immediately added and incubated for 1.5 hours at room temperature. The primary antibodies used were either anti-β-Tubulin III (1:200), monoclonal anti-Vinculin (1:200), or anti-glial fibrillary acidic protein (1:200). Primary antibodies were added to a 0.5% BSA in PBS solution. Following primary staining, cells were washed 3 times, and the secondary staining solution consisting of either goat anti-mouse conjugated to Alexa-Fluor 488 or goat anti-rabbit conjugated to Alexa-Fluor 546 and 4',6-diamidino-2-phenylindole (DAPI) was added to the cells for 30 minutes at room temperature. Samples were then washed 3 times. For samples seeded on silicon sheets, a scalpel was used to cut out an 18mm circular section of the substrate which was placed on a glass slide. For glass bottom samples, the glass was removed from the dish and placed on a glass slide. ProLong Gold

Antifade reagent (Invitrogen) was added to preserve the samples and glass coverslips are affixed using nail polish (company info). Prepared slides were either imaged immediately or stored at -20°C. Imaging was performed on a LSM 5 LIVE confocal microscope (Carl Zeiss, Oberkochen, Germany) with appropriate filter cubes.

2.4.5 TUNEL Assay

Click-iT TUNEL assays (Invitrogen) were performed following the manufacturer's protocol [211]. Briefly, cells were fixed in 4% paraformaldehyde and fragmented strands of DNA were labeled with a fluorescent indicator. Fluorescence imaging was performed on experimental and control populations, and neurons exhibiting fluorescence levels above a threshold set by control samples were considered to be apoptotic.

2.4.6 HSS Membrane Poration Studies

Immediately prior to HSS experiment, membrane impermeable fluorescein dye (Invitrogen) was added to the cell media at a 10μM concentration. Following completion of the experiment, samples were fixed as described previously but TritonX-100 was excluded. Cell nuclei were labeled with DAPI as described earlier. Uptake of the dye was determined by fluorescence microscopy. Cells exhibiting uptake of the dye above a set fluorescence intensity threshold of three standard deviations greater than the control mean were considered to be porated.

2.4.7 **Vinculin Puncta Quantification**

Using a watershed algorithm to separate neighboring structures according to the intensity 'valley' between them, individual FAs could be identified and their respective area quantified. In order to segment very large and granular adhesion sites, as observed on FN- and PLL-coated

substrates respectively, we used a different set of threshold values for watershed segmentation [149,317].

2.4.8 **Pharmacological Interventions**

Calpain inhibitor MDL 28170 (Sigma) was prepared per manufacturer's recommendations. Briefly, MDL 28170 was reconstituted in anhydrous DMSO and neurons were treated with concentrations ranging between 100nM and 1mM in Tyrode's solution. The effects of the calpain inhibitor were determined for both 30 minute pre-incubations and immediate post stretch applications. Rho-associated Kinase (ROCK) inhibitor HA-1077 (Sigma) was prepared by dissolving in water and neurons were treated with concentration ranging between 1nM and 100 μM in Tyrode's solution. The effects of calpain inhibitor were determined for immediate post stretch applications.

2.4.9 **Statistical Analysis**

Statistical significance was measured by ANOVA and subsequent pairwise comparison when comparing multiple values. $p < 0.05$ for all statistically significant differences.

3 Developing a Tool Set for Localizing Injury Forces through Specific Subcellular Structures

3.1 Introduction

Following the implication of mechanochemical coupling in axonal injury, we sought to pursue the importance of trauma forces directed through specific brain extracellular matrix (ECM) components in axonal injury. However, to address the primary limitations of our previous work as well as to facilitate future *in vitro* axonal injury studies focusing on cellular mechanotransduction mechanisms, we identified 3 technological limitations that were necessary to address prior to moving forward.

While the previous study was performed using an established *in vitro* model of Traumatic Brain Injury (TBI), we identified no suitable existing model that would allow the isolation of forces through specific ECM components while providing sufficient control over additional cell-ECM influences. Previous reports have summarized the existing models of TBI as well as their features [201]. To address this shortcoming, we identified an established technique called Magnetic Twisting Cytometry (MTC) [295,292,87,194,5,196,210] that could be adapted as an *in vitro* model of TBI and that could provide the necessary level of control for directing injury forces through specific brain ECM components.

Although traumatic damage to all neural cell processes is likely, Diffuse Axonal Injury (DAI) is focused specifically on neuronal axons. In order to isolate our study to axons, we developed improved seeding and cell culture methods that provided axon rich regions in which injury analysis could be isolated. This was accomplished through the combination of mask seeding and microcontact printing [304] into a technique termed stamp mask culturing.

Finally, since the primary form of pathology associated with DAI is a morphological change within the axon, specifically axonal focal swelling, and visual confirmation of injury is

an acceptable form of analysis. However, in order to minimize the influence of user bias, maximize the efficiency and consistency of analysis, and to provide increased complexity of analysis we sought to develop an automated method to quantitatively identify and measure axonal injury. To do so, we developed a protocol combining semi-automated imaging of live neuronal cultures with post image analysis in both ImageJ and Matlab to identify and quantitatively measure the extent of axonal injury *in vitro*.

3.2 Development of an *in vitro* TBI Model for Delivering Localized Injury Forces through Specific Subcellular Structures

3.2.1 Design Criteria for the Development of an *in vitro* TBI Model Capable of Localizing Forces at the Subcellular Level

In order to address the experimental task of investigating brain ECM-cell interaction mechanisms in axonal injury, we built an *in vitro* device that allows the localization of well defined mechanical stimuli through specific ECM proteins to their receptors on the cell surface. The development of a new device was required because there are currently no *in vitro* assays that allow enough precision to isolate injury forces to multiple cellular sites across multiple cells while minimizing global cell strain that results in non-specific force application. MTC is a technique that is similar to the magnetic tweezer based technology that has previously been used in our lab to study axonal injury, but it has previously been used only to study the mechanical and mechanosensitive properties of cells [293]. We chose MTC because it provided a means to direct localized forces to multiple axons simultaneously through specific ECM-coated microbeads and is known to be compatible with live cell imaging.

3.2.2 Building the MTC *in vitro* Model of TBI

MTC delivers localized forces to cells by manipulating small ferromagnetic beads (~5µm diameter) bound to cell surface receptors. Microbeads are rapidly rotated by applying an initial

magnetizing magnetic pulse (~.1T or 1000 G) followed by an orthogonal twisting magnetic pulse (~.01T or 100G). To use this technique as a means to direct injury inducing forces to our cell populations, we designed and built the necessary device components in house. Four primary components were designed (Fig 3-1A). Charging circuitry converts a standard 110 volt power input to as much as 1 kV for charging the capacitor bank. The capacitor bank consists of multiple 10 uF and 900 uF units and stores charged energy to be rapidly discharged through the coils. Due to the electric circuit design (Figure 3-2), the output current can be modeled as a simple RLC circuit whose waveform morphology is dictated by the circuit resistance, inductance, capacitance, and charge voltage. A pulse shaping network is used to modify the characteristic resistor-inductor-capacitor (RLC) circuit transient into a waveform with appropriate duration and morphology for magnetizing and twisting the beads. Field generating coils convert the discharged electric current into a transient magnetic field. The first three components are combined into a single, mobile power supply cart which allows the user to select appropriate charging voltage as well as discharge waveform duration (Fig. 3-1B). Both coils were initially designed using computer aided drafting (CAD) software (Fig 3-1C,E) prior to actual fabrication (Fig 3-1D,F). The twisting coil includes several important design aspects that facilitate long term live cell imaging of a cell sample following bead twisting. These design features include the incorporation of the coils into a standard microscope stage insert and a closed environmental chamber with cover glass lid to minimize contamination and evaporation during long term microscopic imaging. Each coil was designed in a helmholtz configuration to maximize field uniformity.   Simulations were used to direct the design of the coils, and

40
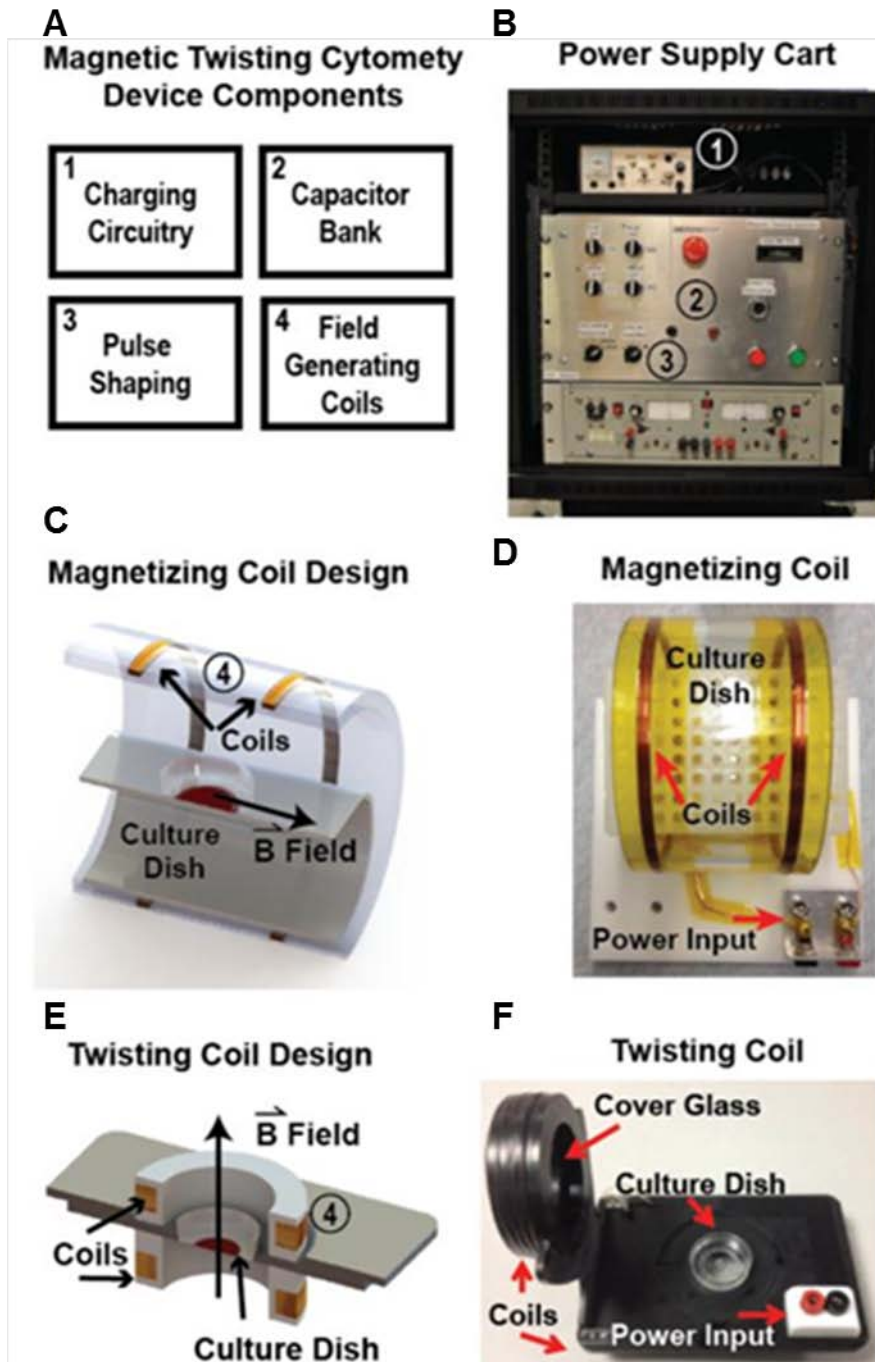
Figure 3-1: Magnetic Twisting Cytometry Device as an in vitro model to study TBI.
(A) Four primary MTC device components were designed and constructed in house. (B) The high voltage charging circuitry, capacitor banks, and pulse shaping network are housed in a single cart both safety and convenience. (C,E) Both the magnetizing and twisting coils were designed using CAD software and supported by simulations of magnetic field generation. (D,F) The coils were fabricated in house and adapted to facilitate long term live cell imaging by incorporating the twisting coil into a standard microscope stage and including a closed cell chamber to minimize contamination and evaporation of bath solution.

following coil construction, we verified the design parameters by directly measuring the

magnetic fields generated by each coil using a small magnetometer probe. The magnetic field
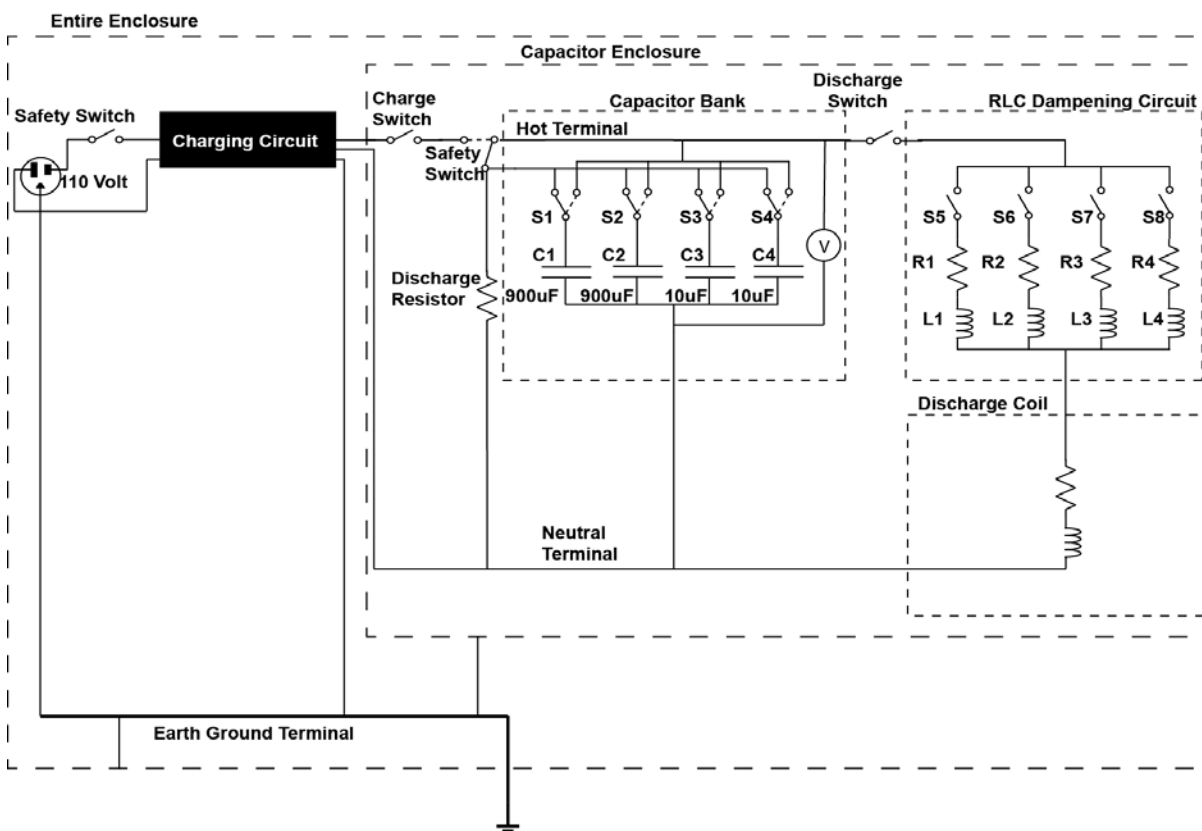
Figure 3-2: Schematic Diagram of MTC Power Supply.
The magnetic twisting cytometry device is driven by a high voltage power supply designed based on a simple resistor-inductor-capacitor (RLC) circuit. A standard 110 volt wall outlet is converted to high voltage through a proprietary circuit. The high voltage outlet then charges a capacitor bank of 900 µF and 10 µF capacitors up to 1 kV. The capacitors are subsequently discharged through a circuit consisting of the coil and a series resistance that is modified to produce transient currents of specified magnitude and duration. Multiple safeguards are built into the power charging circuitry to protect users from potentially dangerous current discharges.

magnitude and orientations were measured in the center of each coil pair, corresponding to the

location in which the culture dish sits, while the current driven through the coil was increased

(Fig. 3-3 A-B). As exected, we observed a linear increase in field magnitude along the axis of

the coil (inset indicates each direction relative to the coil cross section). Measurement of the

slope of this line allowed us to convert current through the coils to magnetic field magnitude for

42
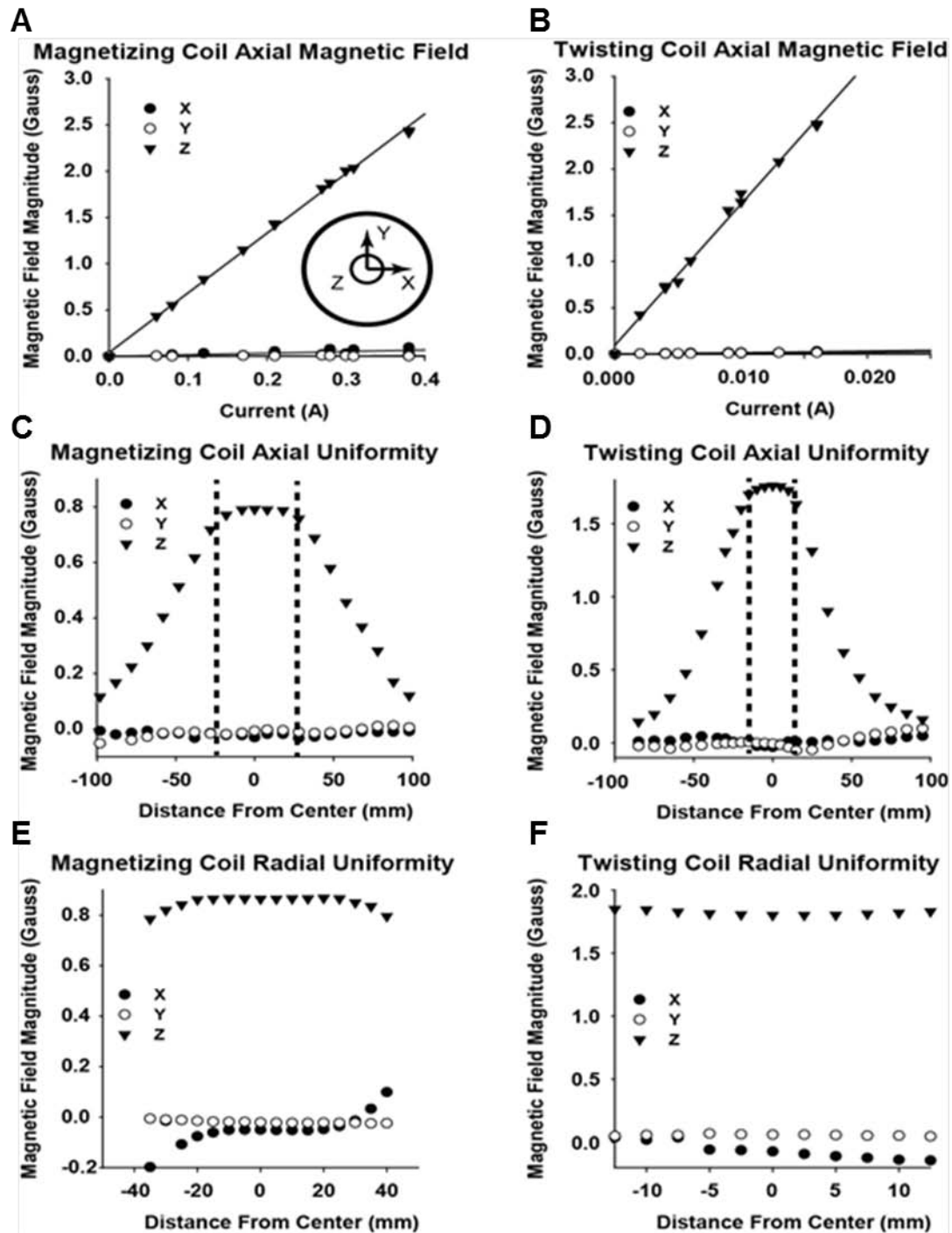
Figure 3-3: Two pairs of electromagnetic coils each in a Helmholtz configuration are used to generate the magnetic fields required for the MTC injury model.
(A) A magnetizing coil is used to initially magnetize small ferromagnetic beads and a (B) twisting coil is used to provide a subsequent orthogonal field causing the beads to rotate and generating a stress at the site of adhesion to the cell. (C-H) The magnetic field strengths and distributions were measured with a magnetometer to verify the experimental design parameters.

both the magnetizing coil (.7 Gauss/Amp) and the twisting coil (160 Gauss/Amp). This also verified that the axial field was much greater in magnitude than either orthogonal field magnitude components. The uniformity of the generated magnetic field was also measured by moving the magnetometer probe in both the axial and radial directions (Fig. 3-3C-F) while keeping the current through the coils constant. As expected, we observed uniform fields within the constraints of the coil (indicated by the dashed lines). Uniformity in field magnitude is important in order to ensure consistent bead torque at all locations within a coverslip.

Twisting of the microbeads is accomplished by applying a transient magnetic field in an orthogonal direction to the microbead magnetic moment resulting in a torque: $\tau = M \times B$ (Fig. 3-4A). The ferromagnetic beads are exposed to a brief, large magnetic field (Fig. 3-4B) generate and align the magnetic moments followed by a brief twiting coil (Fig. 3-4C) that produces the torque. The degree of magnetization is indicated by the magnetic moment, which can be calculated by measuring the decay of the remnant magnetic field as the beads rotate to align with a known twisting field in a medium of known viscocity. We placed a high concentration of ferromagnetic beads in glycerol (Fig. 3-4D), magnetized the beads in one direction, and subsequently applied a low magnitude twisting field in an orthogonal direction. We used a magnetometer to measure the remnant magnetic field strength in the original magnetized direction and observed an exponential decay in field magnitude (Fig. 3-4E). An exponential fit provided the decay constant which, combined with solution viscosity, bead dimensions, and physical constants, was used to calculate the effective stress delivered by each bead [294]. From these results, we calculated a bead calibration factor of 0.314 Pa/Gauss which indicates the effective stress delivered by each bead for a given field strength. This data, in combination with the coil properties previously measured in Figure 3-3, allow the calculation of the bead stress

44
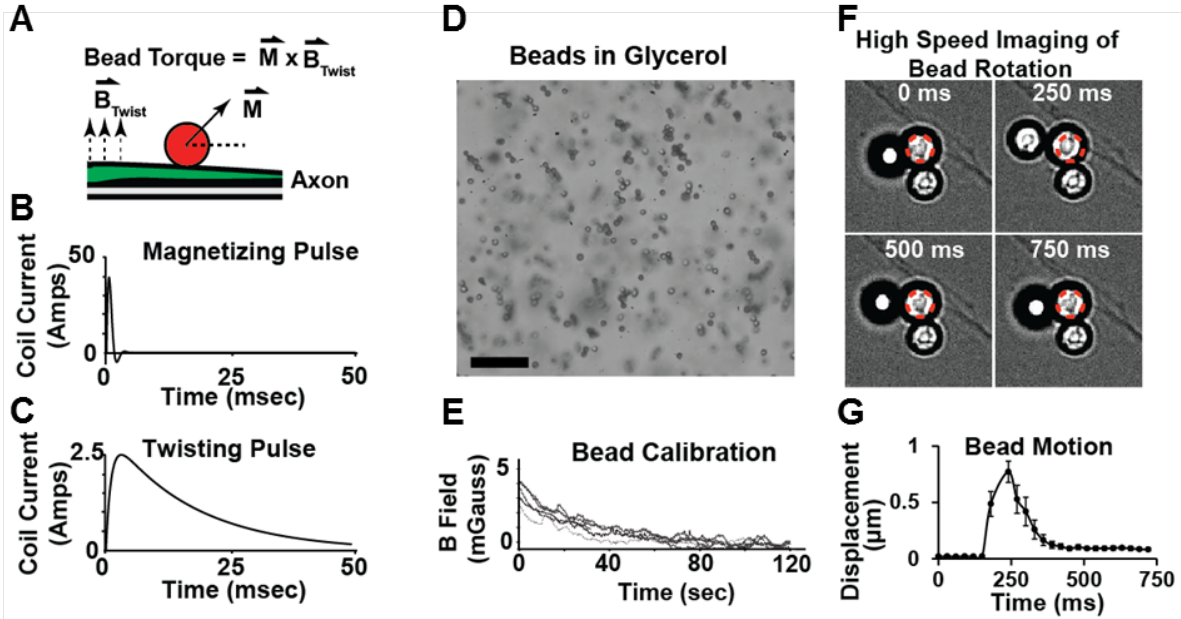
Figure 3-4: Measurement of the induced bead magnetic moment allows for calculation of the induced bead torque for a given magnetic field strength.
(A) Small ferromagnetic beads were placed in a solution of glycerol. (B) The beads were initially magnetized and then exposed to a twisting field while the remnant magnetization along the original magnetization axis was measured in time. The magnetic moment can be is proportional to the exponential decay time constant.

induced by delivering a current pulse through the twisting coil. Two limitations currently exist in determining the exact shear force at the bead adhesion site. First, the force is dependedent upon the surface area of bead binding, and precise imaging studies are needed to experimentally measure this value. Second, the bead rotation cannot currently be measured in real time. Therefore, stimulus values will be reported as the max shear stress delivered by each bead, which is dictated by the peak current discharged through the coil.

In addition to microbead twisting, there is a small degree of microbead translation that will produce a localized strain. High speed imaging during the application of the twisting field captures the projection of bead translation (Fig. 3-4F). Tracking the motion of the centroid of multiple beads (N>100) we measured a typical motion profile (Fig. 3-4G). The motion profile

indicated an absolute displacement of ~.75 μm that occurred over the 50 ms of applied twisting field with a subsequent relaxation to near its original location by ~ 300 ms.

A primary feature of the MTC device is that it can deliver mechanical stimuli at multiple sites across multiple cells in a single sample. However, just as important is its ability to direct these injury forces through microbeads coated with specific proteins or ligands that target specific cell surface receptors. In order to verify microbead coating with proteins of interest, we utilized a basic chemical reaction producing covalently bonded protein coating on the bead surface. The covalent bond was accomplished using a two pot reaction process (Fig 3-5A). The initial step consisted of carboxyl coated microbeads (CFM 40-10, Spherotec) incubated with 100 μM 1-Ethyl-3-(3-dimethylaminpropyl)carbodiimide) (EDC) and 100 μM N-Hydroxysuccinimide (NHS) in a 1.0 M Sodium Acetate Buffer for 1 hour at room temperature. The microbead mixture then underwent a 3x series of centrifugation at 500 G for 1 minute and a subsequent rinse with isotonic buffered saline. The second reaction step consisted of adding the protein of interest at a concentration of 1μM in isotonic buffered saline overnight at 4 $^{\circ}$C. The final coating step consisted of incubating the microbeads in 1% Bovine Serum Albumin (BSA) for 1 hour (also served as storage solution for up to 3 days).

Following microbead coating, the presence of protein on the microbead surface was verified using multiple techniques. We utilized X-ray photoelectron spectroscopy (XPS) to assess the elemental composition of the bead's surface. After incubating beads with fibronectin (FN), a CAM previously used to injure neurons in our studies, beads analyzed via XPS showed marked increase in nitrogen content (Fig. 3-5B). This, combined with the decrease in chromium content, suggest successful FN binding since the carboxyl-coated chromium oxide surface of the bead is now covered with nitrogen-containing FN. Moreover, we observed more positive zeta

potential of the bead following incubation with proteins including Acetylated Low Density Lipoprotein (AcLDL), poly-l-lysine (PLL), and FN (Fig. 3-5C), which suggest successful bead coating as the protein coatings shield the uncoated bead's more negative carboxyl groups. To more specifically determine whether proteins were attached to the beads, we imaged beads coated with fluorescently tagged AcLDL, PLL, or FN (Fig. 3-5D-E). The normalized fluorescence intensity of beads revealed increased signal intensity relative to uncoated beads (Fig. 3-5F), which indicated that proteins were bonded to the bead's surface. We next sought to characterize the ability of beads with various protein coatings to bind neurons. To this end, we seeded 1 million microbeads per well resulting in a saturating coverage of microbeads (Fig. 3-5G) and allowed the microbeads to adhere for 30 minutes. For normal experiments, the microbeads were not perturbed, providing a conistent likelihood for an axon to be in close proximity to a microbead independent of the microbead coating. Only for the purpose of determining if microbead attachment differed significantly with microbead coating, a subset of samples were gently rinsed, fixed, and immunostained (Fig. 3-5H). The number of bound beads per unit length of axon was calculated by counting the number of beads across 1-10 mm of axon. This preliminary analysis revealed variable bead binding with no statistically significant difference in neuronal bead binding for AcLDL, PLL, or FN coatings (Fig. 3-5I), however, due to high variation in the bead binding the rinsing step was omitted from all injury studies. Since beads coated with different proteins attached to neurons to similar degrees, the observed differences in injury rates are likely a function of the specific nature of bead-neuron interactions and not because of differences in net applied force to neurons.
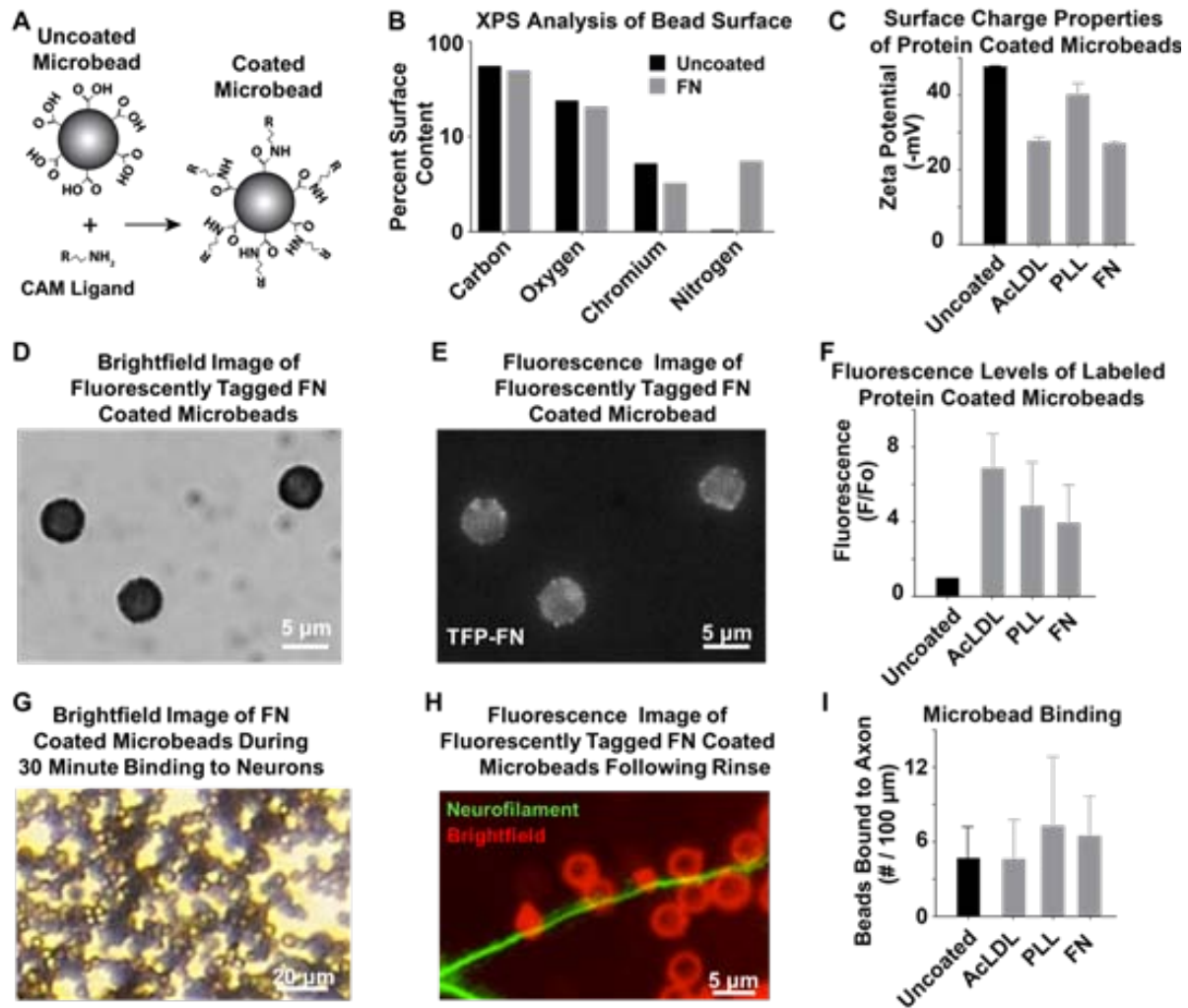
Figure 3-5: Verification of microbead coating with specific ligands.
(A) CAM ligands such as ECM proteins can be covalently bonded to the microbeads in order to target specific molecules that may potentiate brain injury. AcLDL binds a specific membrane receptor that is not a CAM and serves as a control for injury experiments. PLL beads binds non-specifically through charge interaction and serves as another control for injury experiments. FN is an ECM protein that binds specific CAMs such as integrins. Microbead coating can be verified through multiple techniques including (B) measurement of bead surface composition, (C) measurement of bead surface charge, and (D-F) identification of fluorescently tagged CAMs. Following bead coating, adhesion to neurons is accomplished by (G) seeding a high concentration of microbeads followed by a 30 minute incubation period and a gentle rinse to remove unbound beads. The number of bound beads remaining can be quantified by fluorescently labeling (H) the axons with a neurofilament antibody and (I) counting the average number per length of axon, which indicated slight differences in the extent of binding between coatings.

48

3.2.3   Testing the MTC Device as an *in vitro* Model of TBI

Following characterization of the coils and the microbead rotation and translational motion, initial experiments were performed to determine the axonal response to a mechanical stimulus delivered by the MTC device. Using a low throughput magnetic tweezer model, we have previously shown that an acute mechanical pull on Fibronectin (FN) coated beads bound to neurons results in neurite focal swelling and subsequent retraction. We sought to reproduce these results using the new MTC model to verify that MTC could in fact injure axons. Control experiments showed no morphological changes in response to experimental conditions or to bead binding over a 4 hour time window indicating the experimental conditions were not inducing a noticeable injury within the population of neurons (Fig. 3-6A-B). However, application of a single twist using the maximum applied load of 125 Pa per bead resulted in focal swelling within 1 hour post stimulus (Fig. 3-6C). This response was observed in multiple cells on a single coverslip indicating that the MTC device was able to reproduce the characteristic changes in axonal morphology consistent with axonal injury in multiple cells simultaneously. Furthermore, we were able to track these changes in ~25 neurons on a single coverslip which drastically increased our experimental throughput compared to the previous magnetic tweezer model which allowed for analysis of only a single neuron.
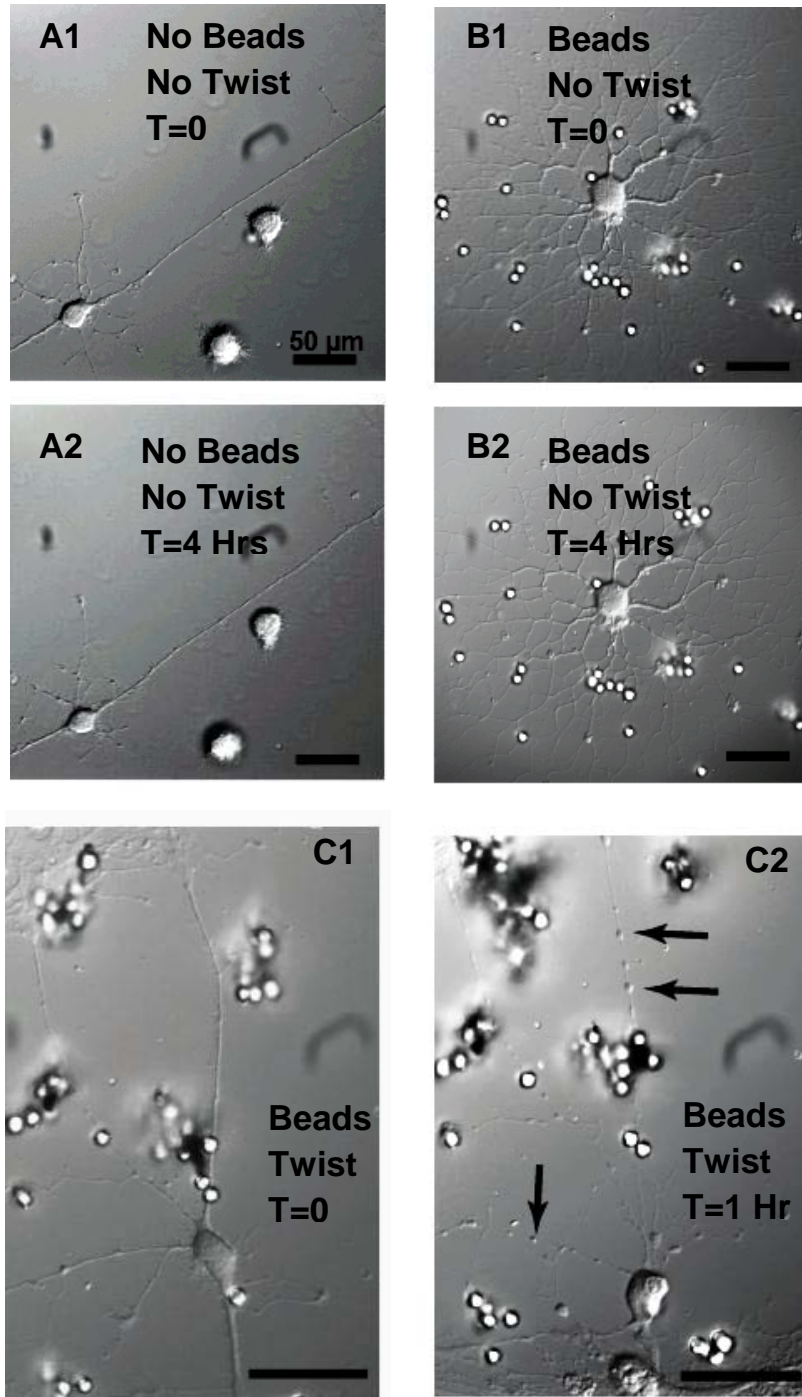
Figure 3-6: Preliminary experiments showed that the MTC device could induce the similar neuronal-axonal injury responses previously observed.
(A1-2) Control experiments consisting of time lapse imaging of neurons under experimental conditions with and (B1-2) without beads attached indicated neurons did not exhibit characteristic morphology changes over a period of 4 hours. (C1) Mechanical stimulation by the MTC device was able to produce the characteristic morphology of focal swellings (arrows) at (C2) 1 hr post bead twist.

After verifying the induction of axonal injury, a set of control experiments was performed in order to determine if evidence of mechanoporation was observed during the MTC mechanical stimulus. In order to rule out this potential event, we performed live, high speed calcium (Ca^{2+}) imaging during the application of the twisting field. FN coated beads were attached to neurons and identified using DIC imaging (Fig. 3-7A). Neurons were then loaded with Fluo4, a Ca^{2+} sensitive fluorescent dye, whose fluorescence level is dependent upon the intracellular concentration of Ca^{2+}. This allowed simultaneous measurements of Ca^{2+} concentrations at multiple locations along the axon (Fig. 3-7B). Due to the large calcium gradient that exists across the cell membrane, if the membrane is torn one would expect to see a rapid increase in intracellular Ca^{2+} levels corresponding to a spike in the Fluo4 signal. In order to test whether such an increase occurs during the mechanical stimulus delivered by the MTC device, we recorded from a neuron loaded with Fluo4 at 250 frames per second (FPS) during a single bead twist. We analyzed the intensity of the fluorescence signal over this time interval (Fig. 3-7C). We observed physiological calcium cycling due to action potential firing but did not observe any change in Ca^{2+} signal during the twist (black arrow). While we cannot rule out mechanoporation, we can conclude that if there is a transient tearing of the membrane the resulting Ca^{2+} flux is much less than that which occurs in the normal axon and thus should not account for the pathological changes observed at later time points.
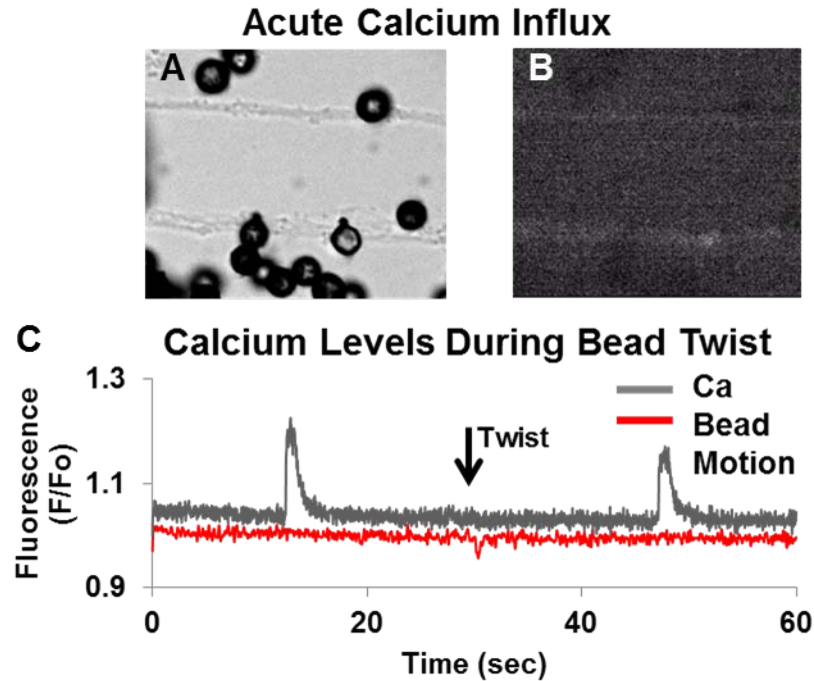
Figure 3-7: Measuring bead twisting induced intracellular calcium (Ca2+) increase as a marker of mechanoporation.
(A) DIC image of a neuron prior to bead twisting illustrates bead binding location and sites analyzed for Ca^{2+} fluorescence. (B) Immunofluorescence image illustrates a single snapshot taken at 250 fps during the bead twist. (C) Example regions show raw Ca^{2+} fluorescence intensity signal at each location illustrated in the images. The dashed line illustrates the approximate time of the bead pull, but no spike is observed in Ca^{2+} intensity, suggesting that the neuron is not experiencing mechanoporation.

In order to better understand the extent of axonal injury induced by the MTC model, we tested analyzed injury rates in neuronal cultures of varying age and varying stimulus intensity. We have previously performed our injury assays on primary cortical neurons harvested from day 2 neonatal Sprague Dawley rats and cultured for 5 days in vitro (DIV). Neurons at this stage, although generally considered immature, exhibit long branched neurites that exhibit injury responses similar to that observed in more mature cells. However, neurons are not typically considered mature until 14-21 DIV. Therefore, in order to accommodate this as well as to maintain consistency with previous results, we performed MTC injury experiments on neurons cultured for 5 and 19 DIV. We also compared the injury rates in response to twisting field

strengths corresponding to capacitor charges of 20 and 100 or induced shear stresses of 6 and 30 Pa per bead, respectively. As expected, we observed a magnitude dependent incidence of neurite focal swelling, in the DIV 19 cells, but we were unable to induce consistent levels of elevated injury rates in the DIV 5 neurons (Fig. 3-8A). One explanation for this is that the magnitude of the mechanical stimulus delivered to each neuron using the MTC injury model may be less than that of previous injury models and insufficient to generate large amounts of injury across the entire coverslip. Interestingly, we did observe neurite retraction, another indicator of injury, in both DIV 5 and DIV 19 neuronal cultures indicating that there is a response to the mechanical stimulus even in the less mature cultures (Fig. 3-8B). Nonetheless, it is an important potential result in that future *in vitro* studies may need to qualify their results based upon the maturity of their cultures. All future injury studies will be performed on the mature 14-21 DIV neuronal cultures.

After verifying that the MTC model can reproduce our previous neuronal injury results, we continued our efforts to understand the effects of directing trauma forces through specific ECM components. Building on our previous results using the high speed stretch injury model, we compared the extent of axonal injury induced by directing forces through PLL coatings compared to FN coatings. PLL will interact non-specifically with the cell membrane due to its large positive charge, yet has no specific ligand-receptor interaction, whereas FN is known to bind specifically to multiple integrin subunits. To this end, we performed live imaging experiments on neurons subjected to MTC stimulus through where multiple neurons from each culture sample were imaged every 5 minutes for one hour allowing timelapse images to be constructed for each neuron. The percentage of neurons that had become injured, indicated by the presence of axonal focal swellings, at each timepoint was recorded for each sample condition
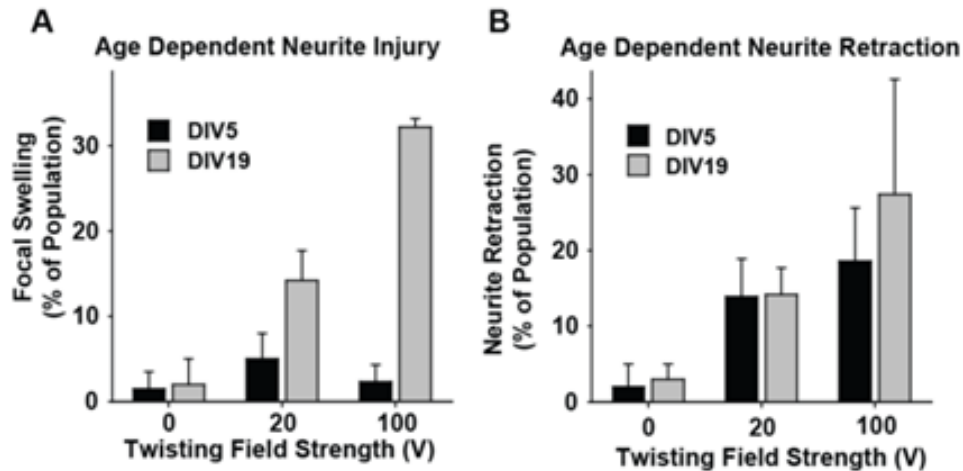
Figure 3-8: Neuronal injury identified in vitro may be dependent upon the days in culture.
(A) Neurite focal swelling exhibited an age and magnitude dependent response using the MTC injury model. (B) Neurite retraction depends upon stimulus magnitude but occurred independent of how long the neurons were cultured.

(Fig. 3-9A). The results indicated that the progression of injury was different in neurons injured through PLL coated beads compared to those injured through FN coated beads. A significant different in injured neurons was observedat 10 minutes following injury but not at 60 minutes (Fig. 3-9B). Additionally, using a sigmoidal fit to the data, a significant difference was observed in the time to 50% of maximum injury percentage (Fig. 3-9C). Together, this data shows that forces delivered through FN coated beads injured neurons quicker than PLL coated beads suggesting a difference in the the cellular response to the applied stimulus. This is important because it supports our previous implication of ECM-cell adhesion in axonal injury and supports the hypothesis of integrin mediated injury.
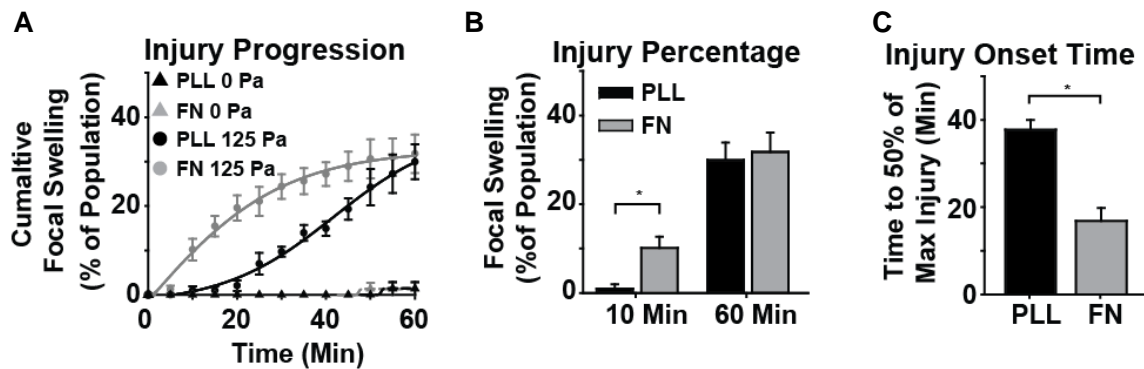
Figure 3-9: Bead coating affects injury rate.
(A) The percentage of neurons exhibiting injury by the indicated time point is recorded for both FN and PLL coated beads. (B) A significant difference in injured percentage is observed at 10 minutes but not at 60 minutes following bead twist corresponding to 30 Pa max shear strain. (C) Using a sigmoidal fit to the data, FN induces injury at a significantly earlier time point than PLL.

To better understand the differences in injury progression observed between FN and PLL coated beads, we aimed to determine the structures through which these beads adhere to the neuron. A primary advantage of the MTC technique is that it allows us to control the cellular structures through which injury forces are delivered by coating the beads with different proteins.

Our hypothesis posits that injury forces encountered during mTBI couple to the neuronal cytoskeleton via mechanically sensitive, transmembrane proteins. One class of such proteins includes integrins, which are a family of transmembrane proteins that mechanically couple the intracellular cytoskeleton of cells to the extracellular space through focal adhesion complexes [292,5,293]. Alternatively, other proteins which do not bind integrins will not result in focal adhesion formation. To test this, we attempted to immunostain for both focal adhesion markers, such as vinculin, and for integrins themselves. We have been successful in identifying evidence of focal adhesion formation near FN coated beads. We observed an increase in the localization of both vinculin (Fig. 3-10A) and β_1 integrin (Fig. 3-10C) to areas of the axon bound by FN coated beads suggesting that the mechanical actuation of these beads engages integrin proteins

55
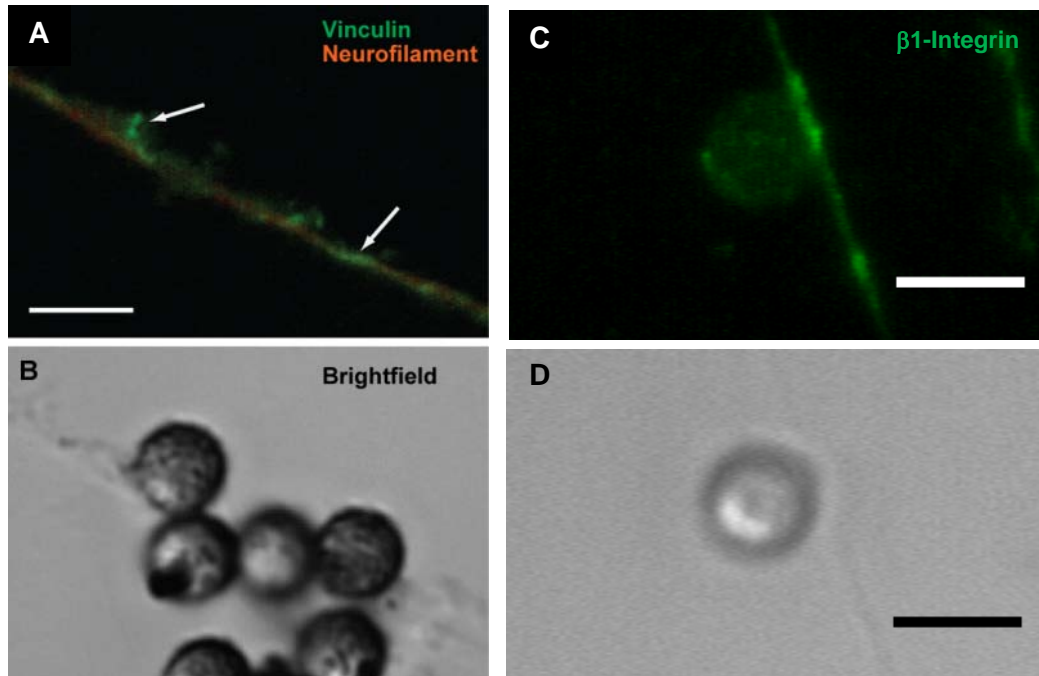
Figure 3-10: Fibronectin coated ferro-magnetic beads bound to neurons recruit integrins and focal adhesion components.
(A) Immunostaining for vinculin (green) reveals the presence of focal adhesions (white arrows) where beads attach to neurons (neurofilament: red). (B) β1 integrins also cluster at bead adhesion sites. (C,D) Bright field images confirm bead colocalization with vinculin and integrin immunofluorescence images. Scale bar = 5 µm.

and is directly transferred to the cytoskeleton of the neuron. Brightfield images indicate the location of bound beads with respect to the axon (Fig. 3-10B,D). Although the colocalization appears more prominent in area of FN bead attachment compared to PLL beads, we unable to produce consistent immunostaining results such that a quantitative analysis could be performed. Therefore, a current limitation exists in that the specific membrane receptors and specifically cell adhesion molecules that are coupled to the ECM coated microbeads is unclear. This is likely due to the difficulty of stabilizing these transient structures during the fixation procedure as well as their small clustering size compared to other adherent cell types. Future work will be necessary to clarify the specific structures through to which these ECM coated beads adhere in neurons.

3.3 Development of Anisotropic Neuronal Substrates to Isolate Axon Rich Regions

3.3.1 Design Requirements for Neuronal Cultures with Isolated Axons

Axonal swelling is the hallmark morphology of DAI and thus remains the most definitive means of identifying injured axons *in vitro*. Unfortunately, due to the intricate structures of neurons and glial cells, it is often difficult to accurately identify these markers. Part of the difficulty lies in the fact that neuronal cultures are typically isotropic and densely seeded to promote viability. In our previous work, we seeded our cultures sparsely in order to increase the likelihood of finding isolated neurons. However, sparse neuronal cultures do not maintain their viability well over the long term culture period necessary for maturation (14-21 DIV). Furthermore, by definition DAI is an injury to axons. While it is unlikely that dendrites are immune to damage, their injury response may vary from that of axons and therefore it may be beneficial to separate these two types of processes in the experimental setting. As is evident from a typical neuronal cortical culture, most neurons exhibit a highly branched, complex tree of processes consisting of a mixture (Fig. 3-11). While immunolabeling techniques as well as subtle morphological differences can distinguish dendritic and axonal processes, clear distinction between these two subsets is often difficult. In order to facilitate studies of axonal injury, it is therefore beneficial to introduce a level of anisotropy into the neuronal cultures such that axons are (1) isolated from dendritic and glial processes, (2) concentrated in a single region to increase analysis throughput, and (3) aligned to decrease the effects of overlapping or directional effects of force application.
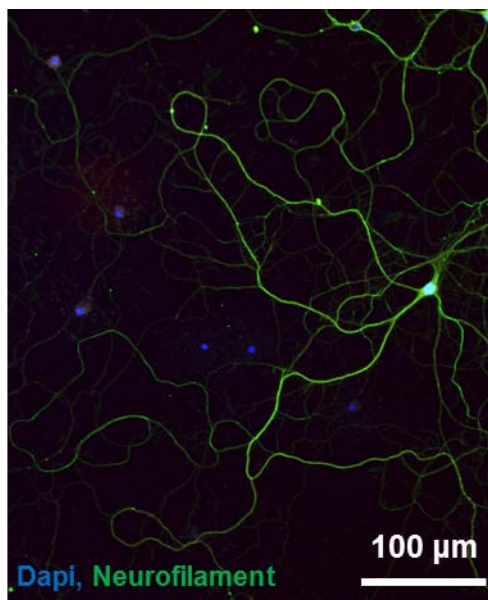
Figure 3-11: Isotropic Neuron with Highly Branched Processes.
Example image of a neuron after 14 days in culture illustrates the extensive branching of its processes. The distinctive morphology presents multiple challenges to identifying axonal injury including distinguishing axons and dendrites, attributing a particular axon to a cell body, and quantifying the degree of axonal injury within a given process. The isotropic morphology also results in a low degree of consistency in general structure across multiple neurons.

3.3.2   Building Stamp Masks to Produce Neuronal Cultures with Isolated Axons

Many strategies have been used successfully to introduce anisotropic cues to cultured cells. We utilized a combination of mask seeding and microcontact printing [304] in a technique termed stamp mask cultures to produce regions of isolated axons with specific degrees of alignment (Fig. 3-12). Mask seeding uses a physical barrier to prevent cell bodies from adhering to regions of a coverslip during the seeding process. Microcontact printing utilizes microscale features imprinted onto the surface of a polymer, typically PDMS, that are inked with adhesive protein and then transferred to a substrate surface. The resulting printed chemical cues direct cell adhesion along certain paths presenting specific boundary cues to the cell. We combined these two techniques by initially molding microscale lines that were 1cm x 15 μm x 5 μm (L x W x H) into one surface of a 1 mm thick slab of PDMS. After molding one surface, an epilog CO_2 laser

was used to cut out a 3x3 grid of squares. Each square was 3 mm x 3mm and separated by 1 mm. After the stamp masks were cut by the laser, they underwent a 3x cycle of rinsing and sonicating in 90% Ethanol to remove any debris left over and to sterilize for cell culture. Following sterilization, the stamp masks were inked with an adhesive chemical composition of 50 μM Laminin reconstituted in .1% Poly-L-Lysine for 1 hour. The stamp masks were then dried and placed on clean glass coverslips sterilized by UVO treatment. PLL was then immediately added to the wells and incubated for an additional hour. The PLL was removed and rinsed 3x with sterile Phosphate Buffered Saline. Neurons from primary harvest of Sprague Dawley rat cortices were seeded at a concentration of 200k cells per cm^2. See section on primary neuronal culture harvest for full protocol. After 1 hour, the stamp masks were removed, coverslips were rinsed 2x and then returned to the incubator.
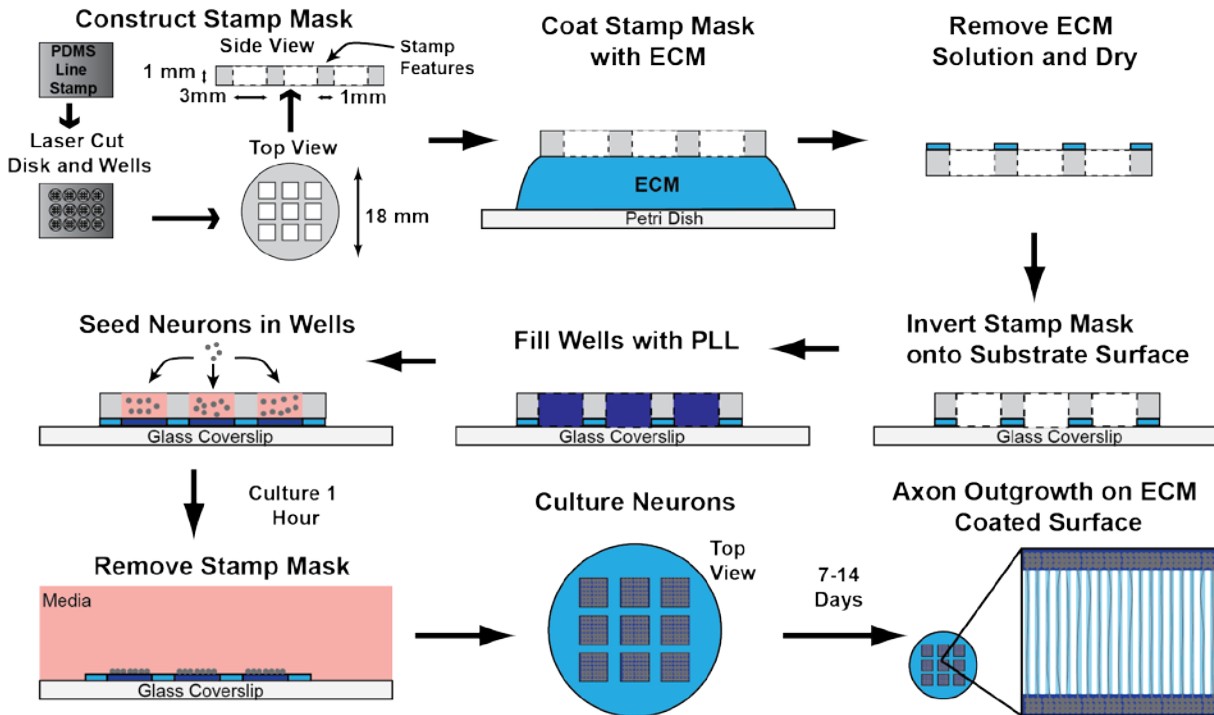
Figure 3-12: Construction of Stamp Mask.
The stamp mask technique utilizes a combination of mask seeding and microcontact printing, also referred to as 'stamping' to produce anisotropic neuronal cultures with regions of isolated axons. The stamp mask is constructed from a PDMS disk that contains microgrooves on one side. A versa laser is used to cut multiple squares out of the disk to create wells for seeding. Prior to seeding, the mask is inked with adhesive proteins, dried, and placed onto a clean glass coverslip. Neurons are seeded into the wells and allowed to adhere to the glass surface. The stamp mask is subsequently removed leaving adhered cell bodies and axon growth cues on the surface. Over 7-14 days, neurons extend axons onto the adhesive ECM proteins creating regions of isolated axons.

3.3.3   Testing the Effectiveness of the Stamp Mask Technique.

The stamp mask procedure utilized the 1 mm barrier regions (Fig. 3-13A) to both isolate a region of the coverslip from cell bodies and to lay down chemical cues to promote axonal growth. Immediately following seeding and removal of the stamp mask, the isolated region was easily visible (Fig. 3-13B). After 14-21 DIV, immunolabeling of neuronal cultures indicated that only axons (indicated with Tau) grew into the isolated region whereas both dendrites (MAP2) and glial cells (GFAP) were confined to the seeding well regions. Therefore, any process found

60

in the central region could be identified as an axon without the use of immunolabeling procedures.

In addition to generating regions of isolated axons, we were able to modify the degree of axonal anisotropy by changing the geometric cues of the microcontact printed area. Whereas the 15 x 15 μm lines indicated previously produced nicely aligned, separated axons, removing these features allowed the printing of an isotropic adhesive surface resulting in an isolated region of non-aligned axons (Fig. 3-14). Although we did not fully characterize the effects of changing the stamp mask features, it was clear that modifying the feature properties such as line width as well as the distance between wells affected the general alignment of the isolated axonal region. Furthermore, modifying the density of neuronal somas seeded in the well regions also influenced the density of axonal processes found in the isolated axon regions. For all future injury studies, we found the optimal parameters to be 15x 15 μm lines with well regions spaced 1.5 mm apart and a seeding density of 200k cells per cm^2.

Dapi, Tau (axons), GFAP (astrocytes)

Dapi, MAP2 (dendrites), GFAP

200 µm

200 µm
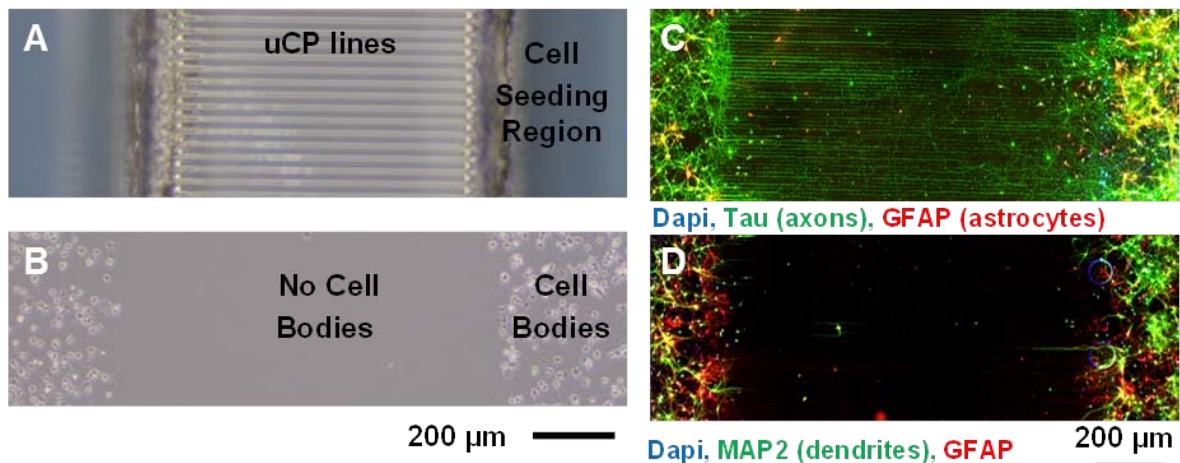
Figure 3-13: Isolation of Axon Rich Region Using Stamp Mask.
Example images from the stamp mask protocol indicate the microcontact printed (ucp) lines on one surface of the stamp mask as well as the separation of cell seeding regions (upper left). After seeding, neuronal cell bodies are separated by a region of uCP adhesive proteins that promotes axonal growth (lower left). After 7-14 days in culture, immunostaining reveals the outgrowth of only axons (upper right) into the center region with dendrites unable to extend across the gap (lower right).
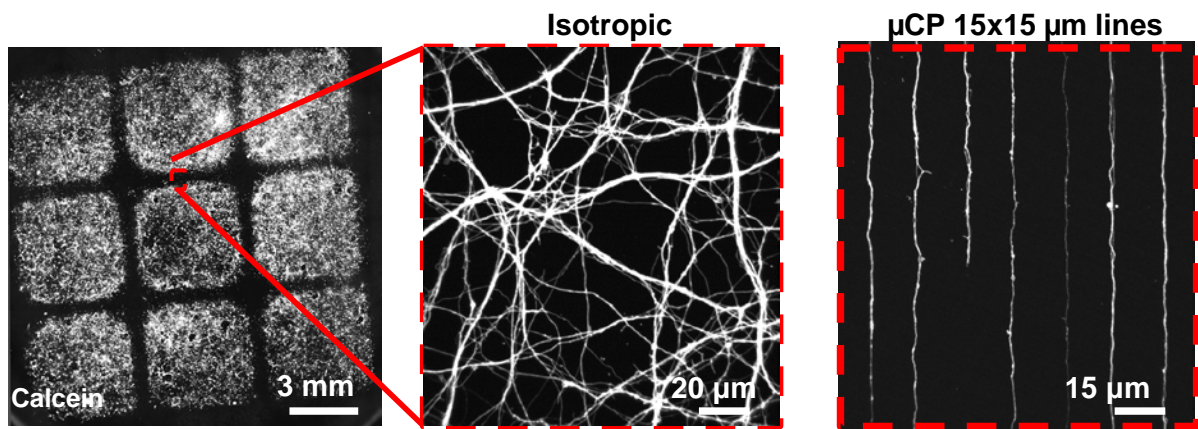
Figure 3-14: Isotropic and Anisotropic Axon Only Regions.
Depending on the microgroove features imprinted onto the PDMS, the isolated axon region can exhibit varying degrees of aligned axons. Using only a smooth surface, isotropic axons are grown in the central region. Using uCP lines of 15 µm width with 15 µm spacing results in highly aligned, anisotropic axons.

62

3.4 Development of an Automated Method for Quantifying Axonal Injury *in vitro*

3.4.1 Design of Automated Analysis of Axonal Morphology.

A major difficulty in studying axonal injury *in vitro* arises in the proper identification of injured axons. Since the only definitive pathology is a morphological change of the axon, the obvious analysis technique is microscopy. However, distinguishing a normal axon from an injured axon is not obvious, and moreover, distinguishing the severity of an injured axon is completely unclear. At what point a normal change in axon diameter becomes pathological is left to the individual researcher to determine and to attempt to keep consistent throughout the analysis.

In order to address this shortcoming, we sought to develop an automated analysis strategy in which (1) no manual identification of morphology is necessary and (2) no preconceived characteristics of axon focal swellings are defined.

3.4.2 Building the Software Package for Automated Analysis of Axon Morphology

We developed a protocol combining semi-automated imaging of live neuronal cultures with post image analysis in both ImageJ and Matlab to identify and quantitatively measure the extent of axonal injury *in vitro*. The process begins with live imaging of neurons that are fluorescently tagged in order to provide sufficient signal to noise ratio as to identify axon segments (Fig. 3-15A). We utilized Calcein to label our neurons as this provided a fluorescent molecule that is confined to the interior of the cell membrane yet is able to diffuse freely throughout the cell volume without attaching to specific structures. Calcein is typically used in live/dead stains to indicate viable cells and therefore provides the additional benefit of verifying the viability of the axons we are imaging. Following time lapse imaging of a field of view (FOV) within the isolated axon regions of our neuronal cultures, the image series undergoes a

sequence of post processing using custom scripts and image processing techniques written in both ImageJ and Matlab software packages. ImageJ scripts are responsible for skeletonizing the first image of each sequence to provide a mask that indicates the coordinate locations of axons within the particular FOV (Fig. 3-15B). Skeletonizing is accomplished through a series of image filtering and morphological analysis that can be found in the attached code. After skeletonizing, the image sequence is passed to Matlab where the morphological properties of the axon are measured at each time point. This process begins with the measurement of the axon cross section at each point along each axon at each time point (Fig. 3-15C). The cross section provides the best estimate of the axon width at a particular point. Multiple options exist for specifying how the cross section is measured. For future injury experiments, and absolute threshold was set where the cross section was measured as the full width at a pixel intensity value of 25 within an 8 bit image. Initial images are background subtracted such that the absolute value provides a constant SNR above background levels of fluorescence. After the width is measured at each point along an axon segment (Fig. 3-15D), the width values are inserted into a matrix (Fig. 3-15E) that provides a quantitative depiction of the morphology of that particular axon in time. The morphology matrix is used in subsequent analysis to identify the presence of injury.
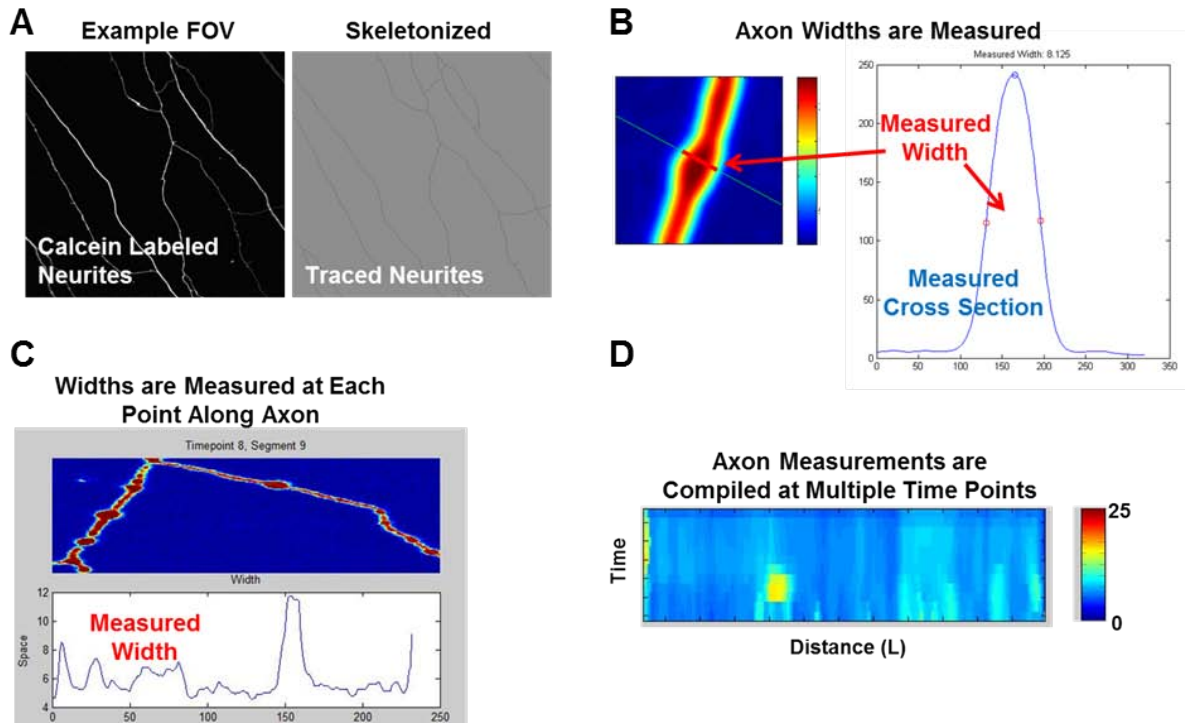
Figure 3-15: Summary of AMA Protocol.
(A) Automated analysis of axon morphology begins with skeletonizing an entire field of view (FOV) that has been imaged throughout the course of an experiment. Skeletonizing results in a 1 pixel wide trace of the axons. **(B)** After tracing, axon width is measured at each discrete point along the axon. The width is quantified by measuring the distance between an absolute threshold of pixel intensity, set to 30 in an 8 bit image for this analysis. **(C)** Width measurements are made along the entire axon segment and for all axons within a FOV. **(D)** Each axon width measurement is made at multiple time points allowing the generation of a map of axon widths in time. This matrix is referred to as the axon morphology map.

3.4.3 Testing the Automated Analysis of Axon Morphology.

Initial testing to ensure the effectiveness of our custom analysis software was performed on fake axon segments drawn in adobe illustrator that will be referred to as pseudo axons. The importance of this verification step is twofold. First, the accuracy of the automated measurement of cross sections was verified. Second, the ability to resolve axonal swellings given the optical resolution of our experimental setup was verified. To do so, multiple axon segments were drawn with varying sizes and number of focal swellings (Fig. 3-16A). These segments were converted
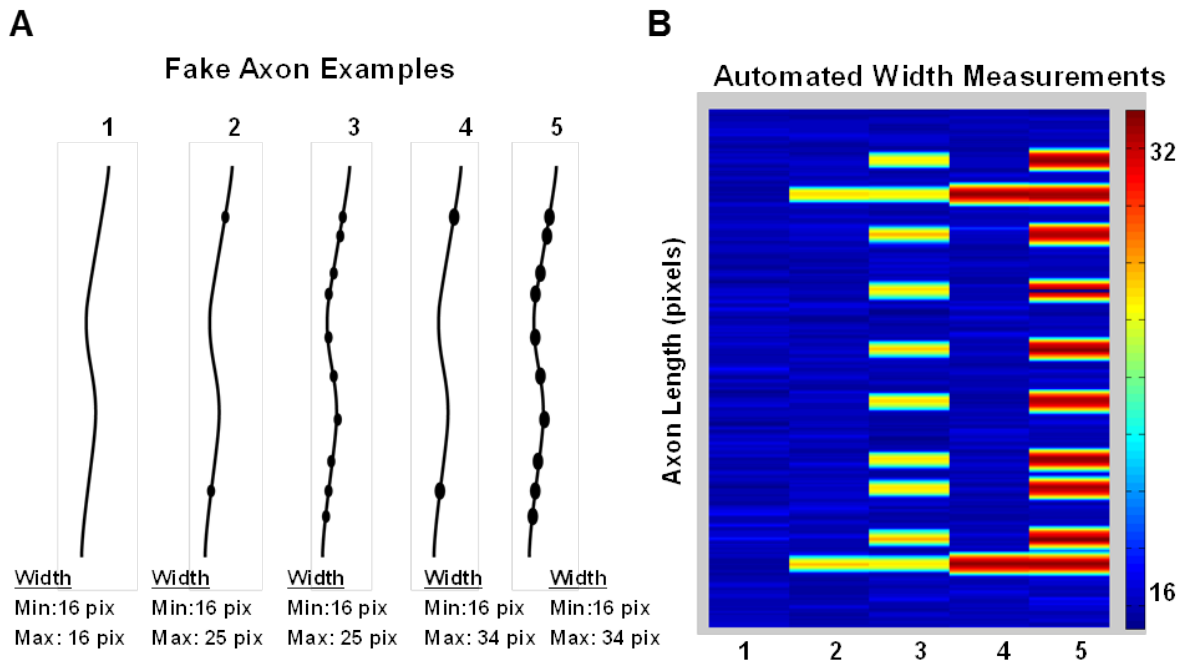
Figure 3-16: Verifying Measurement Accuracy on Pseudo Axon Images.
Verification of the accuracy of axon width measurements was performed using a set of pseudo axons that were drawn in adobe illustrator with specific, known widths and focal swelling sizes. **(A)** Fake axons were constructed to contain multiple width measurements and amounts of focal swellings. **(B)** Automated analysis of the pseudo axons revealed accurate measurement of axon widths and accurate detection of the multiple degrees of axonal swelling.

to tiff images with resolution that matched the output from our imaging system, meaning that the number of pixels that defined a typical real axon segment was also imposed onto the fake axon segments. Subsequent analysis of the pseudo axons was performed and produced a morphology matrix that indicated accurate measurement of both smooth axon segments as well as individual focal swellings (Fig. 3-16B).

After verifying the accuracy of the measurements, it was necessary to define an injury metric that converted the morphology matrix data into a numerical indicator for comparison across conditions. Given that the morphology matrix contains a wealth of information, multiple single parameters could potentially be calculated. In order to maximize robustness we sought a

simple metric that captured the amount of change in axon morphology that occurred in time. We decided on a metric termed the sum of the width gradient squared (SGS) to condense the morphology matrix into a single parameter (Fig. 3-17A). The essence of the metric is that it captures any change in morphology by first taking the geometrical derivative (change of width in space) and then captures the amount of change by summing up the square of this value along the entire segment. It was necessary to control for differences in axon segment lengths, which was accomplished by dividing by the total length of the segment to produce a unit less parameter that effectively indicates the amount of change of the axon width per length of axon. The usefulness of condensing the information of the morphology matrix into a single parameter can be indicated using example segments (Fig. 3-17B). An initially smooth segment can be quantified by a specific SGS that changes at a later time point once axon swellings appear. By normalizing the SGS to the earlier or initial time points, a relative changes in SGS (NSGS) is calculated and can be compared across axon segments.

The automated analysis of axon morphology combined with the NSGS metric was tested on multiple FOV to verify robustness in detecting axon segments and quantifying axon morphology characteristics. An example FOV illustrates how multiple axons (Fig. 3-18A) are segmented (Fig. 3-18B) and subsequently measured to produce quantitative descriptions of length and width measures (Fig. 3-18C,D).

A

$$SGS = \frac{\sqrt{\Sigma\left(\frac{dw_i}{dl_i}\right)^2}}{L}$$

$$NSGS = \frac{SGS}{SGS_{initial}}$$

l_i = axon segment point i
w_i = axon segment width at point i
L = total axon segment length
SGS = sum of gradient squared
NSGS = SGS normalized to initial time point

B

	$T_{initial}$	T_t
dW_i/dl		
SGS	.27	1.6
NSGS	1	5.92
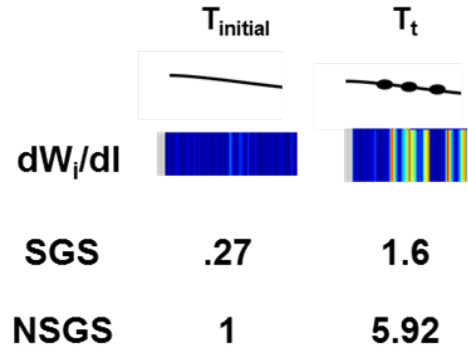
Figure 3-17: Testing Injury Metric on Pseudo Axons.
(**A**) In order to quantify the axon morphology using a single metric, we developed a score based on the sum of the square of the gradient of the axon width, termed SGS. This metric captures the relative amount of change in axon width along the length of the axon. In order to compare the SGS metric in time, it is normalized to an initial point, typically the first time point, to generate a normalized SGS metric or NSGS. (**B**) Analysis of an example segment illustrates how the SGS metric quantifies two segments with varying amounts of focal swelling and how the NSGS metric can quantify the relative amount of change within that segment in time.
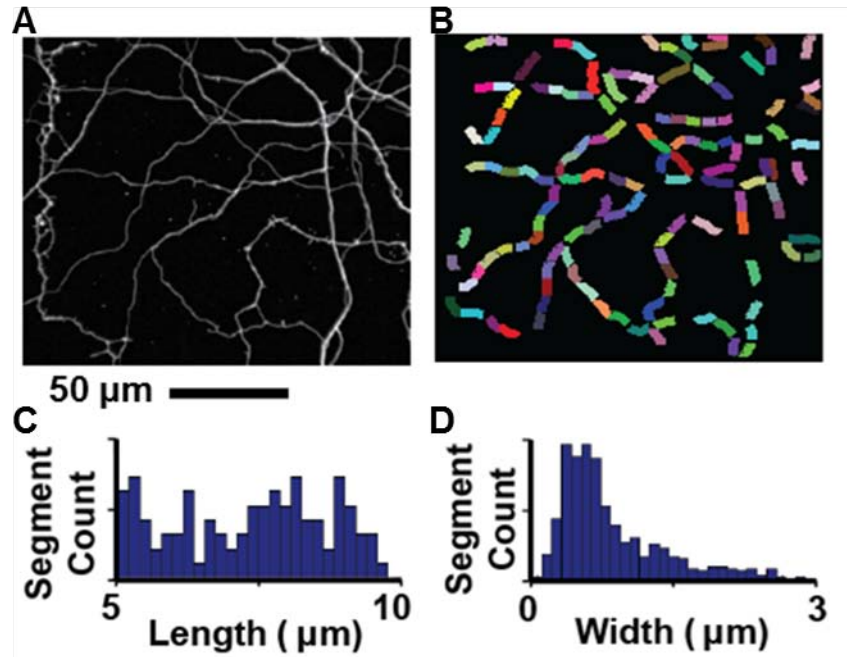
Figure 3-18: AMA Analysis on Example FOV.
Extending the AMA analysis beyond single segments to an entire population is necessary to quantify the amount of axonal injury within a population. A single field of view can be divided into multiple axon segments of constrained length, each of which has a range of potential axon widths.

Individual segments exhibiting focal swellings can be identified and isolated for additional analysis or for demonstration purposes. Figure 3-19 illustrates a specific segment that exhibited axonal swelling. The morphology change is noticeable in the binary image (Fig. 3-19A) and is further identified in the traces of axon width (Fig. 3-19B) and width gradient (Fig. 3-19C). In order to determine the effectiveness of the NSGS parameter in detecting the morphology change, we plotted the temporal progression that indicated an increase around 30 minutes post MTC induced injury (Fig. 3-19D). Future axonal injury studies will use the automated axon morphology analysis strategy combined with additional statistical analysis to pursue the relevant scientific hypothesis.
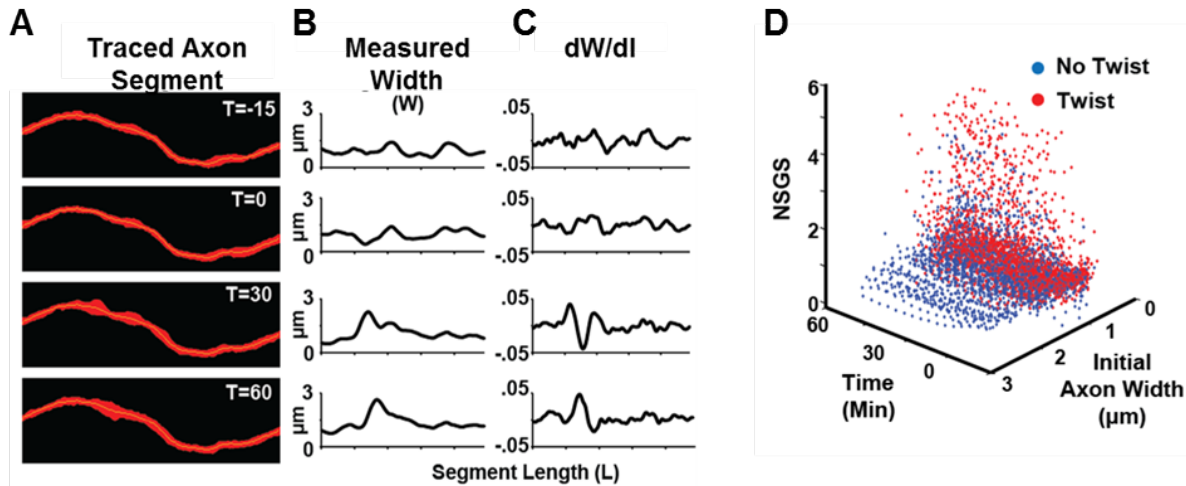
Figure 3-19: NSGS Measurement of Axon Segments.
Each axon segment from a single field of view is analyzed individually in time. Its distinct **(A)** threshold morphology, **(B)** measured width, **(C)** and gradient of the width is calculated. Following this analysis, multiple segments can be compared across conditions generating **(D)** a data set with multiple independent variables.

3.5   Discussion

A large effort was placed in developing this tool set for the sole purpose of addressing our research question. While some of the tools represent novel developments of technologies (e.g. AMA analysis) others consist of a combination or adaptation of existing technologies with novel purpose (e.g. MTC as an injury model, stamp masks for producing isolated axons). Effort was made in writing this dissertation to provide necessary reference to the pre-existing techniques and technology and to clearly indicate where the 'novelty' was in adaptation or combination as opposed to conception.

The primary advancement and contribution of this chapter was in the development of a complete package aimed at advancing the ability of current *in vitro* TBI studies to better address questions of mechanosensitivity of axons. We focused on adapting techniques and strategies from relevant fields that could be applied to our research interests and developing new strategies

and techniques when no existing ones could be found. In particular, a wealth of relevant information, tools, and techniques was found amongst the traditional field of mechanobiology. Although this field is by no means new, there is relatively little crossover between it and *in vitro* TBI. Mechanobiology tends to focus on the basic principles of mechanosensitivity of cells at the cell and sub-cellular level. The tendency is to focus on cells that experience more obvious mechanical interactions such as muscle or endothelial cells, yet many of the structures and processes are ubiquitous and likely relevant to mature neurons as well. It is our intention that by borrowing from existing knowledge within the field of mechanobiology, we can make more timely advances in understanding how mature neurons respond to physical forces during TBI. By developing a package of technologies including the injury model, *in vitro* tissue substrates, and analysis methodology that is amenable to elucidating mechanosensitive structures within the axon, this chapter has served as the foundation for our future TBI studies focused on elucidating mechanosensitive processes related to cell-ECM interactions.

4 Axonal Injury Depends on the Extracellular Matrix through which Trauma Forces are Directed

4.1 Introduction

The non-uniform distribution of axonal injury within the brain previously described in Chapter 1 supports the question of why certain brain regions are more or less susceptible to Traumatic Brain Injury (TBI). Despite previous attempts to explain vulnerabilities from a mechanical standpoint (also outlined in Chapter 1), certain aspects of TBI pathology appear to depend on factors other than purely mechanics and mechanical properties. One particular example is the distribution of Diffuse Axonal Injury (DAI) that is typically described as a multi focal, non-uniform distribution observed diffusely throughout the brain [34]. These injury patterns include multiple isolated regions in which injured neurons are found immediately adjacent to uninjured neurons. We hypothesized that the distribution of injured neurons interspersed with uninjured neurons may be due to factors in the local cellular microenvironment that affect the susceptibility of a neuron or axon to local forces. Given the implication of mechanochemical coupling in axonal injury from Chapter 2, we reasoned that the local extracellular matrix (ECM) composition surrounding a neuron may influence its mechanochemical coupling and thus its susceptibility to trauma.

Despite the high density of cellular components in the brain, the extracellular space constitutes approximately one-fifth of its total volume [273] and is comprised of diverse ECM proteins including glycosaminoglycans (GAG), proteoglycans (PG), and glycoproteins (GP). Hyaluronic Acid (HA), Chondroitin Sulfate Proteoglycans (CSPGs), Tenascin-R (TnR), and Link Proteins together form the primary extracellular scaffolding structure within the brain. Although an extensive analysis of the regional expression levels of individual ECM molecules has only been performed in the mouse brain [64], several reports support the existence of

differential regional expression in multiple species including opossum [44], hedgehog [204], and humans [43]. Table 2 summarizes the extent of known ECM localization reported in the literature for both non-human and human brains, indicating that while less is known about the human distribution, brain ECM is ubiquitously expressed and differentially distributed.

The most prevalent component of the brain's ECM is HA, a GAG formed by a linear polymer of disaccharides [195]. HA is secreted into the extracellular space by membrane bound enzymes called Hyaluronan synthases (HAS) [278] that may localize to neurons [50]. CSPGs are comprised of a protein core to which variable numbers of linear, unbranched chondroitin sulfate GAG chains are covalently bonded. Aggrecan, brevican, neurocan, and versican are prominent CSPGs, commonly referred to as lecticans, that vary in size between ~90kDa (Brevican) up to ~400kDa (versican) [244,320]. The cellular source of CSPGs is controversial, but likely includes both neurons and glial cells [50]. Tenascin-R is a trimeric, modular GP found primarily in the nervous system [279] and has been shown to be synthesized by both neurons and glial cells [50]. Link proteins are a group of small ~38-43 kDa proteins shown to be synthesized by both neurons and glial cells [50]. Additional proteoglycans, such as heparin sulfate proteoglycans (HSPGs), and glycoproteins, such as reelin, also exist in the brain ECM, contributing to its structural and functional diversity.

Unique sub-cellular components form structures within the brain that contribute to the mechanical integrity of the cell. Furthermore, distinct compositions of these components exist within the brain, forming specific cellular microenvironments that serve varying functions.

Table 2: Regional ECM Expression in the Developed CNS

	Non-Human	Human	Reference (N,H)
Cerebral Hemisphere			
Cerebral Cortex	HA, A, B, N, V, P, LP, Tn-R, Tn-C, R, HSPG	HA, CSPG, A, B	[320,66,67,41,16,81,101,202,64], [203,42,251,312,287,225,171]
Amygdala	HA, A, N, B, V, P, LP, Tn-R, Tn-C, L, HSPG	CSPG	[193,197,230,202,288,27,192,101,93,136,65,184,64], [225,203,224]
Hippocampus	HA, A, N, B, V, P, LP, Tn-R, Tn-C, R, HSPG	HA, A, B, R	[320,16,81,101,202,288,93,136,65,184,252,26,28,27,64], [312,171,98]
Thalamus	HA, A, N, B, V, P, LP, Tn-R, Tn-C, HSPG	HA, CSPG, A	[202,27,288,320,40,64], [203,170]
Basal Ganglia	HA, CSPG, A, HSPG	CSPG	[43,312,64]
Hypothalamus	HA, CSPG, N, V, LP, Tn-C, HSPG	CSPG	[193,197,230,64], [203]
Cerebellum	HA, A, B, LP, Tn-C, R, HSPG	HA	[310,237,202,16,309,252,136,65,184,64], [312]
Brainstem	HA, A, N, B, V, P, LP, Tn-R, Tn-C, HSPG	CSPG	[202,27,288,320,40,64], [249]
Spinal Cord			
Gray Matter	HA, CSPG, A, HSPG	HA, Tn-R, A, B, N, V	[64], [142,64]
White Matter	HA, CSPG, A, HSPG	HA, Tn-R	[64], [142,64]

HA: Hyaluronan, CSPG: Chondroitin Sulfate Proteoglycan, A: Aggrecan, B: Brevican, N: Neurocan, V: Versican, HSPG: Heparin Sulfate Proteoglycan, LP: Link protein, TnC: Tenascin-C, TnR: Tenascin-R, R: Reelin

4.1.1 Distinct Cellular Microenvironments Contain Sub-cellular Structures that Influence Physiological Processes in the Brain

The diversity of cell types and ECM within the brain has led to distinct microenvironments in which specific structures comprised of these components influence physiological processes. Organized ECM structures called Perineuronal Nets (PNNs) (Fig. 4-1A) localize to the soma and perisomatic extensions of neurons in multiple brain regions [37,205,227,50,191,43,99]. PNNs preferentially ensheath highly active neurons [205], suggesting they may function as a buffer for cations important in action potential generation [124]. PNNs may also limit plasticity as they are upregulated at the end of critical periods in development [227,49] and stabilize dendritic spine

74

formation [162] potentially by influencing binding of CAMs. Distinct ECM structures also surround synapses, influencing both development and plasticity associated remodeling of these structures (Fig. 4-1B) [323,78]. ECM molecules at the synapse have been shown to both promote and inhibit plasticity, as well as influence the clustering of postsynaptic receptors by limiting diffusion in the membrane [96]. This is accomplished through interactions with CAMs such as integrins and NCAMs [79,71] and transmembrane channels such as voltage dependent calcium channels [207,157]. Traditional adhesions like integrins [56] and cadherins [284] as well as neural specific adhesions like Neuroligin, Neurexin [271] and SynCAM [30,109] influence synaptic connectivity through signaling pathways that directly influence synapse formation and plasticity by regulating cytoskeleton organization [79,80]. Specific CAMs such as Caspr2, contactin, and NrCAM are also important in organizing the myelin structure that forms around axons in the brain [111,229]. Organized ECM scaffolds occupy the space between myelin wrappings, called Nodes of Ranvier (Fig. 4-1C) [19], and may promote clustering of Na^+ channels that is necessary for signal propagation in the axon [272]. Finally, an organized ECM scaffold exists around the vasculature in the brain and influences cellular attachment and organization of the multicellular vascular structures (Fig. 4-1D). ECM comprised of collagen, laminin, and HSPGs surrounds the inner layer of endothelial cells and also engulfs pericytes forming a structure referred to as the tunica intima [113]. In larger vessels, such as arteries and arterioles, a middle layer referred to as the tunica media is formed by multiple layers of ECM and smooth muscle cells as well as an outer layer called the tunica adventitia [135]. The external layer of ECM promotes adhesion of neural cells, such as terminal nerve fibers and astrocyte endfeet, which contribute to numerous vasculature functions including regulating cerebral blood flow and forming the blood brain barrier [1]. Thus, distinct cellular microenvironments
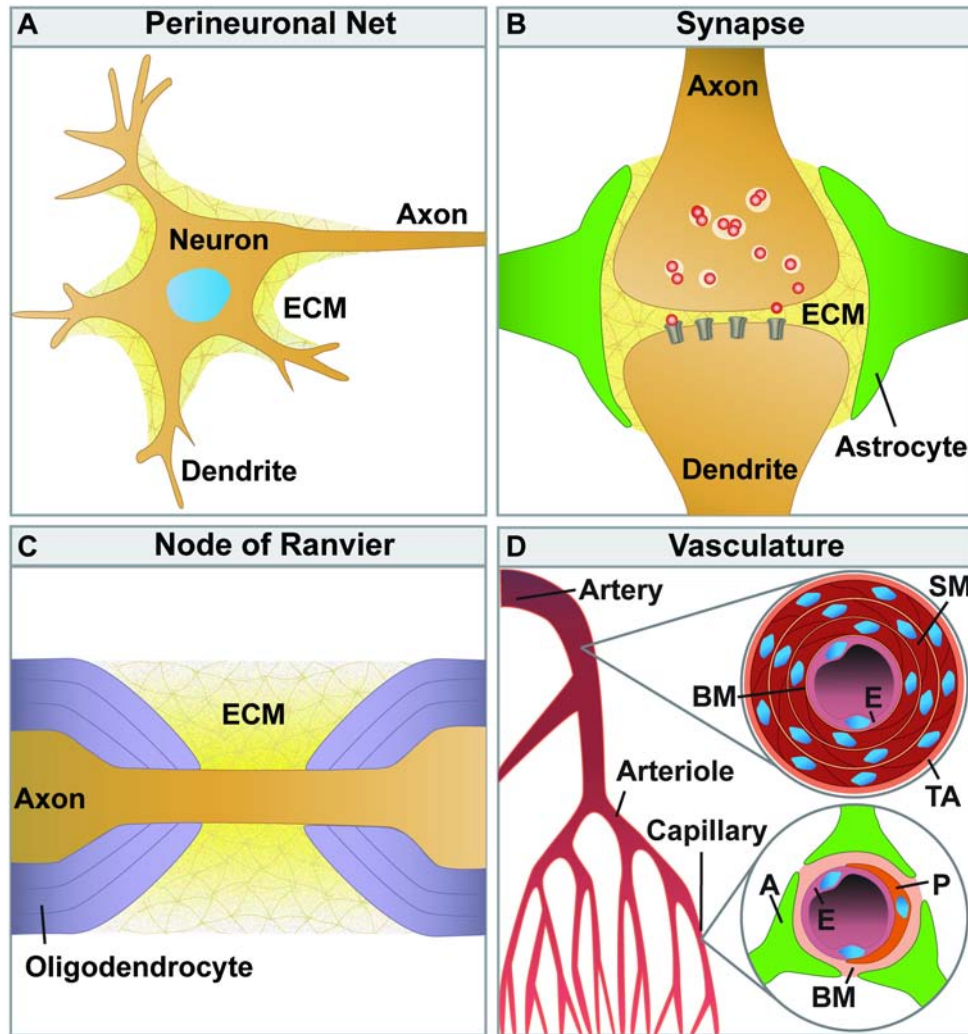
Figure 4-1: Unique cellular microenvironments exist within the brain.
(A) The Perineuronal Net (PNN) is formed by extracellular matrix (ECM) and engulfs the soma and proximal dendrites of neurons. Neuronal structure may be influenced by the PNN through interactions with cell adhesion molecules (CAMs), which together regulate neuronal connectivity. (B) Synapses are formed between neuronal axons and dendrites but are also influenced by supporting ECM and astrocytes. These components are structurally connected through binding of CAMs that influence formation and remodeling of the synapse. (C) Myelinated axons consist of multiple layers of oligodendroctye processes that wrap around the axon with distinct spacing referred to as Nodes of Ranvier (NOR). ECM within the NOR may influence the clustering of ion channels important for axonal signal propagation. (D) The extensive vasculature within the brain varies in size from larger arteries and veins down to small capillaries, each of which has a unique structure. ECM comprised of collagen, laminin, and HSPGs surround the inner layer of endothelial cells (En) and also engulf pericytes (P), forming a basement membrane (BM) for cell attachment. In larger vessels, such as arteries and arterioles, a middle layer referred to as the tunica media is formed by multiple layers of ECM and smooth muscle cells (SM) as well as an outer layer called the tunica adventitia (TA). The external layer of ECM promotes adhesion of neural cells, such as terminal nerve fibers and astrocyte endfeet (A), which contribute to numerous vasculature functions including regulating cerebral blood flow and the blood brain barrier.

influence both cellular structures and functions important to normal brain physiology. Although critical functions of brain specific CAMs and ECM structures are beginning to emerge, their potential influence in mechanotransduction mechanisms remains relatively unexplored.

4.1.2   Brain Extracellular Matrix and CAM Expression in Axons

Unlike other tissue types such as muscle, an understanding of the structure and composition of the ECM directly adjacent to neural cells is not clear. Although a general understanding of components and to some extent localization has been reported, these remain insufficient to correlate with the location of TBI pathology. We previously hypothesized that cell-ECM linkages may direct injury forces through mechanosensitive cellular structures and showed that the extent of focal adhesions correlated with injury sensitivity. Different ECM proteins can interact with different cell surface receptors and CAMs and therefore present a potential to elicit varying severities of injury.

Integrins are expressed heterogeneously throughout the brain and have been shown to be differentially expressed in the adult rat brain [54,226]. Integrins are highly expressed in synaptic regions [243,213] and can modulate synaptic plasticity by regulating ion channel currents [173,255,300]. In the developing nervous system, integrins are involved in dendrite and axon outgrowth [242,277,128,248] and guide synaptogenesis [255,300], and in mature neurons, they influence remodeling of dendritic spines [255,301]. Their ability to modify Ca^{2+} handling and to modulate synaptic strength has also been linked to stabilizing long term memory potentiation [264], suggesting that integrins may be key players in memory and learning [300,54].

Beyond implications in normal functions, the potential for integrins to contribute to the pathophysiology associated with TBI remains unexplored. Previously, TBI related forces at the cellular level have been linked to the cell membrane as well as the underlying cell cytoskeleton.

77

However, no specific conduit for propagating these forces has been proposed or explored. Given the large body of research that indicates CAMs serve as a mechanical linkage between the extracellular space across the membrane to the cytoskeleton, we reasoned that they may serve as that conduit.

In this chapter, we aim to determine if directing injury forces through different components of brain ECM-cell linkages elicit differential injury levels. In doing so, we can answer the question of whether the ECM composition of neuronal microenvironments can explain the differences in injury susceptibility of certain neurons and thus clarify the multi-focal distribution axonal injury observed in DAI.

4.2 Results

4.2.1 ECM Expression in the Brain

Reports of brain ECM immunolabeling are rare and none are sufficient to provide a complete understanding of what ECM are in closest proximity to the axon. In fact, the most quantitative analysis was performed in the mouse with labeling of only 4 components and a semi-quantitative scoring method [64]. Therefore, we performed a series of immunolabeling studies in which we attempted to immunostain the predominant brain ECM components in both tissue sections from adult rat (Fig. 4-2A,B) as well as in mature neuronal cultures at DIV 14-21 (Fig. 4-2C,D). We successfully labeled multiple classes of brain ECM in both tissue and cell culture verifying that components such as TnR, CSPGS, and HA are present. We also observed varying staining patterns that are typically characterized by sparsely labeled neurons with increased density near the soma and perisomatic extensions. These results are consistent with those previously published in the literature. We attempted to further characterize the distribution

78
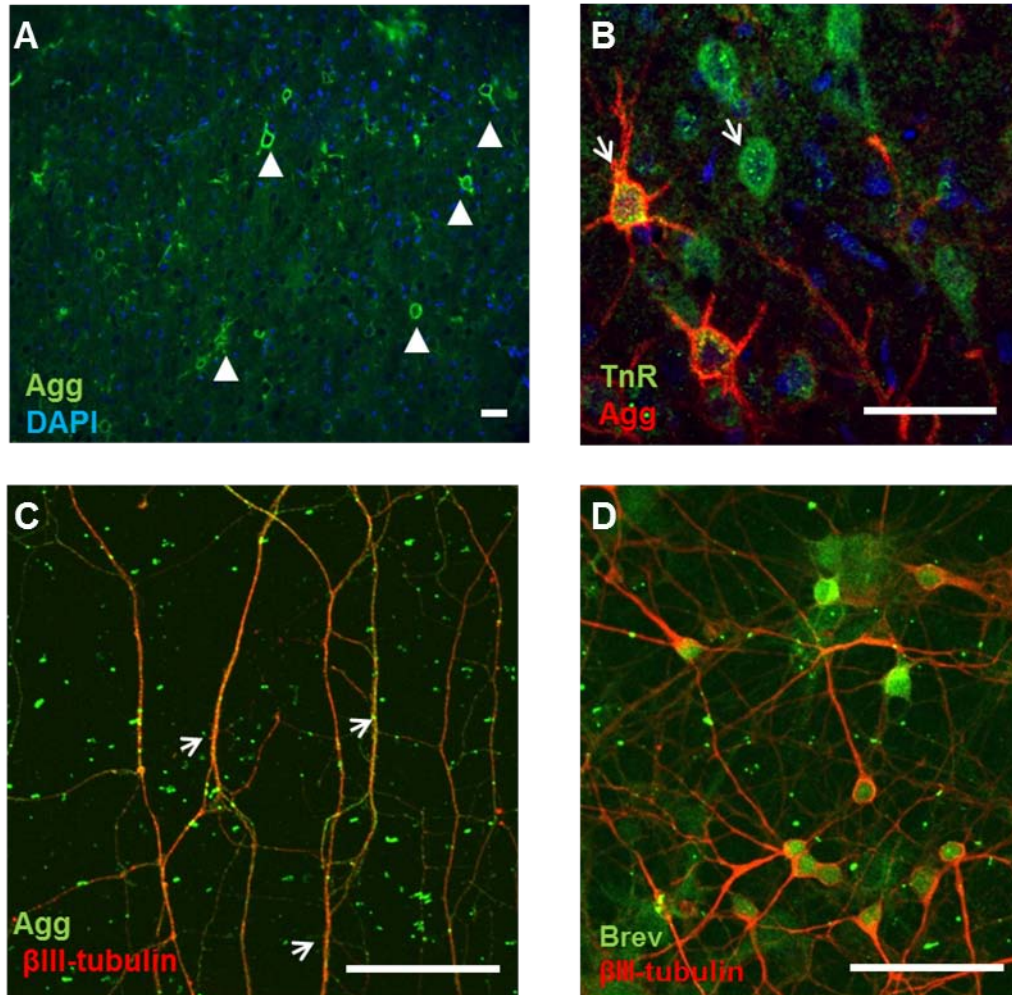
Figure 4-2: Immunolabeling of Brain ECM Molecules.
Adult rat tissue sections indicate ECM distribution of **(A)** Aggrecan and the dual localization of **(B)** Aggrecan and Tenascin-R. Mature neuronal culture DIV 14-21 indicate the presence of **(C)** Aggrecan and **(D)** Brevican near neurons (indicated by β_3 Tubulin). All scale bars indicate 100 µm.

of specific components using colocalization, especially in regions nearest the axon. Unfortunately, the large degree of variability in staining patterns and difficulty in obtaining multiple antibodies resulted in the inability to quantitatively measure which components are predominantly localized near the axon. Instead of pursing a detailed immunolabeling study of brain tissue, we decided to utilize a range of brain ECM molecules in the subsequent axonal injury studies.

79

4.2.2 Brain ECM Dependent Axonal Injury Rates

Since multiple forms of ECM exist in the brain, we sought to determine the effect on axonal injury susceptibility when trauma forces are directed through a specific type of ECM. To do so, we utilized the Magnetic Twisting Cytometry (MTC) model of axonal injury wherein the microbeads were coated with a specific type of ECM (Fig. 4-3A). Coating of microbeads with each type of brain ECM was verified by fluorescently tagging the molecules prior to binding. Subsequently, the microbeads were imaged (Fig. 4-3B) and fluorescence levels were compared to that of stock beads to ensure fluorescence was due to the tagged ECM (Fig. 4-3C).

In order to determine if the brain ECM microbead coating affected axonal injury susceptibility, we performed multiple injury studies using either Bovine Serum Albumen (BSA), Acetylated Low Density Lipoprotein (LDL), FN, TnR, Brev, Agg, or HA coated beads. All microbeads were coated with BSA following their respective ECM coatings. Microbeads coated solely with BSA served as a control to account for potential interactions between the microbead surface and cell surface receptors. LDL coated beads served as another control condition as LDL is known to bind to a cell membrane receptor that influences metabolism but that does not serve as a CAM, and therefore represents non-adhesion binding proteins. The remaining ECM types are all found in the adult brain and represent multiple classes of brain ECM.

Axonal injury experiments consisted of a precise protocol in which the only variation was due to the microbead coating. Experiments began by seeding coated microbeads onto a neuronal culture coverslip at a concentration that was verified to ensure maximum coverage of the coverslip. This number was initially estimated based on the coverslip area and experimentally verified to be ~5 million microbeads. The experimental protocol is illustrated in Figure 4-4.
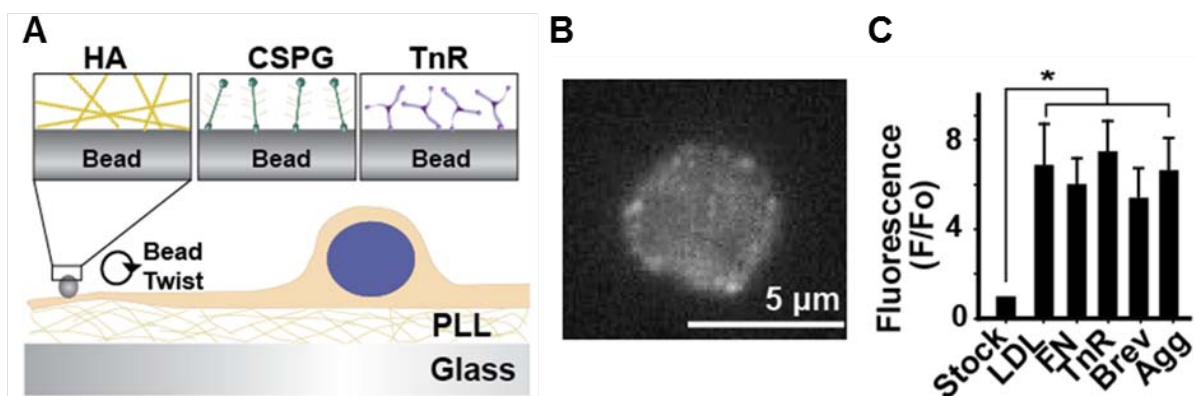
Figure 4-3: Labeled ECM Coated Microbeads.
(A) Schematic illustration indicates how MTC can be used to control the local ECM through which forces are directed to neurons. **(B)** Verification of ECM coating on the microbeads was accomplished using immunofluorescence which indicated **(C)** a significant increase in fluorescence levels compared to control beads when fluorescently tagged proteins were adhered to the microbead surface. All bars SEM for all panels, * $p < 0.05$.

Figure 4-4: Axonal Injury Experimental Protocol.
A precise protocol was followed to induce axonal injury. Microbeads were initially seeded at a density of ~5 million beads per coverslip or ~65 thousand per mm^2. Following seeding, neurons underwent a precisely timed sequence of bead magnetization, neuronal labeling, and imaging. The protocol produced a time series consisting of 15 minutes of pre-twist data followed by 60 minutes of post-twist data.

Following injury experiments, a large data set was generated that was characterized by multiple independent variables. In order to properly determine the effects attributed to bead coating, we had to also account for variability due to additional factors such as presence of the bead, time, and axon width. To do so, we initially pooled the entire data set and determined if there were significant differences in any of these main effects. We found that adhering ECM-

coated microbeads (without twisting) was not sufficient to cause changes in NSGS levels (Fig. 4-5A). However, when the beads were twisted, we did find a significant increase in the NSGS value indicating that microbead twisting did induce axonal injury. Next, we identified a significant difference in the time course of axons subjected to bead twist compared to those that experienced no twist (Fig. 4-5B). There was a small increase in the NSGS value for the no twist condition in time, however, this can likely be attributed to normal fluctuations in axon morphology. Finally, we found that the average initial width of the axon segment also affected its NSGS level. Significant differences were found between the no twist and twist conditions in axons whose initial average width was between 1.25 and 2.25 µm but not in those with widths between 2.25 and 2.75 µm (Fig. 4-5C). Therefore, variations in the NSGS level were found to depend upon bead twist, time, and initial axon width.

After identifying multiple sources of variance in our data set, we then sought to address our primary hypothesis. This is consistent with asking whether there are significant differences in NSGS values that can be attributed to microbead ECM coating, taking into consideration bead twist, time, and initial axon width. We found that when variance due to time and axon width was accounted for, there was no significant difference between ECM coatings when microbeads were adhered but not twisted (Fig. 4-5D). When microbeads were twisted, we did observe a significant difference in NSGS levels attributed to ECM coating (Fig. 4-5E). Specifically, we found no difference between control microbeads coated only with BSA or LDL indicating that directing forces either non-specifically or through non-adhesion receptors did not increase injury levels. FN, TnR, and Brev coated microbeads all exhibited increased injury levels, significantly greater than the other bead coatings, with TnR eliciting the largest degree of injury. Neither Agg
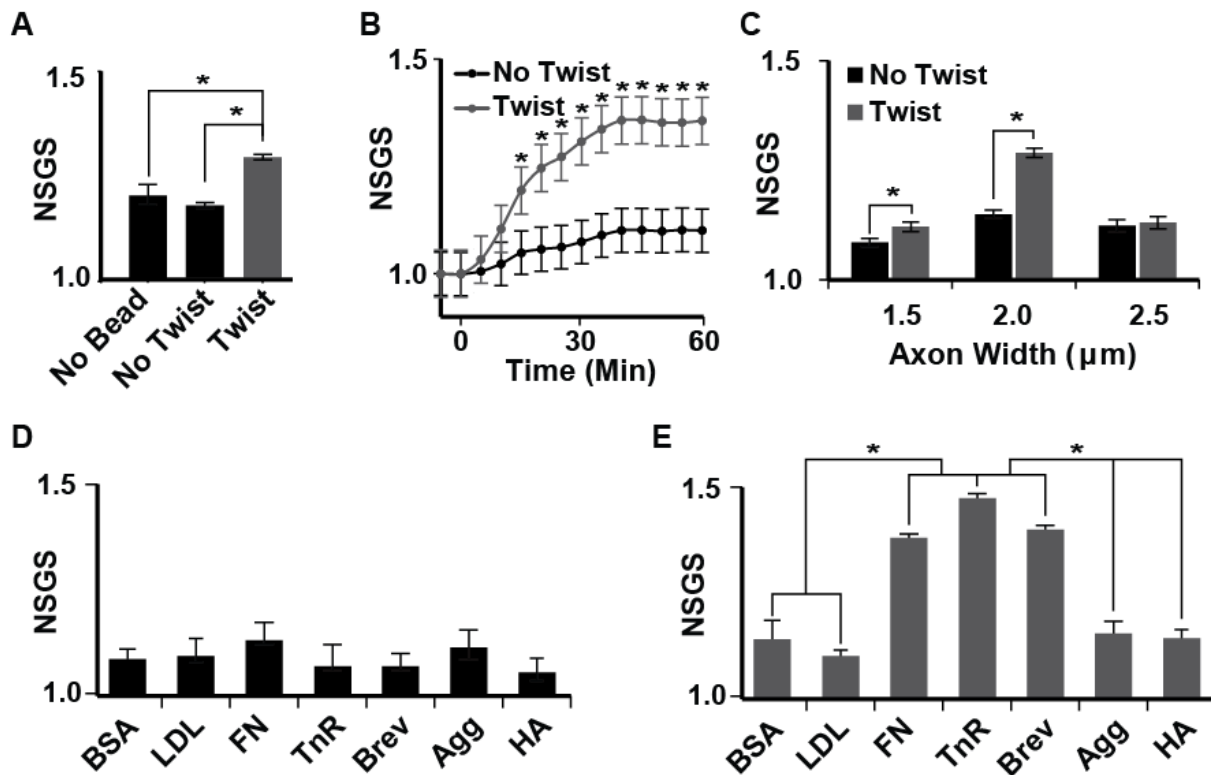
Figure 4-5: Brain ECM Dependent Axonal Injury.
The extent of axonal injury induced by MTC was compared across multiple independent variables. **(A)** Initial tests ensured that there was no statistical difference in samples subjected only to the presence of adhered microbeads. However, when those microbeads were twisted, injury levels did increase significantly. **(B)** Injury levels were also shown to depend upon time following the bead twist. An average onset time of injury can be observed around 10 minutes post twist. **(C)** Injury levels were also shown to depend upon the average initial axon width. These results indicate that axons with lower initial widths are more susceptible to injury compared to their larger counterparts. After controlling for the multiple conditions that contribute to variation in the axonal injury data set, we identified **(D)** no injury dependency on bead coating in samples that were not subjected to bead twist, however **(E)** we did detect a dependency in samples that were subjected to bead twist indicating that certain brain ECM coatings resulted in higher levels of injury. Statistics analyzed using multi-way ANOVA followed by Post hoc Bonferroni pairwise comparison ($\alpha=.05$). All bars SEM.

nor HA coated microbeads elicited injury levels significantly above control or non-adhesion coatings. Taken together, these results suggest that the local ECM composition through which forces are directed to neurons can influence the susceptibility to injury. Furthermore, whether the specific ECM component exhibits affinity for CAMs may be an important factor in determining how injurious the localized forces are to the neuron.

4.2.3 Integrin Dependent Axonal Injury Rates

In order to determine if directing forces through integrins is sufficient to cause axonal injury, we again utilized the MTC model of axonal injury (Fig. 4-6A). Instead of attaching various ECMs to the microbead surface, we instead used the same chemistry to covalently attach integrin antibodies (Abs) for specific subunits. We verified the existence of receptors for specific Abs to be used in injury experiments by immunolabeling neuronal cultures. Two different integrin antibodies to β1 and β3 subunits successfully labeled neurons as well as the axon only regions of the coverslip (Fig. 4-6B). These results indicate that both β1 and β3 integrin subunits are expressed *in vitro* and furthermore that they localize to the axons.

After verifying that both of the β integrin subunits were expressed in axons of our neuronal culture, we attempted to determine their influence on microbead binding. Of the three brain ECM molecules that produced the largest injury rates in previous studies, FN is the best known and most widely studied as an integrin binding ECM. To determine if FN coated microbeads are interacting with integrin subunits in our cultures, we performed Ab blocking experiments in which 1 µM of either β1 or β3 integrin Ab was incubated with the neuronal cultures prior to addition of microbeads. After 30 minutes of incubation, non-adhered beads were gently removed by placing a permanent magnet in the solution above the coverslip surface. The percentage of the coverslip area covered by axons that remained covered by adhered beads was compared to control samples that contained no blocking Ab. We found that with the addition of either β1 or β3 antibody, the amount of bead coverage may be slightly reduced, however, the results contained too much variance to draw a definitive conclusion. Future experiments such as these will be necessary to determine the extent of interaction between specific ECMs cell surface
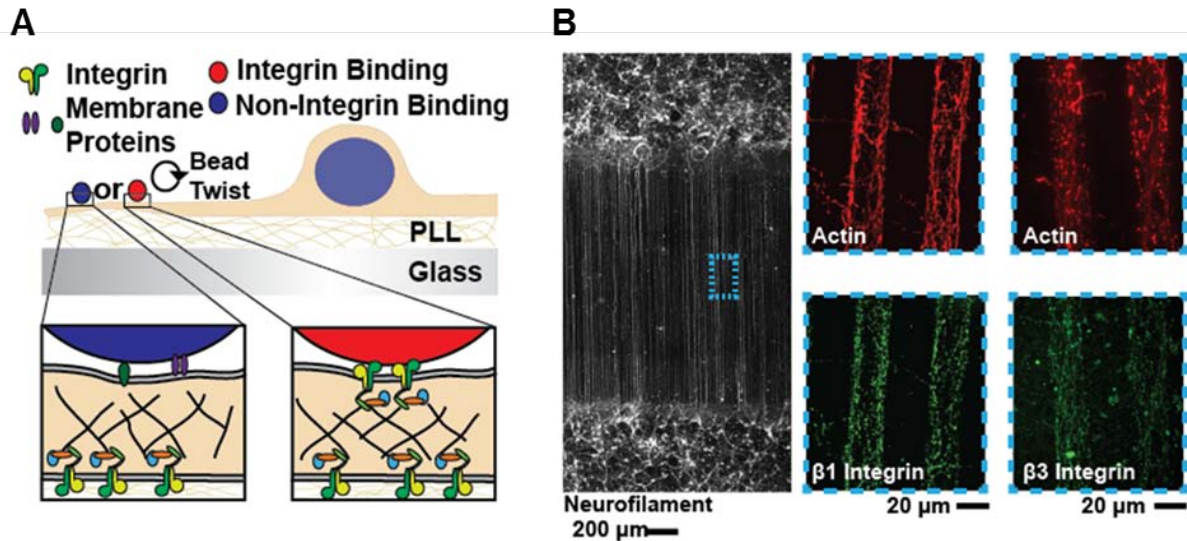
Figure 4-6: Integrin Ab Staining In Axon Rich Regions.
(A) Schematic illustration indicates that integrin binding beads will couple directly into the cytoskeleton whereas non-integrin binding beads will interact with cell surface receptors that do not couple into the cytoskeleton. **(B)** Immunostaining for the presence of integrins in the axon only region of neuronal cultures indicates that both β_1 and β_3 integrins are expressed *in vitro* in axons.

receptors.

Given the shortcoming of directly measuring the effects of integrin blocking Abs on ECM mediated injury, we sought to measure injury levels elicited by directing injury forces specifically through integrins. To do so, we utilized the MTC injury model with microbeads coated with antibodies to either $\beta1$ or $\beta3$ integrins. Experiments were performed as previously indicated. We found that neither $\beta1$ nor $\beta3$ integrin Ab coated beads induced injury when microbeads were adhered but not twisted (Fig. 4-7A). However, following microbead twist, an increase in NSGS levels was observed (Fig. 4-7B). $\beta1$ integrins elicited injury levels that were slightly elevated compared to both control and non-adhesion receptors coatings, however these levels were not statistically different. We did observe statistically greater NSGS levels elicited by $\beta3$ integrin Ab coated microbeads. Moreover, these injury levels were greater than both control and non-adhesion coatings as well as that of the $\beta1$ induced levels. Therefore, this data
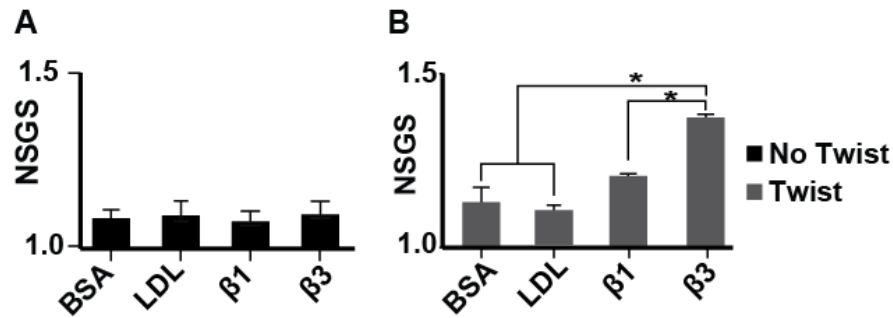
Figure 4-7: Integrin Mediated Axonal Injury.
Axonal injury levels elicited by localizing injury forces through specific integrin subunits were measured. **(A)** No significant differences were observed simply by binding coated microbeads to neurons. **(B)** Injury rates elicited by β_3 integrin bound microbeads were found to be significantly elevated following bead twist compared to control coatings, non-adhesion receptor coatings, and β_1 integrin coatings. Statistics analyzed using multi-way ANOVA followed by Post hoc Bonferroni pairwise comparison ($\alpha=.05$). All bars SEM.

indicates that directing forces through integrins is sufficient to induce axonal injury. Furthermore, the specific subtype of integrin receptor may influence susceptibility to injury.

4.3 Discussion

In this chapter, we explored the implication of focal adhesions and mechanochemical coupling in TBI by asking whether specific cell-ECM adhesions mediate axonal injury. The composition of ECM surrounding a cell has been tied to both selective CAM binding [133] and differential mechanochemical coupling [250]. This indicates that the local ECM composition can influence not only the cell adhesions that form but also the extent of mechanosensitivity of the cell. Little is known about the brain ECM composition, structure, and specific interactions with cell receptors. Therefore, we chose to test the effect of directing injury forces through the most common components of brain ECM. Here we showed that trauma forces directed through different components of the brain ECM elicit differential axonal injury levels. This result is important because it indicates that susceptibility of axons to injury may depend upon the

composition of the cellular microenvironment.   While susceptibility to axonal injury has previously been tied primarily to mechanics, the potential for an extracellular biological influence at the sub-cellular level has not been reported.

One important implication of an ECM dependent susceptibility to axonal injury is that it may provide an explanation for the diffuse injury patterns observed throughout the brain following TBI. While material properties and tissue structure have been proposed to account for these regional vulnerabilities, differences in the sub-cellular compositions or microenvironments near the injured regions have not. Mapping of the composition and distribution of brain ECM currently established in the literature is insufficient to correlate with brain regions that exhibit elevated injury levels following TBI. Therefore, future studies will be necessary to determine if specific compositions of cellular microenvironments may predispose specific regions to injury induced by traumatic forces.

In addition to understanding where an injury may occur within the brain, these results provide a potential explanation of the diffuse injury patterns that is directly related to the mechanism of injury. We discussed a brief overview of cellular mechanotransduction and highlighted some of the key players, and within this work we have focused on the primary components of the brain ECM. While little evidence exists indicating which brain ECM components exhibit specific affinity for CAMs and which exhibit specific mechanosensitive characteristics, we assumed the potential for mechanochemical coupling due to the extensive literature base focused on integrins and ECM coupling. Some reports have indicated specific binding between brain ECM components and integrins subunits (Table 3), although a comprehensive list is not known.

Table 3: Reported Integrin Binding to Brain ECM

Microbead Coating	Reported Neuronal Integrin Binding
Bovine Serum Albumin (BSA)	Non-specific
Low Density Lipoprotein (LDL)	Non-adhesion
Fibronectin (FN)	$\alpha_5\beta_1$, $\alpha_v\beta_3$
Tenascin-R (TnR)	$\alpha_5\beta_1$
Aggrecan (Agg)	β_1* (CSPG binding)
Brevican (Brev)	β_1* (CSPG binding)
Hyaluronic Acid (HA)	None

Summarized from [228] and [307]

Due to its abundance in different tissues, Fibronectin is the best studied of the ECMs that were tested in our experimental model, and as such its interactions with integrins have been widely documented [147,72,62]. While FN may not be as predominant as HA, CSPGs, or TnR in the brain, its interactions with specific integrins, such as the $\alpha_5\beta_1$ and $\alpha_v\beta_3$ subunits known to be expressed in the brain is the best established. Interestingly, TnR is similar in structure to FN, although somewhat less complex [58], but its specific interactions with integrin subunits are much less documented. Nevertheless, there is at least some evidence that suggests the potential for direct interaction with specific integrin subunits for all the primary components of the brain ECM in this study except for HA (summarized in Table 3). Interestingly, FN and TnR exhibited some of the highest injury levels and are also the most established integrin binding ECMs. Brev also exhibited elevated injury levels even though its potential for integrin binding is less established. While this data certainly cannot definitively point to integrins as the mechanosensors, it presents a strong argument that CAMs such as integrins likely potentiate

axonal injury. Interestingly, when injury forces were directed through specific integrin subunits, injury levels were much lower for β_1 integrins compared to FN, TnR, and Brev. However, injury levels elicited by forces directed through β_3 integrins did induce injury levels similar to that of these ECMs. Multiple explanations may exist for these differences: (1) Differences in mechanical strength of ligand-receptor interactions between ECM and antibodies, (2) Differences in the activation state of integrins bound by antibodies as opposed to ECM, and (3) Differences in amount of ligand present on microbead surface between ECM and antibody. Therefore, future studies will be necessary to directly conclude that integrins are the mechanosensors as well as specifically which subunits are implicated. However, the current results due indicate a likely injury mechanism by which exogenous forces are directed through specific ECM to mechanosensitive integrins.

In this chapter, we have focused on the potential for the ECM composition surrounding neurons to influence axonal injury levels. Our findings suggest that variation in injury vulnerability at the cell and sub-cellular level may be due to differences in the ECM composition of the cellular microenvironment. While the cellular microenvironment is influenced by multiple factors, ECM composition may be especially important in TBI due to its potential influence on cellular mechanosensitivity. ECM-cell adhesions are known to be critical to maintaining neuronal structural integrity and therefore provide conduits for distributing mechanical force throughout the cell. It is this specificity that provides the unique mechanosensitive functionality of CAMs and their associated intracellular proteins. While we are limited in our current understanding of the exact cell-ECM linkages within the brain, our findings indicate that specific linkages affect vulnerability to axonal injury and likely provide an injury mechanism that is

linked to mechanochemical coupling that influences the neuronal response to exogenous mechanical force.

4.4 Materials and Methods

4.4.1 Ethics Statement

All procedures were approved by the Harvard Animal Care and Use Committee under Animal Experimentation Protocol permit number 24-01. This protocol, entitled "Harvest and Culture of Neural and Cardiac Tissue from Neonatal Rats and Mice for In Vitro Disease Models," meets the guidelines for the use of vertebrate animals in research and teaching of the Faculty of Arts and Sciences of Harvard University. It also follows recommendations included in the NIH Guide for the care and use of laboratory animals and is in accordance with existing Federal (9 CFR Parts 1,2&3), state and city laws and regulations governing the use of animals in research and teaching.

4.4.2 Neuron Harvest and Culture

Cortical neurons were isolated from 2-day old neonatal Sprague-Dawley rats (Charles River Laboratories, Boston, MA). Harvest protocol was established from Brewer et al., 2007 [38]. Stamp mask technique (Chapter 3) was utilized to form anisotropic substrates with regions of isolated axons. Neurons were cultured for 14-17 days post-harvest.

4.4.3 Immunolabeling of Brain ECM in Tissue Slices

Adult female Sprague-Dawley rats (Charles River Laboratories, Boston, MA) were euthanized using a combination of CO_2 and cervical dislocation. Brains were immediately extracted and placed on ice. Coronal tissue slices at ~30 µm thick were taken sequentially using a custom built tissue slicer. Slices were fixed in 4% paraformaldehyde and 2.5% TritonX-100 in

90

PBS at 4°C for 24 hours. Primary antibodies for Aggrecan, Brevican, and Tenascin-R were incubated at 200 ug/ml in 1% Bovine Serum Albumin (BSA) (Jackson ImmunoResearch, West Grove, PA) in PBS for 1 hour. Secondary antibodies were subsequently incubated at 200 ug/ml in 1% BSA for 1 hour. Immunolabeled tissue slices were mounted and preserved in ProLong Gold Antifade reagent (Invitrogen) and stored at -20°C until imaging. Imaging was performed on an Olympus IX83 Platform with a Hamamatsu Spinning Disk Confocal (Olympus).

4.4.4   Verification of Microbead Coating

Microbead coating with various ECM was verified using immunofluorescence. ECM was initially labeled with a fluorescence tag by incubation with TFM. Unbound dye was subsequently removed using dye removal columns. Labeled ECM was adhered to microbeads using the standard microbead coating protocol (outlined in Chapter 3). Coated microbeads were imaged using an Olympus IX83 Platform with a Hamamatsu Spinning Disk Confocal (Olympus) and fluorescence levels were measured using the same laser intensity and exposure time for each bead coating. Fluorescence levels of control coatings in which no protein was initially added were used to determine base line levels of fluorescence. Microbeads with fluorescence levels significantly greater than control beads were considered coated with ECM.

4.4.5   Immunolabeling Axonal Integrins

Cells were washed 3 times in PBS at 37°C and fixed for 1 minute in 4% paraformaldehyde at room temperature. Cells were then washed 3 times in PBS and an initial blocking step using 5% Bovine Serum Albumin (Jackson ImmunoResearch, West Grove, PA) in PBS was performed for 1 hour at 37°C. The blocking solution was aspirated away and the primary antibody solution was immediately added and incubated for 1.5 hours at room temperature. The primary antibodies used were either anti-β1 integrin (1:200) or anti-β3 integrin

(1:200). Primary antibodies were added to a 0.5% BSA in PBS solution. Following primary staining, cells were washed 3 times, and the secondary staining solution consisting of either goat anti-mouse conjugated to Alexa-Fluor 488 4', 6-diamidino-2-phenylindole (DAPI), and 488 Phalloidin (1:200) (Invitrogen) were added to the cells for 30 minutes at room temperature. Samples were then washed 3 times. ProLong Gold Antifade reagent (Invitrogen) was added to preserve the samples and glass coverslips are affixed using nail polish. Prepared slides were stored at -20°C. Olympus IX83 Platform with a Hamamatsu Spinning Disk Confocal (Olympus).

4.4.6 Microbead Binding to Neurons

Following coating, microbeads were seeded at a density of ~5 million beads per coverslip or ~65 thousand per mm^2. This number corresponded to a saturating coating in which the maximum coverslip area was covered by microbeads. Following microbead seeding, neuronal cultures were returned to the incubator for 30 minutes to allow the formation of adhesions between microbeads and the cells.

4.4.7 Calcein Labeling of Neurons

Neurons were fluorescently labeled using Calcein (Invitrogen). Stock Calcein was reconstituted in 10% pluronic solution in DMSO (Invitrogen) at a concentration of 50 µg in 50 uL. For labeling, 4 uL of Calcein solution was added to 1 mL of imaging media and incubated with the neurons for 2 minutes at room temperature. Neurons were rinsed gently 3x with fresh imaging media followed by a 2 minute rest period and then rinsed 3x again. Neurons were incubated at 37°C for 30 minutes prior to imaging to allow fluorescence levels to stabilize.

4.4.8 Axonal Injury Experiment

Axonal injury experiments followed a precise protocol that is outlined in Figure 4-4. Microbeads are initially adhered to neurons and allowed to incubate for 30 minutes. Neurons were then rinsed gently 3x with imaging media. All media except for 100 uL retained in the central area of the live imaging dish was removed and neurons were carefully transferred to the magnetizing coil while minimizing mechanical perturbation due to motion. Microbeads were then magnetized by a single pulse of ~.1 T parallel to the length of the axon only region. Neurons were subsequently moved to the imaging chamber and 1 ml of imaging media was added. After 30 minutes, neurons were labeled with Calcein. Following another 30 minute period, multiple regions (5-10 fields of view were typical) were designated. Each region was imaged for 10 minutes at 5 minute intervals generating a time lapse of pre-twist images. If samples were to be injured by microbead twist, they were then subjected to a single pulse ~.01 T oriented orthogonally to the magnetizing field. High speed imaging at 50 FPS in brightfield verified rotation of microbeads. Neurons were then imaged again every 5 minutes for 60 minutes generating a time laps of post-twist images. Following live imaging, time lapse images were subjected to post analysis.

4.4.9 Post Processing of Axonal Injury Data

Axonal injury data (time lapse images) was analyzed using custom axon morphology analysis software developed in both ImageJ and Matlab. This process is described in Chapter 3.

4.4.10 Statistical Analysis

Statistical analysis was performed in Matlab following the post processing automated analysis of axon morphology. A multi way ANOVA test was initially used to determine if differences in mean values attributed to independent variables existed. If so, subsequent

pairwise comparisons were run using post hoc Bonferroni analysis to identify differences in main effects. Statistical tests were limited to 3 independent variables due to technical limitations of the software package. Tests were run multiple times with different groupings of independent variables to test necessary comparisons. $\alpha = .05$ for all analyses. All error bars are standard error of the mean.

5   Conclusions

5.1   Importance of Implicating Focal Adhesions and Extracellular Matrix in Axonal Injury

5.1.1   Interpretation of Results

Current limitations in understanding diffuse brain damage associated with TBI may be a result of the complex interactions between mechanical forces and biological structures within the brain.   Previous studies aimed at identifying the cellular mechanisms underlying TBI have tended to focus on the non-specific application of force to tissue or cells within the brain.   In contrast, here we have suggested that a mechanical insult could utilize the extracellular matrix (ECM), cell adhesion molecules (CAMs), and the cytoskeleton as specific conduits through which forces are directed to mechanosensitive focal adhesions (FAs) within the intracellular space (Fig. 5-1).   Although the concept of mechanotransduction, a general process by which force is converted to chemical signaling, is by no means novel to TBI research, here we have focused on a specific class of cellular mechanotransduction previously unexplored in the context of TBI.

Beyond transient membrane tearing, pathological mechanotransduction processes remain relatively unexplored in TBI.   In this dissertation, we have implicated mechanosensitive sub-cellular structures in axonal injury by employing *in vitro* models designed to control the density of FAs through which injurious forces are delivered to neurons.   Using an *in vitro* uniaxial stretch model, we showed that modifying the FA density can influence the percentage of injured neurons, identified by morphological swellings similar to those observed in DAI *in vivo*.   This suggests that the neuronal adhesions to the ECM are an important factor in initiating injury.   Since FAs serve as attachment sites for the cell, it is not surprising that they may influence cellular mechanical events.   However, since FAs also provide sites of mechanochemical

coupling, they may provide a means by which neurons 'sense' trauma forces associated with TBI.

We showed evidence that inhibition of Rho-Associated Kinase (ROCK), a downstream effector of Rho-GTPases, was able to significantly reduce stretch induced injury levels. Activation of Rho-GTPases may initiate at the FA suggesting that these pathways may be activated in neurons following an acute mechanical strain. In addition to supporting mechanochemical coupling at the FA as an injury mechanism, these findings are promising because they present a novel, potential strategy for treating axonal injury. There are currently no therapeutic options for TBI and, even more troubling, there are few treatment strategies that have exhibited promising neuroprotective results. On the other hand, much is understood about the vast signaling capabilities of the FA as well as the extensive physiological pathways they influence [159]. Determining if and which of these pathways play critical roles in TBI may identify numerous targets for pharmacological intervention. Therefore, implicating ROCK signaling in axonal injury presents not only an additional drug target, but more importantly it provides a potential link to the wealth of knowledge within the field focusing on cellular mechanotransduction.

Building on these results, we sought to determine the effects of modifying the extracellular conduit that localizes forces to FAs. To do so, we directed forces through different brain ECM to affect the cell-ECM linkages through which neurons 'sensed' trauma. Using a Magnetic Twisting Cytometry (MTC) injury model, we found that forces directed through Tenascin-R, Brevican, and Fibronectin resulted in elevated injury levels compared to Aggrecan or Hyaluronic Acid. These results indicate that differences in the ECM content of the local cellular microenvironment may affect neuronal susceptibility to injury potentially due to the resulting
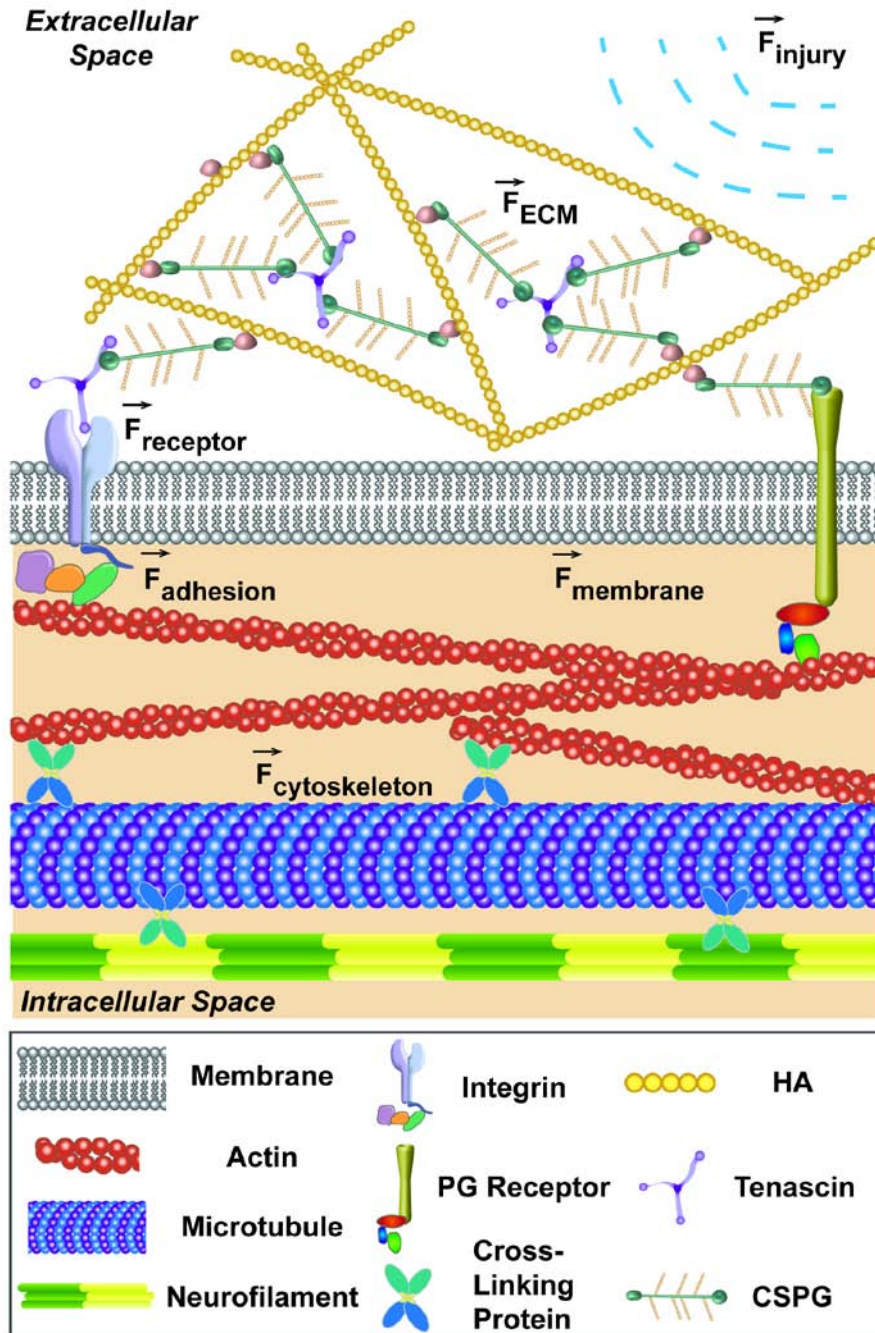
Figure 5-1: Injury forces may be transmitted through mechanosensitive sub-cellular structures that regulate cellular architecture.
The intracellular space is mechanically coupled to the extracellular space through components such as the cytoskeleton, transmembrane CAMs, and ECM. A dynamic force balance exists within cells whereby forces on intracellular components balance forces on extracellular components dictating cellular structure. Cells can respond to external mechanical cues by sensing alterations in this balance through mechanosensitive structures that respond by activating signaling pathways, many of which remodel the cytoskeleton to redistribute forces. A mechanical insult suffered during TBI could alter this force balance by changing the forces distributed throughout the structural elements of the ECM, CAMs, and cytoskeleton.

differences in cell-ECM adhesions. Interestingly, when forces were localizing through non-specific adhesions using either bovine serum albumin or low density lipoprotein coatings, injury levels were low and on the same level as that induced by both Aggrecan and Hyaluronan. Therefore, directing forces specifically through adhesion receptors may be an important factor in initiating axonal injury, potentially because only these adhesions exhibit mechanochemical coupling.

To further implicate the importance of forces directed through cell-ECM adhesions, we measured injury levels elicited by localizing forces through integrins. We again utilized the MTC injury model to determine that directing forces though β integrins, specifically β_1 and β_3 subunits, was sufficient to induce axonal injury. These results indicate that directing injury forces specifically through CAMs such as integrins may be a predominant component of axonal injury and support the implication of FAs in axonal injury. Furthermore, forces directed through β_3 subunits resulted in elevated injury levels compared to forces directed through β_1 subunits. This result suggests that the subtype of integrin may influence vulnerability to injury potentially by influencing the extent of mechanochemical coupling that occurs at the adhesion. Taken together, these findings are important because for the first time, they implicate a family of known mechanosensitive sub-cellular structures in TBI.

5.1.2 What Evidence Supports Cellular Mechanotransduction in TBI

Several previous reports support the implication of cellular mechanotransduction events in TBI. A rapid deformation of 3D collagen gels resulted in a reduction in embedded neuronal viability when collagen concentration was increased, suggesting a potential influence of cell-matrix interactions on injury [69]. The actin cytoskeleton and its regulatory pathways have also been implicated in axon degeneration by reports showing intrinsic activation of Rho signaling

pathways in response to trauma in the optic nerve, increased localization of RhoA with F-actin rich swellings in primary hippocampal neurons, and upregulation of RhoA in both rats subjected to fluid percussion brain injury and in stretch injured organotypic hippocampal slices [100,75,82]. Cytoskeleton and membrane associated proteins such as integrins have been previously hypothesized to influence the axonal morphology associated with DAI in peripheral nerve fibers as well [216]. Evidence also suggests neurite retraction exhibits a strain dependent response that is regulated by stretch sensitive channel activity [95], and mechanically initiated sodium influx has been shown to occur in neurons subjected to rapid stretch *in vitro* [305]. Interestingly, integrins have been linked to these stretch activated channels in sensory neurons and other cell types [174,70]. Therefore, evidence for the involvement of mechanotransduction events beyond transient membrane rupture is emerging, however, future studies are necessary to elucidate and link these components of injury.

In addition to the immediate contribution of mechanotransduction, there is evidence that suggests possible long term cellular changes initiated by mechanical events. Alterations in protein expression have been observed in neurons exposed to a single rapid stretch in which sodium channel expression was greatly increased 24 hours following trauma [315]. This increase in channel expression was linked to an increased susceptibility to subsequent injury. In our lab, we previously showed that vascular smooth muscle cells subjected to a single, rapid stretch exhibited altered calcium handling followed by a phenotypic switch to either contractile or synthetic states depending upon the magnitude of stretch [7]. Furthermore, the increased contractility was mitigated by immediate treatment with a ROCK inhibitor, providing additional evidence for the involvement of Rho-signaling following stretch induced injury. In addition to

providing a potential explanation for the vasospasm observed following blast TBI, these studies illustrate the potential long term effects of cellular remodeling due to a single mechanical event.

The major importance of this research lies in the potential identification of mechanical activation of specific signaling pathways, termed mechanochemical coupling, that likely accompany the initial trauma. Since much of the morbidity associated with TBI is now correlated with progressive degeneration attributed to diffuse damage in the brain, identification of relevant biological signaling pathways is critical for therapeutic intervention. While a few secondary injury cascades associated with diffuse injury such as DAI have been identified, there remain few treatment strategies and no approved pharmacological agents to mitigate this damage. Although potential treatment options such as membrane resealing agents like Poloxamer 188 have shown promising results in animal studies, experimental evidence suggests this may not be the only mechanism leading to diffuse damage. A search of all current and previous NIH clinical studies (performed on 9/25/13 at clinicaltrials.gov) revealed only 10 candidate therapeutics for mTBI, none of which directly target a mechanotransduction mechanism. On the other hand, many therapeutic options currently exist that target cellular mechanotransduction pathways. It is our intent that by applying the current knowledge and principles of cellular mechanotransduction to TBI, future studies may elucidate underlying mechanisms and therapeutic strategies previously unexplored in the context of TBI.

5.2 Limitations of Current Studies and Suggested Future Directions

Herein we have focused on implicating cell-ECM adhesions and their potential to localize forces to mechanosensitive FAs that mediate axonal injury. As we believe this represents a critical advancement in understanding the mechanisms underlying TBI, we also acknowledge that many of our conclusions rely on previous work to connect the dots. Furthermore, much of

the previous work relied on was not conducted in neurons nor verified in the adult central nervous system. While the results reported previously have broad implications, several key limitations must also be addressed.

The initial high speed stretcher studies were intended to minimize deviation from prior *in vitro* TBI studies while incorporating only a small change to study the effect of FAs. In doing so, potential changes due to culturing of neurons on different ECM could not be controlled. While we reported clear differences in FA coverage due to culturing on either Poly-L-Lysine (PLL) or Fibronectin (FN) surfaces, we did not account for potential changes in gene expression or cytoskeleton organization that could also depend upon ECM composition. While it is impossible to control for all biological variation, the particular importance of a consistent culture substrate was a primary motivation for moving to the MTC injury model in which all neurons are cultures similarly prior to injury experiments. Moreover, the global strain induced by substrate stretch is insufficient to localize forces through FAs. We did establish a direct link between adhesion strength and vinculin density (data published in [126]), yet we cannot control for non-specific interactions between cell membrane bound structures and the substrate. Furthermore, multiple mechanisms exist by which mechanical forces are transduced within the cell [185], and, while we have focused on FAs, it is possible that cytoskeleton prestress or changes in the force balance between the cytoskeleton and the ECM post stretch could also provide potential mechanosensitive responses. Therefore, the high speed stretcher experiments provided minimal deviation from established models of TBI, yet presented limitations to isolating the effects of cell-ECM adhesions.

In order to minimize the influence of culture conditions and global strain, we sought to adapt MTC to use as an *in vitro* model of axonal injury. Moving to this mode of mechanical

101

stimulus presented several important limitations as it represented a clear deviation from previously established models of axonal injury and most importantly a clear link between the magnitude of mechanical insult. Whereas strain magnitude and rate were relatively easy to measure in the high speed stretcher experiments, measuring the exact mechanical stimulus produced by the MTC injury model presented many challenges. Although this technique has been previously used to measure mechanical properties of cellular structures, individual measurements are typically acquired by averaging multiple cycles of bead twisting with highly sophisticated magnetometer setups and noise minimization techniques [294]. Incorporating these strategies to measure the mechanical stimulus provided by a single bead twist was deemed beyond the scope of this study as both a magnitude and rate dependency of mechanical stimuli has been previously reported in axonal injury studies. Nonetheless, approximate magnitudes were provided and the potential for future studies to focus on specific force responses using this model is possible.

Although we have provided a detailed description of the known brain ECM content and organization from the literature as well as additional immunostaining of both tissue sections and cell culture, it is clear that a comprehensive understanding is far from complete. Numerous classes and sub-types of ECM molecules have been reported to exist in the brain and even an organized structure is beginning to emerge. A key question remains in elucidating the specific ECM content and respective CAM binding that exists in axons, and moreover how this may differ in myelinated and non-myelinated axons. Therefore, while we have identified specific ECM that may result in elevated sensitivity to mechanical forces, additional information about where this ECM occurs within the brain is necessary to determine if it can fully account for the regional susceptibility and multi-focal patterns observed in DAI [34]. *In vivo* studies are also

likely necessary to account for other differences in cellular microenvironment that were not considered here such as soluble factors or multicellular architecture.

Finally, we presented evidence that brain ECM may direct forces through integrins and that this may be sufficient to induce axonal injury. Integrins are the best studied class of CAMs and have been widely implicated in mechanosensitive pathways in multiple cell types [133,299] and were therefore the logical choice with which to begin. By implicating integrins, we by no means suggest they are solely responsible for distributing forces that are injurious to neurons, but instead suggest they may represent a predominant conduit for force transmission, especially in the case of mild insults, that may provide a means by which neurons can actively respond to the mechanical insult. From our current results, we cannot rule out additional mechanotransduction events, and in fact, suggest that TBI likely causes cellular damage through multiple mechanisms. While the evidence reported herein represents only the initial studies necessary to determine if mechanochemical coupling at the FA causes axonal injury, we believe that it is a promising target for future studies and should provide a foundation for future research.

Both experimental design and interpretation of our findings have relied heavily on previous studies in the field of mechanotransduction. Most of these studies have been performed on non-neuronal cells and those that are performed on neurons tend to focus on the developing nervous system. Even so, there is strong evidence that propagation and distribution of forces through the cytoskeleton is a ubiquitous phenomenon that can initiate mechanotransduction signaling cascades, modulate cytoskeleton remodeling, and even alter ion channel activity without inducing membrane poration [70,208,299]. Interestingly, cytoskeleton remodeling has been shown to occur through integrin mediated activation of Rho signaling proteins that influence microtubule stability and actin dynamics [222,141], providing a potential link to the

103

microtubule breakdown and transport disruption observed in axonal injury. Given the existing evidence that supports the importance of mechanical forces directed through cell-ECM adhesions, future studies aimed at linking integrin mediated cellular mechanotransduction and previously reported secondary injury processes in axonal injury are warranted. These include signaling pathways that regulate cytoskeleton structure and stability such as the class of integrin associated small GTPases including Rho, Rac, and CDC42. We reported a successful decrease in axonal injury using the Rho-Associated Kinase (ROCK) inhibitor HA-1077. ROCK is a downstream effector of Rho and is therefore to our knowledge the first implication of targeting integrin signaling for neuroprotection. While these signaling pathways have been widely studied in non-neuronal cells, future studies will be necessary to determine the effectiveness of targeting pathways to treat TBI.

The diverse content that comprises the brain ECM has the potential to interact with numerous CAMs. While we have focused on integrins and integrin signaling as they are currently the best understood mechanosensors, additional membrane receptors including HAS, CD44, RHAMM, Layilin, and GPI-linked Brevican may also provide conduits into the neuron as they bind directly to HA and may thus serve as a physical link to the brain ECM [97]. Although we found that microbeads coated with HA elicited low injury levels, reports have shown that GPI-linked proteins interact with HA and can transmit extracellular forces to the cytoskeleton [297]. Therefore, while microbeads presented an effective means of controlling the local ECM content, they may not fully recapitulate the native form and extent of adhesion interactions between the neuron and its microenvironment. Furthermore, in addition to the traditional cell-ECM linkages that we have focused on, numerous cell-cell linkages also exist and support structural integrity. Therefore, the existence of brain specific CAMs may provide additional

diversity that influences both the mechanical linkages and mechanochemical coupling that occurs in neurons.

Future studies designed to elucidate the brain specific structures involved in cellular mechanotransduction as well as their associated signaling pathways will improve our ability to understand how the brain responds to exogenous mechanical forces, such as those experienced during TBI. Key aspects to consider include: (1) Identifying the sub-cellular components involved in mechanotransduction within the brain, such as localized ECM and associated CAM expression and binding; (2) Understanding whether heterogeneities in the distribution of mechanosensitive cellular components can explain regional vulnerabilities to TBI; (3) Understanding if these mechanosensitive components can result in activation of signaling pathways that ultimately lead to the secondary injuries associated with TBI.

5.3 Funding Sources

6 References

1. Abbott NJ, Patabendige AAK, Dolman DEM, Yusof SR, Begley DJ (2010) Structure and function of the blood-brain barrier. Neurobiol Dis 37 (1):13-25.
2. Adams JH (1982) Diffuse axonal injury in non-missile head injury. Injury 13 (5):444-445.
3. Adams JH, Graham DI, Gennarelli TA (1983) Head injury in man and experimental animals: neuropathology. Acta Neurochir Suppl (Wien) 32:15-30.
4. Alberts B (1994) Molecular biology of the cell. 3rd edn. Garland Pub., New York.
5. Alenghat FJ, Ingber DE (2002) Mechanotransduction: All Signals Point to Cytoskeleton, Matrix, and Integrins. Sci STKE 2002 (119):pe6-.
6. Alessandri B, Doppenberg E, Zauner A, Woodward J, Choi S, Bullock R (1999) Evidence for time-dependent glutamate-mediated glycolysis in head-injured patients: a microdialysis study. Acta Neurochir Suppl 75:25-28.
7. Alford PW, Dabiri BE, Goss JA, Hemphill MA, Brigham MD, Parker KK (2011) Blast-induced phenotypic switching in cerebral vasospasm. Proc Natl Acad Sci U S A 108 (31):12705-12710.
8. Alford PW, Taber LA (2003) Regional epicardial strain in the embryonic chick heart during the early looping stages. Journal of Biomechanics 36 (8):1135-1141.
9. Amano M, Kaneko T, Maeda A, Nakayama M, Ito M, Yamauchi T, Goto H, Fukata Y, Oshiro N, Shinohara A, Iwamatsu A, Kaibuchi K (2003) Identification of Tau and MAP2 as novel substrates of Rho-kinase and myosin phosphatase. Journal of Neurochemistry 87 (3):780.
10. Angst BD, Marcozzi C, Magee AI (2001) The cadherin superfamily: diversity in form and function. J Cell Sci 114 (Pt 4):629-641.
11. Arfanakis K, Haughton VM, Carew JD, Rogers BP, Dempsey RJ, Meyerand ME (2002) Diffusion tensor MR imaging in diffuse axonal injury. AJNR Am J Neuroradiol 23 (5):794-802.
12. Armonda RA, Bell RS, Vo AH, Ling G, DeGraba TJ, Crandall B, Ecklund J, Campbell WW (2006) Wartime traumatic cerebral vasospasm: recent review of combat casualties. Neurosurgery 59 (6):1215-1225; discussion 1225.
13. Arnadottir J, Chalfie M (2010) Eukaryotic mechanosensitive channels. Annu Rev Biophys 39:111-137.
14. Azevedo FA, Carvalho LR, Grinberg LT, Farfel JM, Ferretti RE, Leite RE, Jacob Filho W, Lent R, Herculano-Houzel S (2009) Equal numbers of neuronal and nonneuronal cells make the human brain an isometrically scaled-up primate brain. J Comp Neurol 513 (5):532-541.
15. Bao HJ, Wang T, Zhang MY, Liu R, Dai DK, Wang YQ, Wang L, Zhang L, Gao YZ, Qin ZH, Chen XP, Tao LY (2012) Poloxamer-188 Attenuates TBI-Induced Blood-Brain Barrier Damage Leading to Decreased Brain Edema and Reduced Cellular Death. Neurochemical Research.
16. Bartsch U, Pesheva P, Raff M, Schachner M (1993) Expression of janusin (J1-160/180) in the retina and optic nerve of the developing and adult mouse. Glia 9 (1):57-69.
17. Bauman RA, Ling G, Tong L, Januszkiewicz A, Agoston D, Delanerolle N, Kim Y, Ritzel D, Bell R, Ecklund J, Armonda R, Bandak F, Parks S (2009) An introductory characterization of a combat-casualty-care relevant swine model of closed head injury resulting from exposure to explosive blast. J Neurotrauma 26 (6):841-860.

18. Bayless KJ, Davis GE (2004) Microtubule depolymerization rapidly collapses capillary tube networks in vitro and angiogenic vessels in vivo through the small GTPase Rho. J Biol Chem 279 (12):11686-11695.

19. Bekku Y, Rauch U, Ninomiya Y, Oohashi T (2009) Brevican distinctively assembles extracellular components at the large diameter nodes of Ranvier in the CNS. Journal of neurochemistry 108 (5):1266-1276.

20. Bendlin BB, Ries ML, Lazar M, Alexander AL, Dempsey RJ, Rowley HA, Sherman JE, Johnson SC (2008) Longitudinal changes in patients with traumatic brain injury assessed with diffusion-tensor and volumetric imaging. Neuroimage 42 (2):503-514.

21. Benson DL, Schnapp LM, Shapiro L, Huntley GW (2000) Making memories stick: cell-adhesion molecules in synaptic plasticity. Trends Cell Biol 10 (11):473-482.

22. Bergsneider M, Hovda DA, Lee SM, Kelly DF, McArthur DL, Vespa PM, Lee JH, Huang SC, Martin NA, Phelps ME, Becker DP (2000) Dissociation of cerebral glucose metabolism and level of consciousness during the period of metabolic depression following human traumatic brain injury. J Neurotrauma 17 (5):389-401.

23. Bernal R, Pullarkat PA, Melo F (2007) Mechanical properties of axons. Physical review letters 99 (1):018301.

24. Bernard-Trifilo JA, Kramar EA, Torp R, Lin CY, Pineda EA, Lynch G, Gall CM (2005) Integrin signaling cascades are operational in adult hippocampal synapses and modulate NMDA receptor physiology. Journal of neurochemistry 93 (4):834-849.

25. Bernick KB, Prevost TP, Suresh S, Socrate S (2011) Biomechanics of single cortical neurons. Acta biomaterialia 7 (3):1210-1219.

26. Bertolotto A, Goia L, Schiffer D (1986) Immunohistochemical study of chondroitin sulfate in human gliomas. Acta Neuropathol 72 (2):189-196.

27. Bertolotto A, Manzardo E, Guglielmone R (1996) Immunohistochemical mapping of perineuronal nets containing chondroitin unsulfated proteoglycan in the rat central nervous system. Cell Tissue Res 283 (2):283-295.

28. Bertolotto A, Palmucci L, Gagliano A, Mongini T, Tarone G (1986) Immunohistochemical localization of chondroitin sulfate in normal and pathological human muscle. Journal of the neurological sciences 73 (3):233-244.

29. Bhattacharjee Y (2008) Neuroscience. Shell shock revisited: solving the puzzle of blast trauma. Science 319 (5862):406-408.

30. Biederer T, Sara Y, Mozhayeva M, Atasoy D, Liu X, Kavalali ET, Sudhof TC (2002) SynCAM, a synaptic adhesion molecule that drives synapse assembly. Science 297 (5586):1525-1531.

31. Billuart P, Winter CG, Maresh A, Zhao X, Luo L (2001) Regulating axon branch stability: the role of p190 RhoGAP in repressing a retraction signaling pathway. Cell 107 (2):195-207.

32. Birukova AA, Fu P, Xing J, Yakubov B, Cokic I, Birukov KG (2010) Mechanotransduction by GEF-H1 as a novel mechanism of ventilator-induced vascular endothelial permeability. Am J Physiol Lung Cell Mol Physiol 298 (6):L837-848.

33. Bito H, Furuyashiki T, Ishihara H, Shibasaki Y, Ohashi K, Mizuno K, Maekawa M, Ishizaki T, Narumiya S (2000) A critical role for a Rho-associated kinase, p160ROCK, in determining axon outgrowth in mammalian CNS neurons. Neuron 26 (2):431-441.

34. Blumbergs PC, Scott G, Manavis J, Wainwright H, Simpson DA, McLean AJ (1995) Topography of axonal injury as defined by amyloid precursor protein and the sector scoring method in mild and severe closed head injury. J Neurotrauma 12 (4):565-572.

35. Borg J, Holm L, Cassidy JD, Peloso PM, Carroll LJ, von Holst H, Ericson K (2004) Diagnostic procedures in mild traumatic brain injury: Results of the WHO Collaborating Centre Task Force on Mild Traumatic Brain Injury. J Rehabil Med 36:61-75.

36. Brangwynne CP, MacKintosh FC, Kumar S, Geisse NA, Talbot J, Mahadevan L, Parker KK, Ingber DE, Weitz DA (2006) Microtubules can bear enhanced compressive loads in living cells because of lateral reinforcement. Journal of Cell Biology 173 (5):733-741.

37. Brauer K, Hartig W, Bigl V, Bruckner G (1993) Distribution of parvalbumin-containing neurons and lectin-binding perineuronal nets in the rat basal forebrain. Brain Res 631 (1):167-170.

38. Brewer GJ, Torricelli JR (2007) Isolation and culture of adult neurons and neurospheres. Nat Protoc 2 (6):1490-1498.

39. Brodal P (2004) The central nervous system : structure and function. 3rd edn. Oxford University Press, Oxford ; New York.

40. Bruckner G, Bringmann A, Koppe G, Hartig W, Brauer K (1996) In vivo and in vitro labelling of perineuronal nets in rat brain. Brain Res 720 (1-2):84-92.

41. Bruckner G, Hartig W, Kacza J, Seeger J, Welt K, Brauer K (1996) Extracellular matrix organization in various regions of rat brain grey matter. J Neurocytol 25 (5):333-346.

42. Bruckner G, Hausen D, Hartig W, Drlicek M, Arendt T, Brauer K (1999) Cortical areas abundant in extracellular matrix chondroitin sulphate proteoglycans are less affected by cytoskeletal changes in Alzheimer's disease. Neuroscience 92 (3):791-805.

43. Bruckner G, Morawski M, Arendt T (2008) Aggrecan-based extracellular matrix is an integral part of the human basal ganglia circuit. Neuroscience 151 (2):489-504.

44. Bruckner G, Pavlica S, Morawski M, Palacios AG, Reichenbach A (2006) Organization of brain extracellular matrix in the Chilean fat-tailed mouse opossum Thylamys elegans (Waterhouse, 1839). J Chem Neuroanat 32 (2-4):143-158.

45. Buki A, Farkas O, Doczi T, Povlishock JT (2003) Preinjury administration of the calpain inhibitor MDL-28170 attenuates traumatically induced axonal injury. J Neurotrauma 20 (3):261-268.

46. Buki A, Farkas O, Doczi T, Povlishock JT (2003) Preinjury administration of the calpain inhibitor MDL-28170 attenuates traumatically induced axonal injury. Journal of neurotrauma 20 (3):261-268.

47. Buki A, Siman R, Trojanowski JQ, Povlishock JT (1999) The role of calpain-mediated spectrin proteolysis in traumatically induced axonal injury. J Neuropathol Exp Neurol 58 (4):365-375.

48. Burridge K (1981) Are Stress Fibers Contractile. Nature 294 (5843):691-692.

49. Carulli D, Pizzorusso T, Kwok JCF, Putignano E, Poli A, Forostyak S, Andrews MR, Deepa SS, Glant TT, Fawcett JW (2010) Animals lacking link protein have attenuated perineuronal nets and persistent plasticity. Brain 133:2331-2347.

50. Carulli D, Rhodes KE, Brown DJ, Bonnert TP, Pollack SJ, Oliver K, Strata P, Fawcett JW (2006) Composition of perineuronal nets in the adult rat cerebellum and the cellular origin of their components. J Comp Neurol 494 (4):559-577.

51. Cavaglia M, Dombrowski SM, Drazba J, Vasanji A, Bokesch PM, Janigro D (2001) Regional variation in brain capillary density and vascular response to ischemia. Brain Res 910 (1-2):81-93.

52. Cernak I (2005) Animal models of head trauma. NeuroRx 2 (3):410-422.

53. Cernak I, Wang ZG, Jiang JX, Bian XW, Savic J (2001) Ultrastructural and functional characteristics of blast injury-induced neurotrauma. Journal of Trauma-Injury Infection and Critical Care 50 (4):695-706.

54. Chan CS, Weeber EJ, Kurup S, Sweatt JD, Davis RL (2003) Integrin requirement for hippocampal synaptic plasticity and spatial memory. J Neurosci 23 (18):7107-7116.

55. Chatelin S, Deck C, Renard F, Kremer S, Heinrich C, Armspach JP, Willinger R (2011) Computation of axonal elongation in head trauma finite element simulation. J Mech Behav Biomed Mater 4 (8):1905-1919.

56. Chavis P, Westbrook G (2001) Integrins mediate functional pre- and postsynaptic maturation at a hippocampal synapse. Nature 411 (6835):317-321.

57. Chen BM, Grinnell AD (1995) Integrins and modulation of transmitter release from motor nerve terminals by stretch. Science 269 (5230):1578-1580.

58. Chiquetehrismann R (1990) What Distinguishes Tenascin from Fibronectin. Faseb Journal 4 (9):2598-2604.

59. Christman CW, Grady MS, Walker SA, Holloway KL, Povlishock JT (1994) Ultrastructural studies of diffuse axonal injury in humans. J Neurotrauma 11 (2):173-186.

60. Cloots RJ, van Dommelen JA, Kleiven S, Geers MG (2013) Multi-scale mechanics of traumatic brain injury: predicting axonal strains from head loads. Biomech Model Mechanobiol 12 (1):137-150.

61. Cloots RJ, van Dommelen JA, Nyberg T, Kleiven S, Geers MG (2011) Micromechanics of diffuse axonal injury: influence of axonal orientation and anisotropy. Biomech Model Mechanobiol 10 (3):413-422.

62. Condic ML, Letourneau PC (1997) Ligand-induced changes in integrin expression regulate neuronal adhesion and neurite outgrowth. Nature 389 (6653):852-856.

63. Corsellis JA, Bruton CJ, Freeman-Browne D (1973) The aftermath of boxing. Psychological medicine 3 (3):270-303.

64. Costa C, Tortosa R, Domenech A, Vidal E, Pumarola M, Bassols A (2007) Mapping of aggrecan, hyaluronic acid, heparan sulphate proteoglycans and aquaporin 4 in the central nervous system of the mouse. J Chem Neuroanat 33 (3):111-123.

65. Costa E, Davis J, Grayson DR, Guidotti A, Pappas GD, Pesold C (2001) Dendritic spine hypoplasticity and downregulation of reelin and GABAergic tone in schizophrenia vulnerability. Neurobiol Dis 8 (5):723-742.

66. Crossin KL, Edelman GM (1986) Mechanisms of cell adhesion in epithelial-mesenchymal transformations. Progress in clinical and biological research 226:81-92.

67. Crossin KL, Hoffman S, Grumet M, Thiery JP, Edelman GM (1986) Site-restricted expression of cytotactin during development of the chicken embryo. The Journal of cell biology 102 (5):1917-1930.

68. Crossin KL, Krushel LA (2000) Cellular signaling by neural cell adhesion molecules of the immunoglobulin superfamily. Dev Dyn 218 (2):260-279.

69. Cullen DK, Lessing MC, LaPlaca MC (2007) Collagen-dependent neurite outgrowth and response to dynamic deformation in three-dimensional neuronal cultures. Ann Biomed Eng 35 (5):835-846.

70. Dabiri BE, Lee H, Parker KK (2012) A potential role for integrin signaling in mechanoelectrical feedback. Prog Biophys Mol Biol 110 (2-3):196-203.
71. Dalva MB, McClelland AC, Kayser MS (2007) Cell adhesion molecules: signalling functions at the synapse. Nat Rev Neurosci 8 (3):206-220.
72. Damsky CH, Werb Z (1992) Signal transduction by integrin receptors for extracellular matrix: cooperative processing of extracellular information. Curr Opin Cell Biol 4 (5):772-781.
73. DeMali KA, Wennerberg K, Burridge K (2003) Integrin signaling to the actin cytoskeleton. Curr Opin Cell Biol 15 (5):572-582.
74. Dennerll TJ, Lamoureux P, Buxbaum RE, Heidemann SR (1989) The cytomechanics of axonal elongation and retraction. The Journal of cell biology 109 (6 Pt 1):3073-3083.
75. Di Pietro V, Amin D, Pernagallo S, Lazzarino G, Tavazzi B, Vagnozzi R, Pringle A, Belli A (2010) Transcriptomics of Traumatic Brain Injury: Gene Expression and Molecular Pathways of Different Grades of Insult in a Rat Organotypic Hippocampal Culture Model. J Neurotraum 27 (2):349-359.
76. DiLeonardi AM, Huh JW, Raghupathi R (2009) Impaired axonal transport and neurofilament compaction occur in separate populations of injured axons following diffuse brain injury in the immature rat. Brain Res 1263:174-182.
77. Discher DE, Janmey P, Wang YL (2005) Tissue cells feel and respond to the stiffness of their substrate. Science 310 (5751):1139-1143.
78. Dityatev A, Schachner M (2003) Extracellular matrix molecules and synaptic plasticity. Nat Rev Neurosci 4 (6):456-468.
79. Dityatev A, Schachner M (2006) The extracellular matrix and synapses. Cell Tissue Res 326 (2):647-654.
80. Dityatev A, Schachner M, Sonderegger P (2010) The dual role of the extracellular matrix in synaptic plasticity and homeostasis. Nat Rev Neurosci 11 (11):735-746.
81. Dorries U, Bartsch U, Nolte C, Roth J, Schachner M (1993) Adaptation of a non-radioactive in situ hybridization method to electron microscopy: detection of tenascin mRNAs in mouse cerebellum with digoxigenin-labelled probes and gold-labelled antibodies. Histochemistry 99 (3):251-262.
82. Dubreuil CI, Marklund N, Deschamps K, McIntosh TK, McKerracher L (2006) Activation of Rho after traumatic brain injury and seizure in rats. Exp Neurol 198 (2):361-369.
83. Dubreuil CI, Winton MJ, McKerracher L (2003) Rho activation patterns after spinal cord injury and the role of activated Rho in apoptosis in the central nervous system. J Cell Biol 162 (2):233-243.
84. Elder GA, Cristian A (2009) Blast-related mild traumatic brain injury: mechanisms of injury and impact on clinical care. Mount Sinai Journal of Medicine: A Journal of Translational and Personalized Medicine 76 (2):111-118.
85. Ellis EF, McKinney JS, Willoughby KA, Liang S, Povlishock JT (1995) A new model for rapid stretch-induced injury of cells in culture: characterization of the model using astrocytes. J Neurotrauma 12 (3):325-339.
86. Erb DE, Povlishock JT (1991) Neuroplasticity following traumatic brain injury: a study of GABAergic terminal loss and recovery in the cat dorsal lateral vestibular nucleus. Exp Brain Res 83 (2):253-267.

87. Fabry B, Maksym GN, Hubmayr RD, Butler JP, Fredberg JJ (1999) Implications of heterogeneous bead behavior on cell mechanical properties measured with magnetic twisting cytometry. J Magn Magn Mater 194 (1-3):120-125.

88. Fahrig R, Nikolov H, Fox AJ, Holdsworth DW (1999) A three-dimensional cerebrovascular flow phantom. Med Phys 26 (8):1589-1599.

89. Fallenstein GT, Hulce VD, Melvin JW (1969) Dynamic mechanical properties of human brain tissue. J Biomech 2 (3):217-226.

90. Farkas O, Lifshitz J, Povlishock JT (2006) Mechanoporation induced by diffuse traumatic brain injury: an irreversible or reversible response to injury? J Neurosci 26 (12):3130-3140.

91. Farkas O, Povlishock JT (2007) Cellular and subcellular change evoked by diffuse traumatic brain injury: a complex web of change extending far beyond focal damage. Prog Brain Res 161:43-59.

92. Faul M, Xu L, Wald M, Coronado V (2010) Traumatic brain injury in the United States: Emergency department visits, hospitalizations and deaths 2002–2006. Atlanta, GA: Centers for Disease Control and Prevention, National Center for Injury Prevention and Control.

93. Ferhat L, Chevassus au Louis N, Jorquera I, Niquet J, Khrestchatisky M, Ben-Ari Y, Represa A (1996) Transient increase of tenascin-C in immature hippocampus: astroglial and neuronal expression. J Neurocytol 25 (1):53-66.

94. Fletcher DA, Mullins RD (2010) Cell mechanics and the cytoskeleton. Nature 463 (7280):485-492.

95. Franze K, Gerdelmann J, Weick M, Betz T, Pawlizak S, Lakadamyali M, Bayer J, Rillich K, Gogler M, Lu YB, Reichenbach A, Janmey P, Kas J (2009) Neurite branch retraction is caused by a threshold-dependent mechanical impact. Biophys J 97 (7):1883-1890.

96. Frischknecht R, Heine M, Perrais D, Seidenbecher CI, Choquet D, Gundelfinger ED (2009) Brain extracellular matrix affects AMPA receptor lateral mobility and short-term synaptic plasticity. Nat Neurosci 12 (7):897-904.

97. Frischknecht R, Seidenbecher CI (2008) The crosstalk of hyaluronan-based extracellular matrix and synapses. Neuron Glia Biol 4:249-257.

98. Frotscher M (2010) Role for Reelin in stabilizing cortical architecture. Trends in neurosciences 33 (9):407-414.

99. Galtrey CM, Kwok JC, Carulli D, Rhodes KE, Fawcett JW (2008) Distribution and synthesis of extracellular matrix proteoglycans, hyaluronan, link proteins and tenascin-R in the rat spinal cord. Eur J Neurosci 27 (6):1373-1390.

100. Garland P, Broom LJ, Quraishe S, Dalton PD, Skipp P, Newman TA, Perry VH (2012) Soluble axoplasm enriched from injured CNS axons reveals the early modulation of the actin cytoskeleton. Plos One 7 (10):e47552.

101. Gates MA, Thomas LB, Howard EM, Laywell ED, Sajin B, Faissner A, Gotz B, Silver J, Steindler DA (1995) Cell and molecular analysis of the developing and adult mouse subventricular zone of the cerebral hemispheres. J Comp Neurol 361 (2):249-266.

102. Gavett BE, Stern RA, McKee AC (2011) Chronic traumatic encephalopathy: a potential late effect of sport-related concussive and subconcussive head trauma. Clin Sports Med 30 (1):179-188, xi.

103. Geddes-Klein DM, Serbest G, Mesfin MN, Cohen AS, Meaney DF (2006) Pharmacologically induced calcium oscillations protect neurons from increases in cytosolic calcium after trauma. Journal of neurochemistry 97 (2):462-474.

104. Geddes DM, Cargill RS, 2nd, LaPlaca MC (2003) Mechanical stretch to neurons results in a strain rate and magnitude-dependent increase in plasma membrane permeability. J Neurotrauma 20 (10):1039-1049.

105. Gennarelli TA (1993) Mechanisms of brain injury. J Emerg Med 11 Suppl 1:5-11.

106. Gennarelli TA (1996) The spectrum of traumatic axonal injury. Neuropath Appl Neuro 22 (6):509-513.

107. Gennarelli TA, Thibault LE, Adams JH, Graham DI, Thompson CJ, Marcincin RP (1982) Diffuse axonal injury and traumatic coma in the primate. Annals of Neurology 12 (6):564-574.

108. Gennarelli TA, Thibault LE, Adams JH, Graham DI, Thompson CJ, Marcincin RP (1982) Diffuse axonal injury and traumatic coma in the primate. Ann Neurol 12 (6):564-574.

109. Giagtzoglou N, Ly CV, Bellen HJ (2009) Cell adhesion, the backbone of the synapse: "vertebrate" and "invertebrate" perspectives. Cold Spring Harb Perspect Biol 1 (4):a003079.

110. Giancotti FG, Ruoslahti E (1999) Integrin signaling. Science 285 (5430):1028-1032.

111. Girault JA, Peles E (2002) Development of nodes of Ranvier. Curr Opin Neurobiol 12 (5):476-485.

112. Giza CC, Hovda DA (2001) The Neurometabolic Cascade of Concussion. J Athl Train 36 (3):228-235.

113. Golding EM (2002) Sequelae following traumatic brain injury. The cerebrovascular perspective. Brain Res Brain Res Rev 38 (3):377-388.

114. Goldstein LE, Fisher AM, Tagge CA, Zhang XL, Velisek L, Sullivan JA, Upreti C, Kracht JM, Ericsson M, Wojnarowicz MW, Goletiani CJ, Maglakelidze GM, Casey N, Moncaster JA, Minaeva O, Moir RD, Nowinski CJ, Stern RA, Cantu RC, Geiling J, Blusztajn JK, Wolozin BL, Ikezu T, Stein TD, Budson AE, Kowall NW, Chargin D, Sharon A, Saman S, Hall GF, Moss WC, Cleveland RO, Tanzi RE, Stanton PK, McKee AC (2012) Chronic traumatic encephalopathy in blast-exposed military veterans and a blast neurotrauma mouse model. Sci Transl Med 4 (134):134ra160.

115. Goodison S, Urquidi V, Tarin D (1999) CD44 cell adhesion molecules. Mol Pathol 52 (4):189-196.

116. Graham DI, McLellan D, Adams JH, Doyle D, Kerr A, Murray LS (1983) The neuropathology of the vegetative state and severe disability after non-missile head injury. Acta Neurochir Suppl (Wien) 32:65-67.

117. Gu L, Li J, Feng DF, Cheng ET, Li DC, Yang XQ, Wang BC (2013) Detection of white matter lesions in the acute stage of diffuse axonal injury predicts long-term cognitive impairments: a clinical diffusion tensor imaging study. J Trauma Acute Care Surg 74 (1):242-247.

118. Gumbiner BM (1993) Breaking through the tight junction barrier. Journal of Cell Biology 123 (6 Pt 2):1631-1633.

119. Gumbiner BM (1993) Proteins associated with the cytoplasmic surface of adhesion molecules. Neuron 11 (4):551-564.

120. Gumbiner BM (1996) Cell adhesion: the molecular basis of tissue architecture and morphogenesis. Cell 84 (3):345-357.

121. Gumbiner BM, McCrea PD (1993) Catenins as mediators of the cytoplasmic functions of cadherins. J Cell Sci Suppl 17:155-158.
122. Hall A (1998) Rho GTPases and the actin cytoskeleton. Science 279 (5350):509-514.
123. Hamill OP, Martinac B (2001) Molecular basis of mechanotransduction in living cells. Physiol Rev 81 (2):685-740.
124. Hartig W, Derouiche A, Welt K, Brauer K, Grosche J, Mader M, Reichenbach A, Bruckner G (1999) Cortical neurons immunoreactive for the potassium channel Kv3.1b subunit are predominantly surrounded by perineuronal nets presumed as a buffering system for cations. Brain Res 842 (1):15-29.
125. Hashimoto R, Nakamura Y, Goto H, Wada Y, Sakoda S, Kaibuchi K, Inagaki M, Takeda M (1998) Domain- and Site-Specific Phosphorylation of Bovine NF-L by Rho-Associated Kinase. Biochemical and Biophysical Research Communications 245 (2):407-411.
126. Hemphill MA, Dabiri BE, Gabriele S, Kerscher L, Franck C, Goss JA, Alford PW, Parker KK (2011) A Possible Role for Integrin Signaling in Diffuse Axonal Injury. Plos One 6 (7).
127. Herrmann H, Bar H, Kreplak L, Strelkov SV, Aebi U (2007) Intermediate filaments: from cell architecture to nanomechanics. Nat Rev Mol Cell Biol 8 (7):562-573.
128. Hoang B, Chiba A (1998) Genetic analysis on the role of integrin during axon guidance in Drosophila. J Neurosci 18 (19):7847-7855.
129. Hoge CW, McGurk D, Thomas JL, Cox AL, Engel CC, Castro CA (2008) Mild traumatic brain injury in U.S. Soldiers returning from Iraq. N Engl J Med 358 (5):453-463.
130. Holbourn AHS (1944) Mechanics of Head Injuries. The Lancet 243 (6293):483.
131. Huang H, Kamm RD, Lee RT (2004) Cell mechanics and mechanotransduction: pathways, probes, and physiology. Am J Physiol Cell Physiol 287 (1):C1-11.
132. Huveneers S, Danen EHJ (2009) Adhesion signaling - crosstalk between integrins, Src and Rho. J Cell Sci 122 (8):1059-1069.
133. Hynes RO (1992) Integrins: versatility, modulation, and signaling in cell adhesion. Cell 69 (1):11-25.
134. Hynes RO (1999) Cell adhesion: old and new questions. Trends Cell Biol 9 (12):M33-37.
135. Iadecola C, Nedergaard M (2007) Glial regulation of the cerebral microvasculature. Nat Neurosci 10 (11):1369-1376.
136. Impagnatiello F, Guidotti AR, Pesold C, Dwivedi Y, Caruncho H, Pisu MG, Uzunov DP, Smalheiser NR, Davis JM, Pandey GN, Pappas GD, Tueting P, Sharma RP, Costa E (1998) A decrease of reelin expression as a putative vulnerability factor in schizophrenia. Proc Natl Acad Sci U S A 95 (26):15718-15723.
137. Inglese M, Makani S, Johnson G, Cohen BA, Silver JA, Gonen O, Grossman RI (2005) Diffuse axonal injury in mild traumatic brain injury: a diffusion tensor imaging study. J Neurosurg 103 (2):298-303.
138. Iwata A, Stys PK, Wolf JA, Chen XH, Taylor AG, Meaney DF, Smith DH (2004) Traumatic axonal injury induces proteolytic cleavage of the voltage-gated sodium channels modulated by tetrodotoxin and protease inhibitors. J Neurosci 24 (19):4605-4613.
139. Jaalouk DE, Lammerding J (2009) Mechanotransduction gone awry. Nat Rev Mol Cell Bio 10 (1):63-73.
140. Jaalouk DE, Lammerding J (2009) Mechanotransduction gone awry. Nat Rev Mol Cell Biol 10 (1):63-73.

141. Jaffe AB, Hall A (2005) Rho GTPases: Biochemistry and biology. Annual review of cell and developmental biology 21:247-269.
142. Jager C, Lendvai D, Seeger G, Bruckner G, Matthews RT, Arendt T, Alpar A, Morawski M (2013) Perineuronal and perisynaptic extracellular matrix in the human spinal cord. Neuroscience.
143. Jalink K, van Corven EJ, Hengeveld T, Morii N, Narumiya S, Moolenaar WH (1994) Inhibition of lysophosphatidate- and thrombin-induced neurite retraction and neuronal cell rounding by ADP ribosylation of the small GTP-binding protein Rho. J Cell Biol 126 (3):801-810.
144. Janmey PA, McCulloch CA (2007) Cell mechanics: integrating cell responses to mechanical stimuli. Annu Rev Biomed Eng 9:1-34.
145. Janowitz T, Menon DK (2010) Exploring new routes for neuroprotective drug development in traumatic brain injury. Sci Transl Med 2 (27):27rv21.
146. Jenkins A, Teasdale G, Hadley MD, Macpherson P, Rowan JO (1986) Brain lesions detected by magnetic resonance imaging in mild and severe head injuries. Lancet 2 (8504):445-446.
147. Johansson S, Svineng G, Wennerberg K, Armulik A, Lohikangas L (1997) Fibronectin-integrin interactions. Front Biosci 2:d126-146.
148. Juliano RL (2002) Signal transduction by cell adhesion receptors and the cytoskeleton: functions of integrins, cadherins, selectins, and immunoglobulin-superfamily members. Annu Rev Pharmacol Toxicol 42:283-323.
149. Kam Z, Zamir E, Geiger B (2001) Probing molecular processes in live cells by quantitative multidimensional microscopy. TRENDS in Cell Biology 11 (8):329-334.
150. Kandel ER, Schwartz JH, Jessell TM (2000) Principles of neural science. 4th edn. McGraw-Hill, Health Professions Division, New York.
151. Kilinc D, Gallo G, Barbee KA (2008) Mechanically-induced membrane poration causes axonal beading and localized cytoskeletal damage. Experimental Neurology 212 (2):422-430.
152. Kilinc D, Gallo G, Barbee KA (2008) Mechanically-induced membrane poration causes axonal beading and localized cytoskeletal damage. Exp Neurol 212 (2):422-430.
153. Kilinc D, Gallo G, Barbee KA (2009) Mechanical membrane injury induces axonal beading through localized activation of calpain. Exp Neurol 219 (2):553-561.
154. Kimura K, Ito M, Amano M, Chihara K, Fukata Y, Nakafuku M, Yamamori B, Feng J, Nakano T, Okawa K, Iwamatsu A, Kaibuchi K (1996) Regulation of Myosin Phosphatase by Rho and Rho-Associated Kinase (Rho- Kinase). Science 273 (5272):245-248.
155. Kiryushko D, Berezin V, Bock E (2004) Regulators of neurite outgrowth: role of cell adhesion molecules. Ann N Y Acad Sci 1014:140-154.
156. Kis A, Kasas S, Babic B, Kulik AJ, Benoit W, Briggs GA, Schonenberger C, Catsicas S, Forro L (2002) Nanomechanics of microtubules. Physical review letters 89 (24):248101.
157. Kochlamazashvili G, Henneberger C, Bukalo O, Dvoretskova E, Senkov O, Lievens PMJ, Westenbroek R, Engel AK, Catterall WA, Rusakov DA, Schachner M, Dityatev A (2010) The Extracellular Matrix Molecule Hyaluronic Acid Regulates Hippocampal Synaptic Plasticity by Modulating Postsynaptic L-Type Ca2+ Channels. Neuron 67 (1):116-128.
158. Kreplak L, Bar H, Leterrier JF, Herrmann H, Aebi U (2005) Exploring the mechanical behavior of single intermediate filaments. J Mol Biol 354 (3):569-577.
159. Kritikou E (2007) The complexity of adhesion. Nat Rev Mol Cell Bio 8 (9):674-674.

160. Kruse SA, Rose GH, Glaser KJ, Manduca A, Felmlee JP, Jack CR, Ehman RL (2008) Magnetic resonance elastography of the brain. Neuroimage 39 (1):231-237.

161. Kupina NC, Nath R, Bernath EE, Inoue J, Mitsuyoshi A, Yuen PW, Wang KK, Hall ED (2001) The novel calpain inhibitor SJA6017 improves functional outcome after delayed administration in a mouse model of diffuse brain injury. J Neurotrauma 18 (11):1229-1240.

162. Kwok JC, Dick G, Wang D, Fawcett JW (2011) Extracellular matrix and perineuronal nets in CNS repair. Dev Neurobiol 71 (11):1073-1089.

163. Langanger G, Moeremans M, Daneels G, Sobieszek A, De Brabander M, De Mey J (1986) The molecular organization of myosin in stress fibers of cultured cells. Journal of Cell Biology 102 (1):200-209.

164. LaPlaca MC, Simon CM, Prado GR, Cullen DK (2007) CNS injury biomechanics and experimental models. Prog Brain Res 161:13-26.

165. Larsen M, Artym VV, Green JA, Yamada KM (2006) The matrix reorganized: extracellular matrix remodeling and integrin signaling. Curr Opin Cell Biol 18 (5):463-471.

166. Lauret C, Hrapko M, van Dommelen JA, Peters GW, Wismans JS (2009) Optical characterization of acceleration-induced strain fields in inhomogeneous brain slices. Med Eng Phys 31 (3):392-399.

167. Lee H, Wintermark M, Gean AD, Ghajar J, Manley GT, Mukherjee P (2008) Focal lesions in acute mild traumatic brain injury and neurocognitive outcome: CT versus 3T MRI. J Neurotrauma 25 (9):1049-1056.

168. Lele TP, Thodeti CK, Ingber DE (2006) Force meets chemistry: Analysis of mechanochemical conversion in focal adhesions using fluorescence recovery after photobleaching. J Cell Biochem 97 (6):1175-1183.

169. Lemons ML, Condic ML (2006) Combined integrin activation and intracellular cAMP cause Rho GTPase dependent growth cone collapse on laminin-1. Exp Neurol 202 (2):324-335.

170. Lendvai D, Morawski M, Bruckner G, Negyessy L, Baksa G, Glasz T, Patonay L, Matthews RT, Arendt T, Alpar A (2012) Perisynaptic aggrecan-based extracellular matrix coats in the human lateral geniculate body devoid of perineuronal nets. J Neurosci Res 90 (2):376-387.

171. Lendvai D, Morawski M, Negyessy L, Gati G, Jager C, Baksa G, Glasz T, Attems J, Tanila H, Arendt T, Harkany T, Alpar A (2013) Neurochemical mapping of the human hippocampus reveals perisynaptic matrix around functional synapses in Alzheimer's disease. Acta Neuropathol 125 (2):215-229.

172. Liao H, Huang W, Schachner M, Guan Y, Guo J, Yan J, Qin J, Bai X, Zhang L (2008) Beta 1 integrin-mediated effects of tenascin-R domains EGFL and FN6-8 on neural stem/progenitor cell proliferation and differentiation in vitro. J Biol Chem 283 (41):27927-27936.

173. Lin CY, Hilgenberg LG, Smith MA, Lynch G, Gall CM (2008) Integrin regulation of cytoplasmic calcium in excitatory neurons depends upon glutamate receptors and release from intracellular stores. Mol Cell Neurosci 37 (4):770-780.

174. Lin YW, Cheng CM, Leduc PR, Chen CC (2009) Understanding Sensory Nerve Mechanotransduction through Localized Elastomeric Matrix Control. Plos One 4 (1).

175. Liu S, Calderwood DA, Ginsberg MH (2000) Integrin cytoplasmic domain-binding proteins. J Cell Sci 113 (Pt 20):3563-3571.

176. Lo CM, Wang HB, Dembo M, Wang YL (2000) Cell movement is guided by the rigidity of the substrate. Biophys J 79 (1):144-152.
177. Lu YB, Franze K, Seifert G, Steinhauser C, Kirchhoff F, Wolburg H, Guck J, Janmey P, Wei EQ, Kas J, Reichenbach A (2006) Viscoelastic properties of individual glial cells and neurons in the CNS. Proc Natl Acad Sci U S A 103 (47):17759-17764.
178. Luo L, O'Leary DD (2005) Axon retraction and degeneration in development and disease. Annu Rev Neurosci 28:127-156.
179. Mac Donald CL, Dikranian K, Song SK, Bayly PV, Holtzman DM, Brody DL (2007) Detection of traumatic axonal injury with diffusion tensor imaging in a mouse model of traumatic brain injury. Experimental Neurology 205 (1):116-131.
180. Mac Donald CL, Dikranian K, Song SK, Bayly PV, Holtzman DM, Brody DL (2007) Detection of traumatic axonal injury with diffusion tensor imaging in a mouse model of traumatic brain injury. Exp Neurol 205 (1):116-131.
181. Mac Donald CL, Johnson AM, Cooper D, Nelson EC, Werner NJ, Shimony JS, Snyder AZ, Raichle ME, Witherow JR, Fang R, Flaherty SF, Brody DL (2011) Detection of blast-related traumatic brain injury in U.S. military personnel. N Engl J Med 364 (22):2091-2100.
182. Mace E, Cohen I, Montaldo G, Miles R, Fink M, Tanter M (2011) In vivo mapping of brain elasticity in small animals using shear wave imaging. IEEE Trans Med Imaging 30 (3):550-558.
183. Main AL, Harvey TS, Baron M, Boyd J, Campbell ID (1992) The three-dimensional structure of the tenth type III module of fibronectin: an insight into RGD-mediated interactions. Cell 71 (4):671-678.
184. Maloku E, Covelo IR, Hanbauer I, Guidotti A, Kadriu B, Hu Q, Davis JM, Costa E (2010) Lower number of cerebellar Purkinje neurons in psychosis is associated with reduced reelin expression. Proc Natl Acad Sci U S A 107 (9):4407-4411.
185. Mammoto A, Mammoto T, Ingber DE (2008) Rho signaling and mechanical control of vascular development. Curr Opin Hematol 15 (3):228-234.
186. Marmarou CR, Walker SA, Davis CL, Povlishock JT (2005) Quantitative analysis of the relationship between intra-axonal neurofilament compaction and impaired axonal transport following diffuse traumatic brain injury. Journal of neurotrauma 22 (10):1066-1080.
187. Matthews BD, Overby DR, Mannix R, Ingber DE (2006) Cellular adaptation to mechanical stress: role of integrins, Rho, cytoskeletal tension and mechanosensitive ion channels. J Cell Sci 119 (3):508-518.
188. Matthews BD, Overby DR, Mannix R, Ingber DE (2006) Cellular adaptation to mechanical stress: role of integrins, Rho, cytoskeletal tension and mechanosensitive ion channels. J Cell Sci 119 (Pt 3):508-518.
189. McKee AC, Cantu RC, Nowinski CJ, Hedley-Whyte ET, Gavett BE, Budson AE, Santini VE, Lee HS, Kubilus CA, Stern RA (2009) Chronic traumatic encephalopathy in athletes: progressive tauopathy after repetitive head injury. J Neuropathol Exp Neurol 68 (7):709-735.
190. McKee AC, Stern RA, Nowinski CJ, Stein TD, Alvarez VE, Daneshvar DH, Lee HS, Wojtowicz SM, Hall G, Baugh CM, Riley DO, Kubilus CA, Cormier KA, Jacobs MA, Martin BR, Abraham CR, Ikezu T, Reichard RR, Wolozin BL, Budson AE, Goldstein

LE, Kowall NW, Cantu RC (2013) The spectrum of disease in chronic traumatic encephalopathy. Brain 136 (Pt 1):43-64.

191. McRae PA, Rocco MM, Kelly G, Brumberg JC, Matthews RT (2007) Sensory deprivation alters aggrecan and perineuronal net expression in the mouse barrel cortex. J Neurosci 27 (20):5405-5413.

192. Mercier F, Arikawa-Hirasawa E (2012) Heparan sulfate niche for cell proliferation in the adult brain. Neuroscience letters 510 (2):67-72.

193. Meyer-Puttlitz B, Junker E, Margolis RU, Margolis RK (1996) Chondroitin sulfate proteoglycans in the developing central nervous system. II. Immunocytochemical localization of neurocan and phosphacan. J Comp Neurol 366 (1):44-54.

194. Meyer CJ, Alenghat FJ, Rim P, Fong JH, Fabry B, Ingber DE (2000) Mechanical control of cyclic AMP signalling and gene transcription through integrins. Nat Cell Biol 2 (9):666-668.

195. Meyer K, Linker A, Rapport MM (1951) The production of monosaccharides from hyaluronic acid by beta-glucuronidase. J Biol Chem 192 (1):275-281.

196. Mijailovich SM, Kojic M, Zivkovic M, Fabry B, Fredberg JJ (2002) A finite element model of cell deformation during magnetic bead twisting. J Appl Physiol 93 (4):1429-1436.

197. Miller B, Sheppard AM, Bicknese AR, Pearlman AL (1995) Chondroitin sulfate proteoglycans in the developing cerebral cortex: the distribution of neurocan distinguishes forming afferent and efferent axonal pathways. J Comp Neurol 355 (4):615-628.

198. Milner R, Campbell IL (2002) The integrin family of cell adhesion molecules has multiple functions within the CNS. J Neurosci Res 69 (3):286-291.

199. Mitra S, Hanson D, Schlaepfer D (2005) Focal adhesion kinase: in command and control of cell motility. Nature Reviews Molecular Cell Biology 6 (1):56-68.

200. Monson KL, Goldsmith W, Barbaro NM, Manley GT (2003) Axial mechanical properties of fresh human cerebral blood vessels. J Biomech Eng 125 (2):288-294.

201. Morales DM, Marklund N, Lebold D, Thompson HJ, Pitkanen A, Maxwell WL, Longhi L, Laurer H, Maegele M, Neugebauer E, Graham DI, Stocchetti N, McIntosh TK (2005) Experimental models of traumatic brain injury: Do we really need to build a better mousetrap? Neuroscience 136 (4):971-989.

202. Morawski M, Bruckner G, Arendt T, Matthews RT (2012) Aggrecan: Beyond cartilage and into the brain. The international journal of biochemistry & cell biology 44 (5):690-693.

203. Morawski M, Bruckner G, Jager C, Seeger G, Arendt T (2010) Neurons associated with aggrecan-based perineuronal nets are protected against tau pathology in subcortical regions in Alzheimer's disease. Neuroscience 169 (3):1347-1363.

204. Morawski M, Bruckner G, Jager C, Seeger G, Kunzle H, Arendt T (2010) Aggrecan-based extracellular matrix shows unique cortical features and conserved subcortical principles of mammalian brain organization in the Madagascan lesser hedgehog tenrec (Echinops telfairi Martin, 1838). Neuroscience 165 (3):831-849.

205. Morris NP, Henderson Z (2000) Perineuronal nets ensheath fast spiking, parvalbumin-immunoreactive neurons in the medial septum/diagonal band complex. Eur J Neurosci 12 (3):828-838.

206. Mueller B, Mack H, Teusch N (2005) Rho kinase, a promising drug target for neurological disorders. Nature Reviews Drug Discovery 4 (5):387-398.

207. Mukhina IV, Korotchenko SA, Dityatev AE (2012) Extracellular matrix molecules, their receptors, and extracellular proteases as synaptic plasticity modulators. Neurochem J+ 6 (2):89-99.

208. Na S, Collin O, Chowdhury F, Tay B, Ouyang M, Wang Y, Wang N (2008) Rapid signal transduction in living cells is a unique feature of mechanotransduction. Proc Natl Acad Sci U S A 105 (18):6626-6631.

209. Na S, Collin O, Chowdhury F, Tay B, Ouyang MX, Wang YX, Wang N (2008) Rapid signal transduction in living cells is a unique feature of mechanotransduction. Proc Natl Acad Sci U S A 105 (18):6626-6631.

210. Na SS, Wang N (2008) Application of Fluorescence Resonance Energy Transfer and Magnetic Twisting Cytometry to Quantify Mechanochemical Signaling Activities in a Living Cell. Sci Signal 1 (34).

211. Nakayama K, Ohkawara T, Hiratochi M, Koh CS, Nagase H (2008) The intracellular domain of amyloid precursor protein induces neuron-specific apoptosis. Neuroscience letters 444 (2):127-131.

212. Nelson WJ, Nusse R (2004) Convergence of Wnt, beta-catenin, and cadherin pathways. Science 303 (5663):1483-1487.

213. Nishimura SL, Boylen KP, Einheber S, Milner TA, Ramos DM, Pytela R (1998) Synaptic and glial localization of the integrin alphavbeta8 in mouse and rat brain. Brain Res 791 (1-2):271-282.

214. Nowinski WL, Puspitasari F, Volkau I, Orrison WW, Jr., Knopp MV (2013) Quantification of the Human Cerebrovasculature: A 7Tesla and 320-Row CT In Vivo Study. J Comput Assist Tomogr 37 (1):117-122.

215. O'Meara RW, Michalski JP, Kothary R (2011) Integrin signaling in oligodendrocytes and its importance in CNS myelination. Journal of signal transduction 2011:354091.

216. Ochs S, Pourmand R, Jersild RA, Friedman RN (1997) The origin and nature of beading: A reversible transformation of the shape of nerve fibers. Prog Neurobiol 52 (5):391-426.

217. Ohashi K, Nagata K, Maekawa M, Ishizaki T, Narumiya S, Mizuno K (2000) Rho-associated Kinase ROCK Activates LIM-kinase 1 by Phosphorylation at Threonine 508 within the Activation Loop. Journal of Biological Chemistry 275 (5):3577-3582.

218. Omalu BI, Hamilton RL, Kamboh MI, DeKosky ST, Bailes J (2010) Chronic traumatic encephalopathy (CTE) in a National Football League Player: Case report and emerging medicolegal practice questions. J Forensic Nurs 6 (1):40-46.

219. Ommaya AK, Gennarelli TA (1974) Cerebral concussion and traumatic unconsciousness. Correlation of experimental and clinical observations of blunt head injuries. Brain 97 (4):633-654.

220. Ommaya AK, Goldsmith W, Thibault L (2002) Biomechanics and neuropathology of adult and paediatric head injury. Br J Neurosurg 16 (3):220-242.

221. Ommaya AK, Grubb RL, Jr., Naumann RA (1971) Coup and contre-coup injury: observations on the mechanics of visible brain injuries in the rhesus monkey. J Neurosurg 35 (5):503-516.

222. Palazzo AF, Eng CH, Schlaepfer DD, Marcantonio EE, Gundersen GG (2004) Localized stabilization of microtubules by integrin- and FAK-facilitated Rho signaling. Science 303 (5659):836-839.

223. Panicker AK, Buhusi M, Thelen K, Maness PF (2003) Cellular signalling mechanisms of neural cell adhesion molecules. Front Biosci 8:D900-D911.

224. Pantazopoulos H, Murray EA, Berretta S (2008) Total number, distribution, and phenotype of cells expressing chondroitin sulfate proteoglycans in the normal human amygdala. Brain Res 1207:84-95.

225. Pantazopoulos H, Woo TU, Lim MP, Lange N, Berretta S (2010) Extracellular matrix-glial abnormalities in the amygdala and entorhinal cortex of subjects diagnosed with schizophrenia. Archives of general psychiatry 67 (2):155-166.

226. Pinkstaff JK, Detterich J, Lynch G, Gall C (1999) Integrin subunit gene expression is regionally differentiated in adult brain. J Neurosci 19 (5):1541-1556.

227. Pizzorusso T, Medini P, Berardi N, Chierzi S, Fawcett JW, Maffei L (2002) Reactivation of ocular dominance plasticity in the adult visual cortex. Science 298 (5596):1248-1251.

228. Plow EF, Haas TA, Zhang L, Loftus J, Smith JW (2000) Ligand binding to integrins. J Biol Chem 275 (29):21785-21788.

229. Poliak S, Peles E (2003) The local differentiation of myelinated axons at nodes of Ranvier. Nat Rev Neurosci 4 (12):968-980.

230. Popp S, Andersen JS, Maurel P, Margolis RU (2003) Localization of aggrecan and versican in the developing rat central nervous system. Dev Dyn 227 (1):143-149.

231. Posmantur R, Kampfl A, Siman R, Liu J, Zhao X, Clifton GL, Hayes RL (1997) A calpain inhibitor attenuates cortical cytoskeletal protein loss after experimental traumatic brain injury in the rat. Neuroscience 77 (3):875-888.

232. Povlishock J, Christman C (1995) The pathobiology of traumatically induced axonal injury in animals and humans: a review of current thoughts. Journal of neurotrauma 12 (4):555-564.

233. Povlishock JT (1992) Traumatically induced axonal injury: pathogenesis and pathobiological implications. Brain Pathol 2 (1):1-12.

234. Povlishock JT, Becker DP, Cheng CL, Vaughan GW (1983) Axonal change in minor head injury. J Neuropathol Exp Neurol 42 (3):225-242.

235. Povlishock JT, Katz DI (2005) Update of neuropathology and neurological recovery after traumatic brain injury. J Head Trauma Rehabil 20 (1):76-94.

236. Prange MT, Margulies SS (2002) Regional, directional, and age-dependent properties of the brain undergoing large deformation. J Biomech Eng 124 (2):244-252.

237. Prieto AL, Jones FS, Cunningham BA, Crossin KL, Edelman GM (1990) Localization during development of alternatively spliced forms of cytotactin mRNA by in situ hybridization. The Journal of cell biology 111 (2):685-698.

238. Raghupathi R, Graham DI, McIntosh TK (2000) Apoptosis after traumatic brain injury. J Neurotrauma 17 (10):927-938.

239. Rajkowska G, Goldman-Rakic PS (1995) Cytoarchitectonic definition of prefrontal areas in the normal human cortex: I. Remapping of areas 9 and 46 using quantitative criteria. Cereb Cortex 5 (4):307-322.

240. Reeves TM, Greer JE, Vanderveer AS, Phillips LL (2010) Proteolysis of submembrane cytoskeletal proteins ankyrin-G and alphaII-spectrin following diffuse brain injury: a role in white matter vulnerability at Nodes of Ranvier. Brain Pathol 20 (6):1055-1068.

241. Reeves TM, Phillips LL, Povlishock JT (2005) Myelinated and unmyelinated axons of the corpus callosum differ in vulnerability and functional recovery following traumatic brain injury. Exp Neurol 196 (1):126-137.

242. Robles E, Gomez TM (2006) Focal adhesion kinase signaling at sites of integrin-mediated adhesion controls axon pathfinding. Nat Neurosci 9 (10):1274-1283.

243. Rodriguez MA, Pesold C, Liu WS, Kriho V, Guidotti A, Pappas GD, Costa E (2000) Colocalization of integrin receptors and reelin in dendritic spine postsynaptic densities of adult nonhuman primate cortex. Proc Natl Acad Sci U S A 97 (7):3550-3555.

244. Ruoslahti E (1996) Brain extracellular matrix. Glycobiology 6 (5):489-492.

245. Saatman KE, Creed J, Raghupathi R (2010) Calpain as a therapeutic target in traumatic brain injury. Neurotherapeutics 7 (1):31-42.

246. Saatman KE, Murai H, Bartus RT, Smith DH, Hayward NJ, Perri BR, McIntosh TK (1996) Calpain inhibitor AK295 attenuates motor and cognitive deficits following experimental brain injury in the rat. Proc Natl Acad Sci U S A 93 (8):3428-3433.

247. Schmid RS, Anton ES (2003) Role of integrins in the development of the cerebral cortex. Cereb Cortex 13 (3):219-224.

248. Schmidt CE, Dai J, Lauffenburger DA, Sheetz MP, Horwitz AF (1995) Integrin-cytoskeletal interactions in neuronal growth cones. J Neurosci 15 (5 Pt 1):3400-3407.

249. Schmidt E, Wolski TP, Jr., Kulesza RJ, Jr. (2010) Distribution of perineuronal nets in the human superior olivary complex. Hear Res 265 (1-2):15-24.

250. Schwartz MA, Schaller MD, Ginsberg MH (1995) Integrins: emerging paradigms of signal transduction. Annual review of cell and developmental biology 11:549-599.

251. Seeger G, Luth HJ, Winkelmann E, Brauer K (1996) Distribution patterns of Wisteria floribunda agglutinin binding sites and parvalbumin-immunoreactive neurons in the human visual cortex: a double-labelling study. Journal fur Hirnforschung 37 (3):351-366.

252. Sekeljic V, Andjus PR (2012) Tenascin-C and its functions in neuronal plasticity. The international journal of biochemistry & cell biology 44 (6):825-829.

253. Seong J, Lu SY, Wang YX (2011) Live Cell Imaging of Src/FAK Signaling by FRET. Cell Mol Bioeng 4 (2):138-147.

254. Serbest G, Horwitz J, Jost M, Barbee KA (2005) Mechanisms of cell death and neuroprotection by poloxamer 188 after mechanical trauma. Faseb Journal 19 (14):308-+.

255. Shi Y, Ethell IM (2006) Integrins control dendritic spine plasticity in hippocampal neurons through NMDA receptor and Ca2+/calmodulin-dependent protein kinase II-mediated actin reorganization. Journal of Neuroscience 26 (6):1813-1822.

256. Shuck LZ, Advani SH (1972) Rheological Response of Human Brain-Tissue in Shear. J Basic Eng-T Asme 94 (4):905-911.

257. Siechen S, Yang S, Chiba A, Saif T (2009) Mechanical tension contributes to clustering of neurotransmitter vesicles at presynaptic terminals. Proc Natl Acad Sci U S A 106 (31):12611-12616.

258. Smith DH, Chen XH, Xu BN, McIntosh TK, Gennarelli TA, Meaney DF (1997) Characterization of diffuse axonal pathology and selective hippocampal damage following inertial brain trauma in the pig. J Neuropathol Exp Neurol 56 (7):822-834.

259. Smith DH, Meaney DF (2000) Axonal damage in traumatic brain injury. Neuroscientist 6 (6):483-495.

260. Smith DH, Wolf JA, Lusardi TA, Lee VM, Meaney DF (1999) High tolerance and delayed elastic response of cultured axons to dynamic stretch injury. J Neurosci 19 (11):4263-4269.

261. Smith SJ (1988) Neuronal cytomechanics: the actin-based motility of growth cones. Science 242 (4879):708-715.

262. Spaethling JM, Klein DM, Singh P, Meaney DF (2008) Calcium-permeable AMPA receptors appear in cortical neurons after traumatic mechanical injury and contribute to neuronal fate. J Neurotrauma 25 (10):1207-1216.

263. Sponheim SR, McGuire KA, Kang SS, Davenport ND, Aviyente S, Bernat EM, Lim KO (2011) Evidence of disrupted functional connectivity in the brain after combat-related blast injury. NeuroImage 54 (Supplement 1):S21-S29.

264. Staubli U, Chun D, Lynch G (1998) Time-dependent reversal of long-term potentiation by an integrin antagonist. J Neurosci 18 (9):3460-3469.

265. Stern RA, Riley DO, Daneshvar DH, Nowinski CJ, Cantu RC, McKee AC (2011) Long-term consequences of repetitive brain trauma: chronic traumatic encephalopathy. PM R 3 (10 Suppl 2):S460-467.

266. Stevens GR, Zhang C, Berg MM, Lambert MP, Barber K, Cantallops I, Routtenberg A, Klein WL (1996) CNS neuronal focal adhesion kinase forms clusters that co-localize with vinculin. J Neurosci Res 46 (4):445-455.

267. Stone JR, Okonkwo DO, Dialo AO, Rubin DG, Mutlu LK, Povlishock JT, Helm GA (2004) Impaired axonal transport and altered axolemmal permeability occur in distinct populations of damaged axons following traumatic brain injury. Exp Neurol 190 (1):59-69.

268. Stone JR, Okonkwo DO, Dialo AO, Rubin DG, Mutlu LK, Povlishock JT, Helm GA (2004) Impaired axonal transport and altered axolemmal permeability occur in distinct populations of damaged axons following traumatic brain injury. Experimental Neurology 190 (1):59-69.

269. Strich SJ (1956) Diffuse degeneration of the cerebral white matter in severe dementia following head injury. J Neurol Neurosurg Psychiatry 19 (3):163-185.

270. Su L, Lv X, Miao J (2008) Integrin beta 4 in neural cells. Neuromolecular Med 10 (4):316-321.

271. Sudhof TC (2008) Neuroligins and neurexins link synaptic function to cognitive disease. Nature 455 (7215):903-911.

272. Susuki K, Rasband MN (2008) Molecular mechanisms of node of Ranvier formation. Curr Opin Cell Biol 20 (6):616-623.

273. Sykova E, Nicholson C (2008) Diffusion in brain extracellular space. Physiol Rev 88 (4):1277-1340.

274. Tagliaferri F, Compagnone C, Korsic M, Servadei F, Kraus J (2006) A systematic review of brain injury epidemiology in Europe. Acta Neurochir (Wien) 148 (3):255-268; discussion 268.

275. Tang-Schomer MD, Patel AR, Baas PW, Smith DH (2010) Mechanical breaking of microtubules in axons during dynamic stretch injury underlies delayed elasticity, microtubule disassembly, and axon degeneration. FASEB J 24 (5):1401-1410.

276. Thibault KL, Margulies SS (1998) Age-dependent material properties of the porcine cerebrum: effect on pediatric inertial head injury criteria. J Biomech 31 (12):1119-1126.

277. Tomaselli KJ, Neugebauer KM, Bixby JL, Lilien J, Reichardt LF (1988) N-cadherin and integrins: two receptor systems that mediate neuronal process outgrowth on astrocyte surfaces. Neuron 1 (1):33-43.

278. Toole BP (2004) Hyaluronan: from extracellular glue to pericellular cue. Nature reviews Cancer 4 (7):528-539.

279. Tucker RP, Chiquet-Ehrismann R (2009) The regulation of tenascin expression by tissue microenvironments. Biochim Biophys Acta 1793 (5):888-892.

280. Turley EA, Noble PW, Bourguignon LY (2002) Signaling properties of hyaluronan receptors. J Biol Chem 277 (7):4589-4592.

281. Tyler WJ (2012) The mechanobiology of brain function. Nat Rev Neurosci 13 (12):867-878.

282. Tzima E (2006) Role of small GTPases in endothelial cytoskeletal dynamics and the shear stress response. Circ Res 98 (2):176-185.

283. Tzima E, del Pozo MA, Shattil SJ, Chien S, Schwartz MA (2001) Activation of integrins in endothelial cells by fluid shear stress mediates Rho-dependent cytoskeletal alignment. EMBO J 20 (17):4639-4647.

284. Uchida N, Honjo Y, Johnson KR, Wheelock MJ, Takeichi M (1996) The catenin/cadherin adhesion system is localized in synaptic junctions bordering transmitter release zones. Journal of Cell Biology 135 (3):767-779.

285. Underhill C (1992) CD44: the hyaluronan receptor. J Cell Sci 103 (Pt 2):293-298.

286. Vappou J, Breton E, Choquet P, Willinger R, Constantinesco A (2008) Assessment of in vivo and post-mortem mechanical behavior of brain tissue using magnetic resonance elastography. J Biomech 41 (14):2954-2959.

287. Virgintino D, Perissinotto D, Girolamo F, Mucignat MT, Montanini L, Errede M, Kaneiwa T, Yamada S, Sugahara K, Roncali L, Perris R (2009) Differential distribution of aggrecan isoforms in perineuronal nets of the human cerebral cortex. J Cell Mol Med 13 (9B):3151-3173.

288. Vitellaro-Zuccarello L, Meroni A, Amadeo A, De Biasi S (2001) Chondroitin sulfate proteoglycans in the rat thalamus: expression during postnatal development and correlation with calcium-binding proteins in adults. Cell Tissue Res 306 (1):15-26.

289. Vogel V, Sheetz M (2006) Local force and geometry sensing regulate cell functions. Nat Rev Mol Cell Biol 7 (4):265-275.

290. Walsh FS, Doherty P (1997) Neural cell adhesion molecules of the immunoglobulin superfamily: role in axon growth and guidance. Annual review of cell and developmental biology 13:425-456.

291. Wang JH, Thampatty BP (2006) An introductory review of cell mechanobiology. Biomech Model Mechanobiol 5 (1):1-16.

292. Wang N, Butler JP, Ingber DE (1993) Mechanotransduction across the Cell-Surface and through the Cytoskeleton. Science 260 (5111):1124-1127.

293. Wang N, Butler JP, Ingber DE (1993) Mechanotransduction across the cell surface and through the cytoskeleton. Science 260 (5111):1124-1127.

294. Wang N, Ingber DE (1994) Control of Cytoskeletal Mechanics by Extracellular-Matrix, Cell-Shape, and Mechanical Tension. Biophysical Journal 66 (6):2181-2189.

295. Wang N, Ingber DE (1995) Probing transmembrane mechanical coupling and cytomechanics using magnetic twisting cytometry. Biochemistry and cell biology = Biochimie et biologie cellulaire 73 (7-8):327-335.

296. Wang N, Naruse K, Stamenovic D, Fredberg JJ, Mijailovich SM, Tolic-Norrelykke IM, Polte T, Mannix R, Ingber DE (2001) Mechanical behavior in living cells consistent with the tensegrity model. Proc Natl Acad Sci U S A 98 (14):7765-7770.

297. Wang N, Planus E, Pouchelet M, Fredberg JJ, Barlovatz-Meimon G (1995) Urokinase receptor mediates mechanical force transfer across the cell surface. Am J Physiol 268 (4 Pt 1):C1062-1066.

298. Wang N, Tytell JD, Ingber DE (2009) Mechanotransduction at a distance: mechanically coupling the extracellular matrix with the nucleus. Nat Rev Mol Cell Biol 10 (1):75-82.

299. Wang Y, Botvinick EL, Zhao Y, Berns MW, Usami S, Tsien RY, Chien S (2005) Visualizing the mechanical activation of Src. Nature 434 (7036):1040-1045.

300. Watson PM, Humphries MJ, Relton J, Rothwell NJ, Verkhratsky A, Gibson RM (2007) Integrin-binding RGD peptides induce rapid intracellular calcium increases and MAPK signaling in cortical neurons. Mol Cell Neurosci 34 (2):147-154.

301. Webb DJ, Zhang H, Majumdar D, Horwitz AF (2007) alpha5 integrin signaling regulates the formation of spines and synapses in hippocampal neurons. J Biol Chem 282 (10):6929-6935.

302. Wernig F, Mayr M, Xu QB (2003) Mechanical stretch-induced apoptosis in smooth muscle cells is mediated by beta(1)-integrin signaling pathways. Hypertension 41 (4):903-911.

303. Wheelock MJ, Johnson KR (2003) Cadherin-mediated cellular signaling. Curr Opin Cell Biol 15 (5):509-514.

304. Wilbur JL, Kumar A, Kim E, Whitesides GM (1994) Microfabrication by Microcontact Printing of Self-Assembled Monolayers. Adv Mater 6 (7-8):600-604.

305. Wolf JA, Stys PK, Lusardi T, Meaney D, Smith DH (2001) Traumatic axonal injury induces calcium influx modulated by tetrodotoxin-sensitive sodium channels. J Neurosci 21 (6):1923-1930.

306. Wright RM, Post A, Hoshizaki B, Ramesh KT (2013) A Multiscale Computational Approach to Estimating Axonal Damage under Inertial Loading of the Head. J Neurotrauma 30 (2):102-118.

307. Wu C, Dedhar S (2001) Integrin-linked kinase (ILK) and its interactors: a new paradigm for the coupling of extracellular matrix to actin cytoskeleton and signaling complexes. The Journal of cell biology 155 (4):505-510.

308. Yakovlev AG, Faden AI (2004) Mechanisms of neural cell death: implications for development of neuroprotective treatment strategies. NeuroRx 1 (1):5-16.

309. Yamada H, Fredette B, Shitara K, Hagihara K, Miura R, Ranscht B, Stallcup WB, Yamaguchi Y (1997) The brain chondroitin sulfate proteoglycan brevican associates with astrocytes ensheathing cerebellar glomeruli and inhibits neurite outgrowth from granule neurons. J Neurosci 17 (20):7784-7795.

310. Yamada H, Watanabe K, Shimonaka M, Yamaguchi Y (1994) Molecular cloning of brevican, a novel brain proteoglycan of the aggrecan/versican family. J Biol Chem 269 (13):10119-10126.

311. Yasuda R, Murakoshi H (2011) The mechanisms underlying the spatial spreading of signaling activity. Current Opinion in Neurobiology 21 (2):313-321.

312. Yasuhara O, Akiyama H, McGeer EG, McGeer PL (1994) Immunohistochemical localization of hyaluronic acid in rat and human brain. Brain Res 635 (1-2):269-282.

313. Yeung T, Georges PC, Flanagan LA, Marg B, Ortiz M, Funaki M, Zahir N, Ming WY, Weaver V, Janmey PA (2005) Effects of substrate stiffness on cell morphology, cytoskeletal structure, and adhesion. Cell Motil Cytoskel 60 (1):24-34.

314. Yoshino A, Hovda DA, Katayama Y, Kawamata T, Becker DP (1992) Hippocampal CA3 lesion prevents postconcussive metabolic dysfunction in CA1. J Cereb Blood Flow Metab 12 (6):996-1006.

315. Yuen TJ, Browne KD, Iwata A, Smith DH (2009) Sodium channelopathy induced by mild axonal trauma worsens outcome after a repeat injury. J Neurosci Res 87 (16):3620-3625.

316. Zaidel-Bar R, Kam Z, Geiger B (2005) Polarized downregulation of the paxillin-p130(CAS)-Rac1 pathway induced by shear flow. J Cell Sci 118 (17):3997-4007.

317. Zamir E, Katz B, Aota S, Yamada K, Geiger B, Kam Z (1999) Molecular diversity of cell-matrix adhesions. Journal of Cell Science 112 (11):1655-1670.

318. Zhang LY, Yang KH, King AI (2001) Comparison of brain responses between frontal and lateral impacts by finite element modeling. J Neurotraum 18 (1):21-30.

319. Zhao XH, Laschinger C, Arora P, Szaszi K, Kapus A, McCulloch CA (2007) Force activates smooth muscle alpha-actin promoter activity through the Rho signaling pathway. J Cell Sci 120 (10):1801-1809.

320. Zimmermann DR, Dours-Zimmermann MT (2008) Extracellular matrix of the central nervous system: from neglect to challenge. Histochem Cell Biol 130 (4):635-653.

321. Zlokovic BV (2008) The blood-brain barrier in health and chronic neurodegenerative disorders. Neuron 57 (2):178-201.

322. Zouridakis G, Patidar U, Situ N, Rezaie R, Castillo EM, Levin HS, Papanicolaou AC (2012) Functional Connectivity Changes in Mild Traumatic Brain Injury Assessed Using Magnetoencephalography. J Mech Med Biol 12 (2).

323. Zuber B, Nikonenko I, Klauser P, Muller D, Dubochet J (2005) The mammalian central nervous synaptic cleft contains a high density of periodically organized complexes. Proc Natl Acad Sci U S A 102 (52):19192-19197.